TU Delft

Delft University of Technology

Development of an Integrated Analytical Model to Predict the Wet Collapse Pressure of Flexible Risers

Li, X.

DOI
10.4233/uuid:404cd375-f152-4a28-b324-8727497a517d

Publication date
2021

Document Version
Final published version

Citation (APA)
Li, X. (2021). *Development of an Integrated Analytical Model to Predict the Wet Collapse Pressure of Flexible Risers* (T2021/9 ed.). [Dissertation (TU Delft), Delft University of Technology]. TRAIL Research School. https://doi.org/10.4233/uuid:404cd375-f152-4a28-b324-8727497a517d

Important note
To cite this publication, please use the final published version (if applicable).
Please check the document version above.

Copyright
Other than for strictly personal use, it is not permitted to download, forward or distribute the text or part of it, without the consent of the author(s) and/or copyright holder(s), unless the work is under an open content license such as Creative Commons.

Takedown policy
Please contact us and provide details if you believe this document breaches copyrights.
We will remove access to the work immediately and investigate your claim.

This work is downloaded from Delft University of Technology.
For technical reasons the number of authors shown on this cover page is limited to a maximum of 10.

Development of an Integrated Analytical Model to Predict the Wet Collapse Pressure of Flexible Risers

Xiao LI

The research leading to this dissertation is partly funded by Delft University of Technology (TU Delft) and China Scholarship Council (CSC) under the grant 201606950011.

Development of an Integrated Analytical Model to Predict the Wet Collapse Pressure of Flexible Risers

Dissertation

for the purpose of obtaining the degree of doctor
at Delft University of Technology
by the authority of the Rector Magnificus, Prof. dr. ir. T.H.J.J. van den Hagen
chair of the Board for Doctorates
to be defended publicly on
Thursday 4th, February 2021 at 12:30 o'clock

by

Xiao LI
Master of Engineering in Naval Architecture and Ocean Engineering
Wuhan University of Technology, Wuhan, China
born in Jingzhou, Hubei, China

This dissertation has been approved by the promotors.

Composition of the doctoral committee:

Rector Magnificus	Chairperson
Prof. ir. J. J. Hopman	Delft University of Technology, promotor
Dr. X. Jiang	Delft University of Technology, copromotor

Independent members:

Prof. dr. ir. A. van Keulen	Delft University of Technology
Prof. ir. F. S. K. Bijlaard	Delft University of Technology
Prof. dr. S. Sævik	Norwegian University of Science and Technology, Norway.
Prof. dr. Y. Bai	Zhejiang University, China
Dr. ir. J. H. den Besten	Delft University of Technology

TRAIL Thesis Series no. T2021/9, the Netherlands Research School TRAIL

TRAIL
P.O. BOX 5017
2600 GA Delft
The Netherlands
E-mail: info@rsTRAIL.nl

ISBN: 978-90-5584-285-8

Copyright © 2021 by Xiao LI

All rights reserved. No part of the material protected by this copyright notice may be reproduced or utilized in any form or by any means, electronic or mechanical, including photocopying, recording or by any information storage and retrieval system, without written permission of the author.

Printed in the Netherlands

Preface

Every Ph.D. research is a long journey and now my journey is about to reach its end. The accomplishment of this journey would not have been possible without the encouragement and collaboration of a large and diverse community of people. I am really cherish the time that worked with them, and it was their advice, support and friendship that brought me to this journey's end.

First of all, I would like to express my gratitude to the China Scholarship Council. This dissertation would not be existed without its financial support.

My profound gratitude goes to my supervision team, Prof. Hans Hopman and Dr. Xiaoli Jiang, for their great support and guidance during these years. I would like to thank Hans, my promotor, for his valuable mentorship, both personally and academically. He was always available and willing to answer my queries, and what I've learned from him was more than what I desired for. I also sincerely thank my co-promotor, Xiaoli, for her insightful comments, inspirational discussions and scientific attitude that guided me through this research. She was always the first person to celebrate my best ideas, and explicate the pitfalls graciously in my research.

I would like to further extend my gratitude to all my committee members. Great thanks to Prof. Frans Bijlaard, Prof. Fred van Keulen, Prof. Yong Bai, Prof. Svein Sævik, and Dr. Henk den Besten for their precious time and efforts for reviewing and committing on my thesis. I am looking forward to the upcoming discussions during the defense ceremony. Additionally, I would like to thank Prof. Chiara Bisagni and Dr. Sape Miedema for being the committee members of my Go/No go meeting. Their comments and suggestions benefited my research a lot.

Many thanks to my colleagues and friends. Thanks to my office-mates, Carmen, Alina, Harleigh, and Zhongchen, Javad, Hamid, Weizheng and Wenjing who stayed shortly, and many other colleagues, for casual talks and helps. I truly appreciate the help from the supporting staff and secretariats in the department of Maritime and Transport Engineering and TRAIL Research School. Among them, a big thanks to Dineke, Patty, Anouk, Monique,

Pauline, Gracia and Conchita for always being kind and helpful. My special thanks go to Mr. Dick Mensch for your help of translating the English summary into Dutch. It was always enjoyable to talk with you.

Finally, I would like to thank my parents for their endless love, support and encouragement.

Xiao Li

Delft, Jan 2021

Contents

Chapter 1

Introduction

With fewer remaining easy-to-access onshore oil and gas reservoirs, offshore fields have been targeted by the industry to find production growth. Over the past 40 years, the water depth of the sub-sea fields for oil and gas production has increased from 125 meters (1977, Roncador field) to 2900 meters (2016, Stones field) (Vidigal da Silva & Damiens, 2016; Moore et al., 2017). As the oil and gas exploitation continuously moves into ever deeper water, there is an increasing demand for the development and qualification of production riser systems to enable this expansion. Flexible riser, a primary riser device for floating production, is being required to meet such a demand.

1.1 Background

The flexible riser is one kind of flexible pipes which transports fluid between subsea facilities and topside structures (Fergestad & Ltveit, 2017), as shown in Figure 1.1 (Shen & Jukes, 2015). It is basically a multilayered pipe structure which consists of helical wound metallic strips and tapes, and extruded polymeric layers (Rahmati et al., 2016). A typical internal configuration of the flexible riser is shown in Figure 1.2 (NOV, 2014). The carcass and the pressure armor are two self-interlocking layers wound by metal strips with constant pitches, which take external and internal pressure, separately. The polymeric inner liner in-between is a leak-proof barrier to contain fluids in the pipe bore. Tensile armors form in pairs to provide tension, bending and torsional resistances. The outer sheath is the water barrier for the seawater outside. In Table 1.1, the function and most commonly used materials of each layer are summarized.

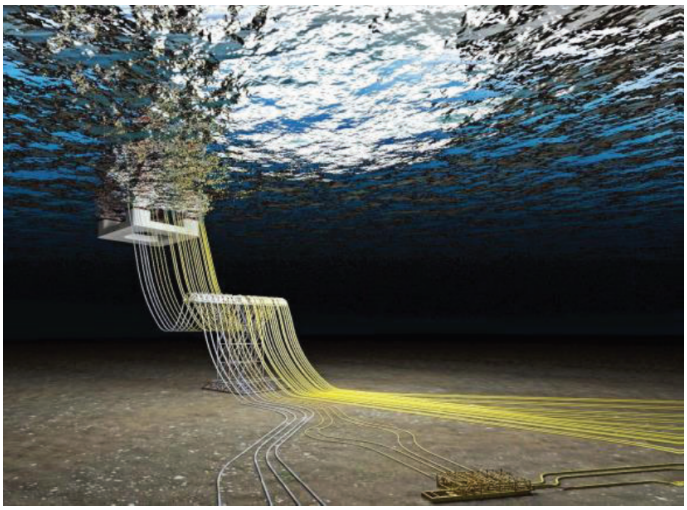

Figure 1.1: Overview of flexible risers (Shen & Jukes, 2015)

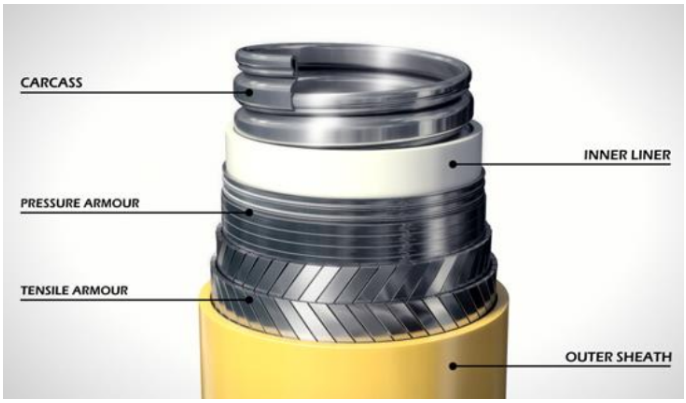

Figure 1.2: Typical configuration of a flexible riser (NOV, 2014)

Since the first flexible risers were installed in 1978 (Machado & Dumay, 1980), this pipe-like structure had served the shallow water production with an established technology. However, the application of flexible risers to deep water gives rise to the increase of cost and technical challenges (Eyssautier et al., 2018), requiring the development of the flexible riser technology. Harsh operating environments in deep and ultra-deep water fields impose a variety of potential failure modes on flexible risers, such as collapse, burst, lateral/ bird-caging buckling or fatigue, etc (Muren, 2007). Among those different failure modes, collapse failure, as shown in Figure 1.3 (Fernando, 2015), is always a primary challenge for riser operators to cope with (Shen

Table 1.1: Name, material and function of each layer within a flexible riser

Layer	Material	Function
Carcass	Duplex steel	External pressure resistance
Pressure armour	Carbon steel	Hoop and radial load resistance
Tensile armour	Carbon steel	Axial and torsional load resistance
Inner liner	HDPE, XLPE, PA, PVDF	Internal fluid containment
Outer sheath	HDPE, PA, TPE	External fluid barrier

& Jukes, 2015).

Collapse of flexible risers refers to radial buckling of the internal carcass structures under external hydro-static water pressure. High valued external pressure, which increases about ten atmospheres for every 100 meters of water depth, makes flexible risers vulnerable to be collapsed in deep water fields. Anti-collapse capability is usually regarded as an essential qualification factor for those flexible risers used in ultra-deep water production (Simpson & Lima, 2019). With flexible risers being contemplated for water depths of nearly 3000 meters, their anti-collapse capability may govern riser design and the final production cost (Wolodko & DeGeer, 2006; Lohr & Pena, 2017; 4Subsea, 2013).

Figure 1.3: Collapse failure of the flexible riser (Fernando, 2015)

1.2 Research motivation

The understanding of collapse failure and related riser performance characteristics is important for designing reliable flexible riser systems (Sævik &

Ye, 2016). Collapse failure of flexible risers is commonly divided into two types, dry and wet collapse, depending on the annulus conditions of flexible risers (API17B Fifth Edition, 2014). Dry collapse may occur when the outer sheath is intact and all layers within the riser play a role together to resist the hydro-static pressure. In this scenario, the interlocked carcass and the pressure armor are the main layers for resisting the collapse, as they contribute the most to radial stiffness. Once the outer sheath is breached, the seawater floods the riser annulus and the external pressure acts directly on the inner sheath. This situation, named wet collapse, represents the most extreme loading condition since the whole external pressure is resisted by the carcass alone. Other layers, mainly the pressure armor, contributes to the collapse resistance by restraining the radial deformation of the carcass.

The collapse capacity of a flexible riser is mainly designed based on its wet collapse resistance (Sævik & Ye, 2016) since the outer sheath can be easily damaged in the ocean environment. According to the latest survey of flexible pipe failure / damage mechanisms carried out by O'Brien et al. (O'Brien et al., 2011), the outer sheath remains the most common failure, as illustrated in Figure 1.4. For the sections of flexible risers lying on the seabed, their outer sheath could be worn out due to large amounts of movements, as shown in Figure 1.5 (Crome, 2013). As there is a high risk for the outer sheath to be breached, flexible risers are therefore required to operate under a flooded annulus situation without collapse.

Various standards have been developed with regard to the design of flexible risers (DNV-OS-C501, 2010; DNV-RP-A203, 2011; API17B Fifth Edition, 2014; API17J Fourth Edition, 2014). Among them, API 17B and 17J (API17B Fifth Edition, 2014; API17J Fourth Edition, 2014) are two widely acceptable specifications that issued by American Petroleum Institute. For flexible risers applied to ultra-deep water production, those specifications, however, did not provide specific approaches for reference to calculate their critical collapse pressure. In their latest versions (2014), no prescriptive methodology was given to guide the anti-collapse design of flexible risers. In other words, how to predict the critical pressure is still a gray area for riser designers (Kalman et al., 2014).

As the industry is moving towards ultra-deep water fields for more petroleum product, the flexible risers are required to have strong collapse capacities. The hydro-static collapse design of flexible risers shall be confirmed by the wet collapse calculations. Mostly, collapse analyses are performed through numerical simulations, which are less feasible for the design stage

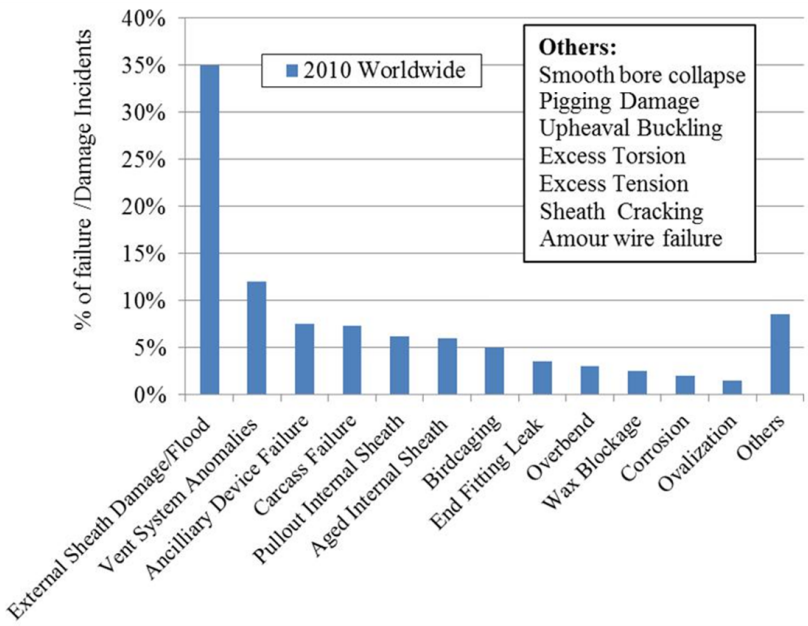

Figure 1.4: Flexible pipe failure/damage mechanisms (O'Brien et al., 2011)

Figure 1.5: Damaged outer sheath (Crome, 2013)

of flexible risers in comparison with the analytical models. To date, the analytical models in public literature for predicting the wet collapse pressure of
90 flexible risers are limited. To meet this demand, an analytical model is presented in this dissertation to facilitate the collapse analysis in design stage.

1.3 Research objective and questions

In this dissertation, the main objective is to develop an analytical model for predicting the wet collapse pressure of flexible risers, aiming to facilitate the collapse analysis in their pipe design stage. To achieve this goal, the following main research question should be answered:

- How to develop an integrated analytical model for predicting the wet collapse pressure of the flexible risers?

This main research question can be further broken down into several sub-questions as below:

1. Are there any analytical models developed for the collapse studies of flexible risers?
2. What are the limitations of those analytical models in predicting the wet collapse pressure of flexible risers?
3. How to address the complex interlocked layers of the flexible riser in the prediction model?
4. How to take the initial ovalization and the inter-layer gap into account?
5. What is the buckling mechanism of curved risers subjected to wet collapse?
6. How to incorporate the curvature effect into the analytical model?
7. How to formulate an integrated analytical model by involving the geometric imperfections and pipe curvature in its wet collapse prediction?
8. How to verify the proposed integrated analytical model?

1.4 Research scope

As mentioned in section 1.2, there are two types of collapse failure of flexible risers, dry and wet collapse, depending on the annulus conditions of flexible risers. Compared to the dry collapse, the wet collapse is a more severe situation for flexible risers since the entire external pressure is resisted by the

carcass and the pressure armor only. Therefore, the research work presented in this thesis focuses on the wet collapse issue of flexible risers.

In the initial design phase (cross-section configuration design), the main work is to determine proper cross-section dimensions for the production risers based on their functional requirements (API17B Fifth Edition, 2014; Bai et al., 2017). As the analytical model aims to serve this design phase, some time dependent factors like carcass erosion (Tadjiev, 2016; Helgaker et al., 2017) and corrosion (Sousa et al., 2015) will not be considered. Additionally, factors related to material imperfections will not be taken into account in the model development, either. This is due to the fact that those factors are difficult to measure and calculate in practice, e.g. the cold work degree and residual stress, and the effects brought by them to the collapse resistance could be positive (Zhang et al., 2003; Fernando et al., 2017).

It should be noted that collapse can also be caused by depressurization if the riser is manufactured with a multi-layered inner sheath (Fernando, 2016). The fluid transported in riser bore can penetrate the annular space between the sheath layers by means of flow paths through the end-fitting (Lambert et al., 2012). When the riser bore is depressurized, a huge differential pressure can be formed due to the trapped fluid, which might lead to the carcass collapse. As this thesis focuses on the hydro-static pressure-induced collapse, therefore, this kind of collapse is not within our research scope.

1.5 Outline of the dissertation

The remainder of this dissertation is made up of six chapters, which has an outline as follows:

- **Chapter 2** gives an overview of the recent advances on collapse studies of flexible risers. The approaches developed for predicting the critical collapse pressure of flexible risers are presented in this chapter as well as the research gaps within this issue. Answers to the sub-questions 1–2 will be given in this chapter.

- **Chapter 3** presents an equivalent layer method to address the complex profiles of the interlocked metallic layers. By using this equivalent layer method, those interlocked layers could be treated as homogeneous rings in the collapse analysis. This chapter is mainly used to answer the third sub-question.

- With the equivalent layer method proposed in the last chapter, **Chapter 4** presents a theoretical framework of this analytical model. Based on this theoretical framework, the geometric imperfections are thereby taken into account. In this chapter, the fourth sub-question will be solved.

- As a further step to predict the wet collapse pressure, **Chapter 5** investigates the curved collapse mechanism of flexible risers. Based on this mechanism study, the analytical model is extended to incorporate the curvature effect in the wet collapse analysis. This chapter gives the answers to the sub-questions 5 and 6.

- In **Chapter 6**, the proposed analytical model is used to study the effect of a combination of the initial geometric imperfections and the pipe curvature on the wet collapse resistance of flexible risers. 3D FE full models are employed to verify its prediction accuracy. The answers to the last two sub-questions are provided by this chapter.

- On the basis of the previous chapters, **Chapter 7** presents the conclusions of this dissertation as well as the recommendations for the future research.

Chapter 2

Literature review

In this chapter, we review the collapse-related research of flexible pipes. This answers the first two research questions. Collapse is a complex phenomenon related to the material properties, the geometry of the pipe and its overall surface topography and, therefore, makes the prediction of critical pressure challenging. Related prediction approaches of flexible risers have been developed for decades, yet a comprehensive review of their predictive capabilities, efficiency and drawbacks is lacking. As this project aims to develop an effective prediction model of riser collapse, there is a necessity to review the recent advances on collapse studies of flexible risers and highlight the gaps in existing prediction methods.

To this end, the chapter is intended to introduce the development of collapse studies of flexible risers and elucidate the limitations of existing available prediction methods, which is organized as: in Section 2.1, the existing prediction approaches of critical pressure of flexible risers are listed, followed by Section 2.2 that elaborates the technical challenges that need to be faced in the model development. Section 2.3 concludes the work.

This chapter is published as a journal article: Li, X., Jiang, X., Hopman, H. (2018). A review on predicting critical collapse pressure of flexible risers for ultra-deep oil and gas production, *Appl Ocean Res*, 80, 1–10.

2.1 Prediction approaches of collapse pressure

Collapse studies have been conducted extensively by many researchers since the inception of the flexible risers around the 1970s (Chaperon et al., 1991). For the most part, those studies are limited to highly simplified models (Cooke & Kenny, 2014). Buckling theories of rings are adopted to develop the analytical models (Sævik & Ye, 2016; Chen et al., 2015; Bai et al., 2016). In the meanwhile, numerical simulations are also developed as an alternative. With the aid of experimental calibration, those models could thereby be used to predict the critical collapse pressure of flexible risers.

2.1.1 Hydro-static tests

Over the past decades, numerous experimental programs have been conducted to study the collapse behaviors of flexible pipes that prepared for deep water environment (Novitsky & Gray, 2003). Although such kind of experiments are costly, they are the foundation to develop related analytical and numerical approaches.

It is known that collapse tests of flexible pipes are very costly, which require specialized hyperbaric chambers and end fitting equipment (Novitsky & Gray, 2003; Rosas et al., 2014), as displayed in Figure 2.1 (Miyazaki et al., 2018). Such kind of tests were performed by Souza (Souza, 2002) at the COPPE/UFRJ Submarine Technology Laboratory. The tests were conducted in a horizontal hyperbaric chamber with a capacity of 10000 psi, as shown in Figure 2.2. The samples with two different internal diamaters (ID), 4 and 8 inches, were placed in that hyperbaric chamber and pressurized to collapse. The test results showed that the pressure armor has a positive effect on the collapse resistance. For the pipe samples without pressure armor, collapse caused large openings on their interlocked carcass. But with the pressure armor, the openings on the carcass were negligible after the pipe collapse. Due to the internal diameter limitation of that chamber, all the samples were test in straight configuration.

Owing to the structural flexibility, flexible risers are curved naturally in the touchdown zone (TDZ) and buoyed regions, as sketched in Figure 2.3 (Anderson & O'Connor, 2012). To investigate the curvature effect on the collapse resistance of flexible pipes, curved collapse tests were conducted by Clevelario et al. (Clevelario et al., 2010), as shown in Figure 2.4. The

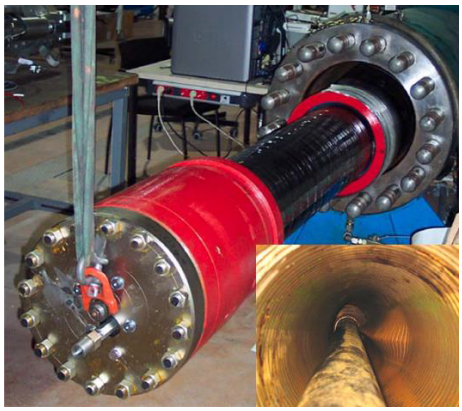

Figure 2.1: Hyperbaric chamber and end fittings for the collapse test (Miyazaki et al., 2018)

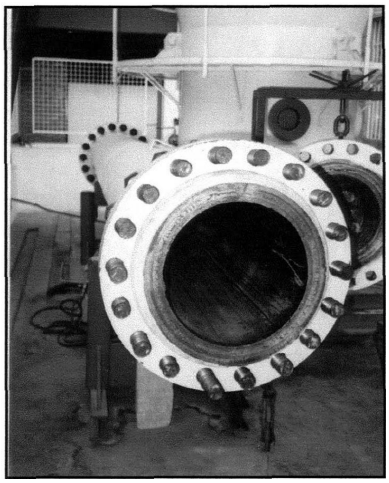

Figure 2.2: Hyperbaric chamber used in Souza's experimental tests (Souza, 2002)

samples with two different ID, 4 and 6 inches, were both used for straight and curved tests. The carcass, the inner liner, and the pressure armor were remained in all the samples, while additional tensile armors were added to those curved ones to withstand the axial compression loads generated by the reverse end cap effect (Fyrileiv & Collberg, 2005). Those curved samples were bent to 1.5 times the storage bending radius (SBR) (Bai & Bai, 2005) to investigate their curved collapse behaviors under external pressure. The curvature radii of those test samples were determined by the global analyses

of the test samples, as illustrated in Figure 2.5, which could not be reached in all possible environmental and operational conditions. Each samples' curved collapse pressure was recorded and compared with its straight counterpart. The comparison showed that the reduction of the collapse strength induced by curvature could go up to 10%, indicating the curvature effect cannot be neglected in the collapse analysis of flexible risers.

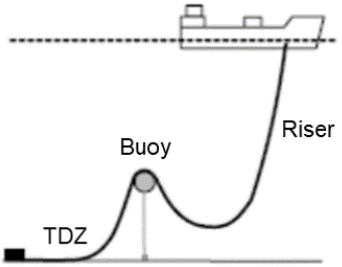

Figure 2.3: Riser in a curved configuration (Anderson & O'Connor, 2012)

Figure 2.4: Curved collapse test samples (Clevelario et al., 2010)

2.1.2 Analytical methods

Due to the geometric complexity of the interlocked layer profile, the development of analytical approaches is still limited to highly simplified models. The main difficulty in using those analytical models always lies in the determination of the equivalent properties for the interlocked metallic layers.

Up to now, many equivalent layer methods have been proposed to address this issue (de Sousa et al., 2001; Martins et al., 2003), which treat those interlocked layers as equivalent tube structures. Considering the helicoidal ge-

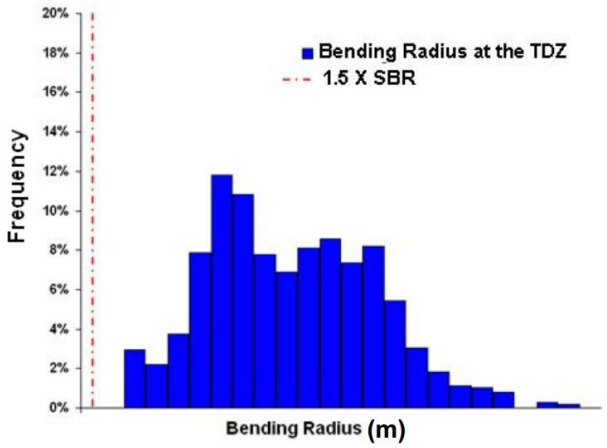

Figure 2.5: Global analysis result – TDZ bending radius histogram (Clevelario et al., 2010)

ometry of the carcass imposes a directional dependency on its structural mechanical properties, a fictitious orthotropic shell was built based on the analogy between grids and plates (Timoshenko & Woinowsky-Krieger, 1959), as shown in 2.6. This idea was first proposed by Cruz and Dias (Cruz & Dias, 1997), who treated the spiral wound carcass as a shell with distinct stiffness in two orthogonal directions. Based on the equivalence of membrane, bending and torsional stiffness between the carcass and the orthotropic tubular shell, the equivalent properties for the latter one were determined.

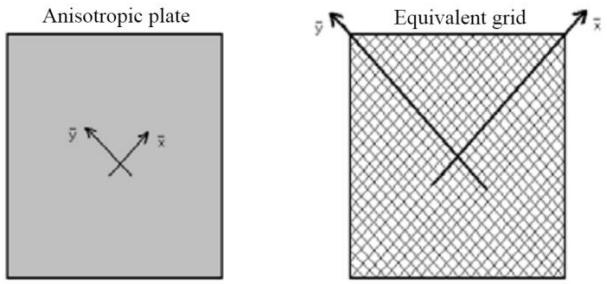

Figure 2.6: Analogy between plates and grids (Ribeiro et al., 2003)

This method is often used to study the responses of carcass layer subjected to axial loads (Ribeiro et al., 2003; Yue et al., 2013; Provasi et al., 2016) or crush (de Sousa et al., 2009, 2001; Soki et al., 2015; Caleyron et al., 2014) due to its orthotropic mechanical properties. Since the external

pressure is mainly resisted by the radial stiffness of the carcass, the treatment of the carcass as a homogeneous ring by discarding its large lay angle in the collapse studies is more acceptable to academics. To support this treatment, Gay Neto and Martins (Gay Neto & Martins, 2012) investigated the lay angle effect of the carcass strips on the collapse prediction of flexible pipes. According to their investigation, the effect brought by the carcass lay angle was negligible to the collapse prediction. Therefore, the lay angle effect was excluded in the equivalent treatment for collapse problems, allowing the usage of the buckling theories of circular rings in the development of analytical models (Timoshenko & Gere, 1961).

In recent years, many equivalent methods were proposed in terms of one property of the carcass, e.g. the cross-sectional area, the bending stiffness or the strain energy (Chen et al., 2015; Zhang et al., 2003; Loureiro & Pasqualino, 2012; Martins et al., 2003; Tang et al., 2016). Area equivalent method (Zhang et al., 2003) was carried out based on the equivalence of cross-sectional areas between structures. One another similar method calculated the equivalent thickness of the interlocked layer based on the fraction fill coefficient of its cross-sectional area (Chen et al., 2015). As the equivalent thickness of the carcass is simply determined by the area equivalency in those methods, the actual material distribution in the layer profile is neglected. As the result, the predictions of collapse pressure based on those equivalent methods are less accurate (Cuamatzi-Melendez et al., 2017).

Considering that the collapse of pipe-like structures is a bending-dominated problem (Timoshenko & Gere, 1961), some other equivalent methods came forward to build this equivalency based on the structural bending stiffness. One bending stiffness equivalence method employed by Loureiro and Pasqualino (Loureiro & Pasqualino, 2012) obtained the equivalent thickness of the carcass based on its sectional bending stiffness, which originated from above-mentioned equivalent orthotropic shell method. Another similar method proposed by Martins et al. (Martins et al., 2003) used the bending stiffness per unit axial length as the basis to determine the equivalent thickness of the carcass. Both of these two methods require using the minimum moment of inertia of the carcass profile to calculate equivalent properties. Due to the neglect of geometric nonlinearities of the interlocked layers in these two methods, the actual structural bending stiffness of the carcass is always overestimated (de Sousa et al., 2018).

Since most equivalent methods were unable to consider the material elastic-plasticity, Tang et al. (Tang et al., 2016) proposed a method based

on the circumferential strain energy equivalence. This method calculated the equivalent thickness by assuming that both the carcass and the equivalent ring stored the same circumferential strain energy when they were subjected to a given displacement-controlled hoop load. As the numerical simulation was used to obtain the strain energy absorption of the carcass, therefore, the geometric nonlinearities of this interlocked layer could be taken into account. To ensure only the hoop strain was generated in the carcass, a Dirichlet-type boundary condition (Huet, 1990) was applied in the numerical model to restrain the radial and axial deformations of the carcass. However, this boundary condition enhanced the structural stiffness of the carcass, lowering its absorbed strain energy. As a result, the equivalent thickness of the carcass was underestimated, leading to a much conservative prediction of the collapse pressure.

Table 2.1 summarizes the common equivalent layer methods and their characteristics. To gain an insight into their reliability in the equivalent treatment of the carcass, an investigation was carried out by Lloyds Register Energy (Edmans, 2014a,b). In this investigation, mathematical models built based on those equivalent method were used to predict the collapse pressure of a flexible pipe. The results showed that there was a considerable variation in the prediction of collapse pressure for the given pipe, indicating that further development of equivalent methods was needed.

Table 2.1: Summary of existing equivalent ring methods

Equivalent method	Authors	Geometric factors		Material factors		FEM required
		Section geometry	Initial imperfections	Linear elasticity	Elastic-plasticity	
Bending stiffness per unit area	Cruz et al. (1997)	Y	N	Y	N	N
Bending stiffness per unit length	Martins et al. (2003)	Y	N	Y	N	N
Area equivalent	Zhang et al. (2003)	Y	N	N	N	N
Actual interlocked layer thickness (with a fraction fill coefficient)	Chen et al. (2015)	Y	N	N	N	N
Strain energy equivalent	Tang et al. (2016)	Y	Y	Y	Y	Y

With the help of the equivalent layer methods, the collapse of flexible pipes can be simplified as ring buckling problems. Therefore, the analytical models for the collapse analysis of flexible pipes are developed based on the ring buckling theories (Cooke & Kenny, 2014). As the differential equation for the deflection curve of a bending ring can be expressed as (Timoshenko

& Gere, 1961)

$$\frac{\mathrm{d}^2\omega}{\mathrm{d}\theta^2} + \omega = -\frac{MR^2}{EI} \tag{2.1}$$

Then the critical collapse pressure of the ring within the elastic limit is obtained as

$$P_{\mathrm{cr}} = \frac{3EI}{R^3} \tag{2.2}$$

Where θ is the angle along the circumference; ω is the radial deflection; M is the bending moment due to the loading; R is the mean radius of the ring; E and I are the Young's modulus and moment of inertia of the ring, respectively; P_{cr} is the critical collapse pressure.

Considering the flexible pipe is a concentric structure, improvement has been made to the above prediction equation. If no radial gaps are present between the layers, the sum of elastic collapse pressure from the carcass and the pressure armor is regarded as the critical pressure of the whole flexible pipe (Shen & Jukes, 2015)

$$P_{\mathrm{cr}} = \sum_{n=1}^{m} \frac{3(EI)_n}{(1-\upsilon^2)R_n^3} \tag{2.3}$$

Where the subscript 'n' represents the parameters of corresponding metallic layers, m denotes the total number of the related layers, υ denotes the Poisson's ratio. However, such a formula is not applicable for the wet collapse situation. The wet collapse of flexible pipes can be described as the radial buckling of the confined carcass under external pressure (Bai et al., 2016). In terms of this kind of buckling, a closed-form analytical solution of a thin-walled ring confined in a rigid cavity was presented by Glock (Glock, 1977)

$$P_{\mathrm{cr}} = \frac{EI}{1-\upsilon^2}\left(\frac{t}{D}\right)^{2.2} \tag{2.4}$$

Where t is thickness of the cylinder and D is the mean diameter. Glock's formula was then extended to consider a tightly (small gap) or loosely fitted (large gap) concentric rings (Boot, 1998; Thépot, 2001). Although those formulae could account for the gap effect, they overestimate the wet collapse pressure since the pressure armor supports the carcass more like an elastic medium rather than a rigid cavity. In this regard, an elastic ring model with

horizontal spring supports was proposed by Bai et al. (Bai et al., 2016). This model treats the pressure armor as springs which support the inner carcass at the horizontal direction, as depicted in Figure 2.7.

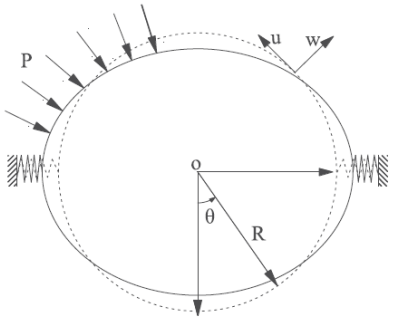

Figure 2.7: Buckling of the cylinder with spring supports (Bai et al., 2016)

With this model, the formula for predicting the collapse pressure of the carcass takes the form

$$P_{\mathrm{cr}} = \frac{3E_{\mathrm{i}}I_{\mathrm{i}}}{R_{\mathrm{i}}^3} + \frac{2}{3}\frac{8E_{\mathrm{o}}I_{\mathrm{o}}}{(\pi^2-7)R_{\mathrm{o}}^3} \tag{2.5}$$

Where the subscripts 'i' and 'o' represent the inner and outer ring, separately. This model gives an elastic solution of the critical pressure for the risers subjected to wet collapse, without considering the effects of initial imperfections. For the flexible risers used in deep water condition, however, collapse usually occurs with the material plasticity of the inner carcass layers (Chen et al., 2015), especially under the influences of initial imperfections. To address this issue, Clinedinst (Clinedinst, 1939) suggested that replacing Young's modulus with a "reduced modulus" to consider the effect of material plasticity on the collapse pressure. This reduced modulus could be calculated based on the stress-strain curve of the pipe material, which takes form as

$$E_{\mathrm{R}} = \frac{4E\frac{\mathrm{d}\sigma}{\mathrm{d}\varepsilon}}{(\sqrt{E}+\sqrt{\frac{\mathrm{d}\sigma}{\mathrm{d}\varepsilon}})^2} \tag{2.6}$$

Where the subscript 'R' represents reduced material properties, $\mathrm{d}\sigma/\mathrm{d}\varepsilon$ is the slope of the stress-strain curve of the material at the stress σ and strain ε caused by the critical load.

Timoshenko and Gere (Timoshenko & Gere, 1961) gave another solution to the plastic collapse, who assumed that the pipe collapses when its material plasticity begins. Based on this assumption, the formula for calculating the plastic collapse pressure is given as

$$P_Y^2 - [\frac{\sigma_Y t}{R} + (1+6\frac{\omega_0}{t})P_{cr}]P_Y + \frac{\sigma_Y t}{R}P_{cr} = 0 \tag{2.7}$$

Where P_Y is the plastic collapse pressure of the pipe; σ_Y is the material yield stress; ω_0 is the maximum initial radial deviation from a circle; P_{cr} is the elastic critical pressure that calculated through Eq.(2.2). Although Eq.(2.7) gives a solution for the plastic collapse, it might underestimate the actual collapse pressure. For the flexible riser used in ultra-deep water production, collapse does not occur until the elastic-plastic boundary has penetrated some way through the carcass wall thickness, as shown in Figure 2.8 (Adams et al., 1998; Abbassian & Parfitt, 1998).

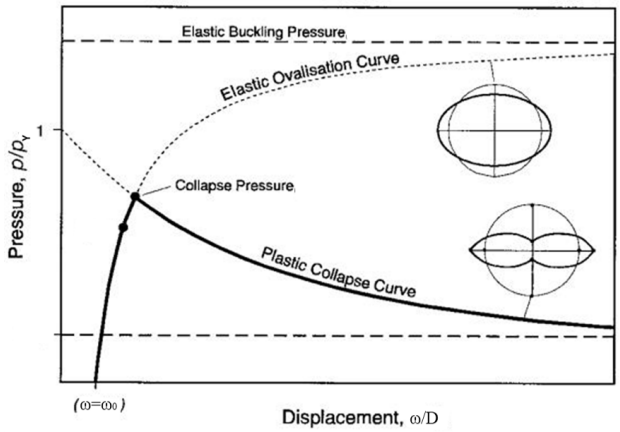

Figure 2.8: Elastic ovalization and plastic collapse curves defining collapse pressure (Abbassian & Parfitt, 1998)

2.1.3 Numerical simulations

Numerical simulation stands as a powerful tool in the collapse analysis of flexible risers. Compared to analytical approaches, numerical simulations allow better insight into the structural integrity and layer interactions during the riser collapses. Nowadays, the finite element analysis (FEA) has been

developed as a common approach to predict the critical collapse pressure of flexible pipes.

Flexible riser is a multi-layered pipe, however, there is no necessity to simulate all the layers of this structure in collapse models. Generally, collapse models are constructed with the carcass, the liner and the pressure armor since those layers are the main components for collapse resistance (Gay Neto et al., 2016). Finite element models of flexible risers could be divided into two types: 3D full FE models and simplified FE models. The 3D full FE models refer to modeling the interlocked layers with their actual rolled shapes, as shown in Figure 2.9 (NOV, 2015; Gay Neto & Martins, 2012). Such kind of FE models preserve the layer geometric details, which can be used to investigate the issues related to stress concentrations (Gay Neto et al., 2016).

Figure 2.9: Details of the carcass profile (NOV, 2015) and the 3D full FE model (Gay Neto & Martins, 2012)

Although 3D full FE models preserve the details of layer profiles, they are quite cumbersome and time consuming in collapse analysis. To reduce the computational cost, simplified FE model are developed as an alternative strategy (Santos & Pesce, 2019). By using the equivalent layer methods, the flexible risers can be simplified as 2D FE ring models. Mostly, those 2D models are adopted to investigate the effects of initial geometric imperfections or pressure armor on the collapse resistance of the carcass (Malta et al., 2012; Bai et al., 2016; Cuamatzi-Melendez et al., 2017). 2D FE models are easy to be built though, they are unable to deal with the pipe curvature directly. In this regard, 3D simplified FE models are developed.

There are two ways to construct 3D simplified FE models. One common simplification is to replace the self-interlocking layers with equivalent tubes. Such kind of simplification can be found in the work of Lu et al. (Lu et al., 2008), which simplified the metallic layers to helical spring-like tubes that made of strips with equivalent rectangular cross section, as shown in Figure 2.10. Another simplification is to reduce the model length using a representative volume element (RVE) model with periodic conditions. This method was adopted in the work of Gay Neto et al. (Gay Neto et al., 2016, 2017a), which presented a two-pitch model that showed in Figure 2.11 to simulate the "infinitely long" flexible pipe. With the aid of displacement couplings and kinematic constrains at the cutting regions (connected to the rest of the flexible pipe), the curved pipe could be represented by this two-pitch model. Those simplified FE models require less computational cost, but their quality highly depends on the adopted equivalent layer methods and the periodic conditions.

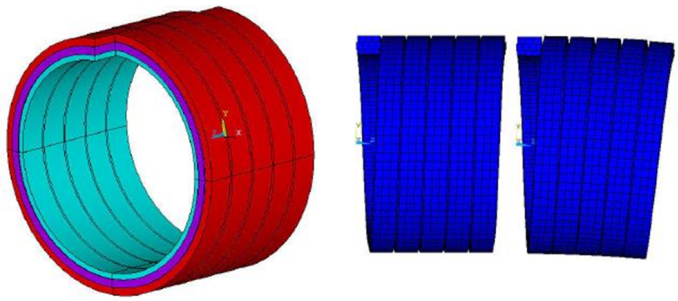

Figure 2.10: 3D Simplified FE model: an equivalent helical spring-like tube (Lu et al., 2008)

As mentioned above, most FE models remove the layers above the pressure armor (except the external sheath). However, there might be a need to investigate the "bending moment effect" that brings by those layers. This effect comes primarily from the tensile armors and plastic layers, as illustrated in Figure 2.12 (Sævik & Ye, 2016). The bending stresses in those layers gives an harmonic squeeze load intensity with the combination of the global curvature, which will increase the ovality of the inner layers. This effect may cause an impact on the critical pressure of the flexible pipes, and further investigations might be needed.

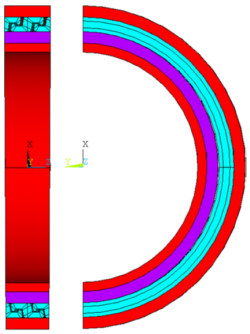

Figure 2.11: 3D Simplified FE model: representative volume element (RVE) model (Gay Neto et al., 2016, 2017a)

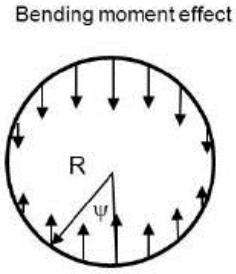

Figure 2.12: Bending moment effect (Sævik & Ye, 2016)

2.2 Technical challenges

To ensure the structural safety of flexible risers in ocean environment, a lower bound collapse concept is adopted in anti-collapse design by considering the possible worst geometric configuration and material properties (Zhang et al., 2003). Based on this concept, factors like initial imperfections should be involved in the collapse analysis as they affect the collapse capacity of flexible risers (Clevelario et al., 2010; Zhang et al., 2003). Related studies have been carried out by scientists for years, which aim to quantify those factors and introduce them into the prediction models.

2.2.1 Geometric imperfections

In practice the pipe product is manufactured to specified tolerance, as a result it always deviate to some degree from an ideally perfect geometric shape (Kyriakides & Corona, 2007). This poses geometric imperfections to

pipe structures and might bring safety hazards to their ultra-deep production. Plenty of studies have been conducted to investigate the effect of various geometric imperfections on collapse capacity of flexible risers. Those works indicate that the collapse capacity is strongly influenced by the initial ovalization and the inter-layer gap as they are the imperfections affect the riser cross section. Once the material of the metallic layer is yielded, radial instability occurs with the increase of external pressure due to those small nonuniformities (Simonen & Shippell, 1982). As stated by Kyriakides (Kyriakides & Corona, 2007), "when the structure stays elastic it is not imperfection sensitive. By contrast, when in-elasticity sets in it becomes imperfection sensitive".

Since the initial ovalization of carcass weakens the collapse capacity of flexible risers, American Petroleum Institute (API) requires the operators to include this imperfection in their collapse analyses. In API 17J, this initial ovalization of the carcass is defined as (API17J Fourth Edition, 2014)

$$\Delta_0 = \frac{D_{\max} - D_{\min}}{D_{\max} + D_{\min}} \tag{2.8}$$

Where $D_{\max}$ and $D_{\min}$ are maximum and minimum pipe diameter, respectively. According to the requirement of API 17J, a minimum ovality of 0.2% should be used if no other data exists (API17J Fourth Edition, 2014).

Numerical techniques were employed by researchers to gain an insight into the ovalization effect on riser collapse. Gay Neto and Martins (Gay Neto & Martins, 2012) modeled the carcass with a set of initial ovalization and then computed its critical pressure numerically. The finite element models exhibited a clear reduction of critical pressure with the increase of initial ovalization level. Considering that API 17B (API17B Fifth Edition, 2014) allowed the collapse analyses to take the pressure armor into account, Malta et al. (Malta et al., 2012) studied the effects of ovalization on the collapse modes of carcass with 2D FE models. In their work, the carcass layer was confined within the pressure armor onto which two types of initial ovalization condition (singly or doubly) was imposed, respectively. According to the analysis results, they found the initial ovalization types did have an impact on the post-buckling behavior (eight/ heart shape collapse mode (Paumier et al., 2009), see Figure 2.13) of carcass. The doubly initial ovalization always caused an eight collapse mode while the singly ovalization interfered the final modes together with the pressure armor thickness. Although the relationship between critical pressure and collapse modes is still under in-

vestigation, some studies (El-Sawy & Sweedan, 2010; Bakeer et al., 1999; Boot, 1998) indicated that the heart shape buckling pattern might yield a lower critical pressure.

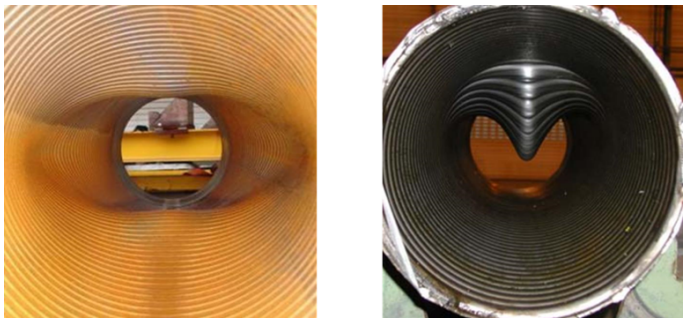

Figure 2.13: Eight shape (left) and heart shape (right) collapse modes (Paumier et al., 2009)

As mentioned above, inter-layer gap is an another major imperfection that affects the collapse resistance of flexible risers. The radial gap between the inner sheath and the pressure armor reduces the supporting effect of the latter after the riser annulus is flooded (Simonen & Shippell, 1982; Lambert et al., 2012; Bai et al., 2017). This imperfection can be caused by the volume change or the extrusion of the liner (Axelsson & Skjerve, 2014; Fernando, 2016), as shown in Figure 2.14 (Davidson et al., 2016). Although tensile armors can reduce the inter-layer gaps by squeezing the pressure armor, it is hard to close them completely if the riser is under a low longitudinal tension.

Figure 2.14: Extrusion of the liner into the adjacent interlocked carcass (Davidson et al., 2016)

At present, numerical simulation is the main approach to address this gap effect issue. Axelsson and Skjerve (Axelsson & Skjerve, 2014) investigated the sensitivity of wet collapse pressure to radial gaps between riser layers. In their 3D FE models, the inter-layer gap was simulated as an airbag layer

which has no interference on the behaviors of the surrounding layers. With the increase of thickness of this airbag layer, a significant drop of wet collapse pressure occurred. A similar phenomenon was observed by Gay Neto and Martins (Gay Neto & Martins, 2014). In their work, the loading pressure peaked twice during the radial deflection of the carcass. A lower peak was reached prior to the gap closure, followed by the second one induced by wet collapse. This phenomenon indicated that a premature radial stiffness reduction of the riser could be caused by the nonzero inter-layer gap.

2.2.2 Manufacturing-related factors

Due to the cold work during the carcass manufacturing process, strain hardening occurs and leads to a high degree of stress-induced material an-isotropy (Pesce et al., 2010). This cold work makes the material properties varied throughout the formed profile of the carcass strip, as shown in Figure 2.15, complicating the collapse behaviors of carcass layer along with the geometric anisotropy.

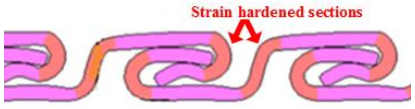

Figure 2.15: Material imperfection induced by cold work along the carcass profile (Axelsson & Skjerve, 2014)

Adopting the average stress-strain curve based on the carcass cross section is one available way to incorporate this material imperfection. This approach was first employed by Zhang et al. (Zhang et al., 2003), who provided the equivalent layer a typical stress-strain curve according to the cold work level of the original carcass. However, the authors admitted that the level of cold work was difficult to measure directly and depended on "a number of factors related to the design and manufacturing process". To address this problem, Nogueria and Netto (Nogueria & Netto, 2010) proposed a methodology to estimate the average stress-strain curve of the carcass. They first applied loads to the crown point of a half sectional carcass wire specimen and recorded its load-displacement curve. A corresponding FE model of the specimen was then constructed, attempting to reproduce experimental load-displacement curve by repeatedly adjusting the material parameters.

This onerous method was improved by Lacerda et al. (Lacerda, 2014; Lacerda et al., 2015), who simplified the nonlinear average stress-strain curve as a bi-linear curve. This bi-linear curve was decided by three material parameters, Young's modulus, yield stress and tangent modulus. The Young's modulus was determined by the linear portion of the load-displacement curve of the test specimen, and the yield stress and the tangent modulus were calibrated by the rest elastic-plastic portion. If a simple bi-linear curve was not able to reproduce the experimental results accurately, a tri-linear curve could be employed.

Using average stress-strain curves is a compromise to the limitation of current techniques on measuring the cold work level, which means discarding the geometric details of the carcass profile. To avoid an incorrect predictions of stress concentrations, Axelsson (Axelsson & Skjerve, 2014) constructed a FE model with the actual carcass profile and applied different stress-strain curves to the corresponding cold formed sections. In their work, a hardness measurement technique was used to define those curves based on the material hardness of the curved sections. Since the relationship between the steel hardness H_v and yield stress σ_y can be expressed as below (Boyer & Gall, 1985; Callister, 1992; Pavlina & Van Tyne, 2008; Zhang et al., 2011), the yield stress was therefore determined.

$$H_v \approx 3\sigma_Y \tag{2.9}$$

Residual stress (RS) is another manufacturing-related factor that may cause earlier onset of plasticity and trigger the early collapse of the flexible riser (Grognec et al., 2019). It is generated from two stages during the pipe manufacture, see in Figure 2.16 (Nielsen, 2014): one is the roll bending stage where the metallic wire experiences a sequence of bending and twisting events; another is the interlocking stage, where the profiled wire is wound onto a bobbin (Alavandimath, 2009). Due to the practical difficulties, there is no available post-deformation stress relief operation that could be conducted to the flexible riser product (Fernando et al., 2004). Those product, therefore, contain unknown magnitude of RS in the cross-section of their armor wires.

Since the stress in the wires during service is a combination of the RS and the stress triggered by external loading (Barnes, 2014; Fernando et al., 2017), estimating the RS accurately is of great importance. To estimate the RS in the interlocked layers of flexible pipes, numerical approaches are adopted by some researchers to make the first attempt. Tang et al. (Tang et al., 2015) simulated the cold-forming process of the carcass wire with FE software

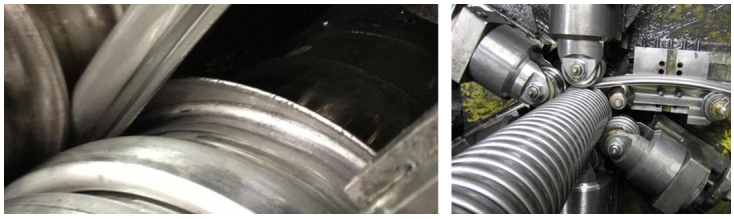

Figure 2.16: Manufacture process of carcass layer (Nielsen, 2014)

MARC and obtained the distribution of residual stress along the carcass profile. Those RS were then input into an identical model in ANSYS for the collapse analyses. Although the numerical results showed the RS caused a significant decrease (nearly 8%) on collapse pressure, the lack of test data made it less persuasive.

To facilitate the stress analyses of flexible risers, an establishment of preliminary studies for the measurement techniques of RS is required. Conventional destructive methods such as hole-drilling (Steinzig & Ponslet, 2003) are no longer applicable as they are unable to measure the stress distribution along the interlocked layer profile. By contrast, non-destructive approaches are gaining popularity among researchers for their advantages of determining the in-situ stress state on the manufactured risers.

Fernando et al. (Fernando et al., 2004) first used the x-ray diffraction method to measure the distribution of RS in pressure armor. By measuring the changes in the spacing of the lattice planes between pre- and post-manufactured pressure armor wires (Anderoglu, 2004), the magnitude of the RS was evaluated. However, this method could only measure the stress state near the armor surface, which failed to give a correct evaluation on the magnitudes of stresses along the wires' cross-section. In this regard, another measurement technique, the Neutron Diffraction method, was adopted in their later research (Fernando et al., 2015) for its large penetration depth (Allen et al., 1981).

This technique, as shown in Figure 2.17, was similar to x-ray diffraction but due to its different scattering properties (neutrons interact primarily with the nuclei of atoms), additional information could be obtained (Pynn, 2009). With the aid of the neutron diffraction method, three orthogonal strains (hoop, axial and radial based on riser coordinate) at gauge points in the wire's cross section were measured, and thus the residual stress distribution on the whole wire section was depicted. Despite the limited gauge points was unable to cover all localized hot spots on the wire cross section,

this technique performed a potential way to measure the residual stress in the interlocked layers of riser product.

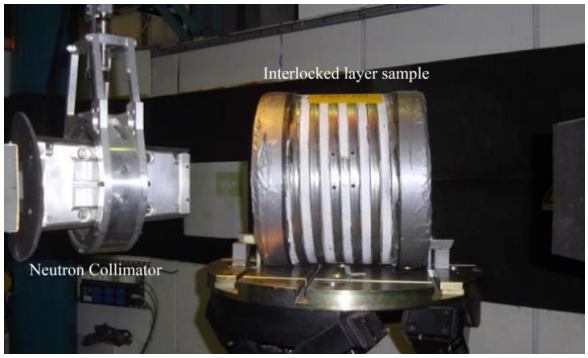

Figure 2.17: Neutron diffraction technique (Fernando et al., 2015)

2.2.3 Curvature effect

During deep-water installation and operation, the flexible risers experience bending within the touchdown zone and buoyed areas. This bending condition could affect the structural stability of flexible risers for service in such extreme water depth, leading to curved collapse with the combination of external hydraulic pressure. Since many factors related to collapse capacity can be affected by the pipe curvature, such as the changes in void fraction of carcass layers and gap between layers (Clevelario et al., 2010), which pose difficulties to the prediction of curved collapse pressure .

To investigate the curvature effect in curved collapse of flexible pipes, a 3D full FE model was constructed by Gay Neto et al. (Gay Neto et al., 2012). Case studies were performed on that 3D model to investigate the curvature effect on wet and dry collapse of flexible pipes, respectively. According to the numerical results, the influence of pipe curvature on the collapse strength is negligible if the outer sheaths of flexible risers remain intact (Gay Neto et al., 2012, 2016). Once the outer sheaths are breached, however, the collapse strength of the curved flexible risers can be largely reduced. The curved collapse tests done by companies such as Technip (Paumier et al., 2009) and Wellstream (Lu et al., 2008; Clevelario et al., 2010) also showed that the wet collapse pressure could be reduced up to 20% when the pipe samples were bent to their minimum bending radius (MBR), indicating that wet collapse pressure of flexible risers is susceptible to the pipe curvature.

Although this curvature effect has been evidenced, the estimation of collapse pressure for a curved flexible risers remains challenges. FE models in curved collapse analyses are required to be constructed adequately long in order to introduce the pipe curvature and eliminate the end effects (Gay Neto et al., 2012; Axelsson & Skjerve, 2014). As a result, those 3D FE models are always cumbersome and time-consuming. Comparing to finite element methods, analytical approaches are much more efficient. However, there is a lack of analytical models for predicting the wet collapse pressure of curved flexible risers in public literature. The main difficulty of developing such an analytical model is to determine the dominant factors for triggering the reduction of curved collapse resistance.

Two possible factors were pointed out by researchers to explain the curvature effect. One is the curvature-induced pitch elongation of the carcass, which reduces the radial stiffness of its extrados, i.e. the section of the pipe which is undergoing tension during the bending process (the opposite section is called intrados) (Gay Neto et al., 2012). Another is the squeeze effect from the flattened region of the curved inner liner (von Kármán fattening effect (von Kármán, 1911)), which imposes an additional ovalization onto the cross section of the carcass (Loureiro & Pasqualino, 2012). Due to the structural complexity of flexible risers, the way in which the pipe curvature affects the wet collapse strength is still not fully understood (Clevelario et al., 2010; Loureiro & Pasqualino, 2012; Edmans, 2014a).

2.3 Summary

In this chapter, literature towards the collapse studies of flexible pipes has been reviewed. To date, most collapse analyses of flexible pipes were conducted numerically. This is less feasible for the design stage of flexible risers. Although analytical approaches are usually a first natural choice for predicting the collapse pressure of flexible risers, few of them are available in public literature to address this collapse issue. The difficulties for developing such analytical approaches mainly come from three aspects: (1) the lack of an effective equivalent layer method; (2) how to deal with geometric imperfections like pipe ovality and inter-layer gap; (3) how to address the global curvature effect with a two-dimensional ring model. In the following chapters, focuses will be put on solving these three aspects.

Chapter 3

Equivalent layer method

How to address the interlocked metallic layers of flexible risers is always a challenge lies in the the collapse analysis. To overcome it, the treatment of the interlocked layer as an equivalent layer is widely adopted. Mostly, the equivalent properties are determined based on their bending stiffness. As discussed in previous chapter, however, the geometry nonlinearities of the interlocked layers make the estimation of their actual bending stiffness difficult.

Considering the actual bending stiffness can be reflected by the relationship between applied load and absorbed strain energy, therefore, the strain energy equivalence is used as an alternative. This chapter presents a strain energy-based equivalent layer method, which obtains the equivalent properties of the carcass based on its strain energy and membrane stiffness. With this proposed equivalent method, the 3rd research question is answered.

The structure of this chapter is as follows: following the introduction, the Section 3.1 presents the establishment of the strain energy-based equivalent method. Section 3.2 provides a feasible FE simulation for offering the strain energy of the carcass to the proposed equivalent method, which were verified by the test data given in the work of (Tang et al., 2016). In Section 3.3, the equivalent model is constructed based on the proposed method and examined by related case study. The final Section 3.4 concludes the work.

This chapter is published as a journal article: Li, X., Jiang, X., Hopman, H. (2018). A strain energy-based equivalent layer method for the prediction of critical collapse pressure of flexible riser, *Ocean Eng*, 164, 248–258.

3.1 Equivalent layer method based on strain energy equivalence

The aim of equivalent layer method is to construct a tubular layer which could perform similar collapse behaviors of the carcass. Many researchers impose equity between them on the bending stiffness since the wet collapse resistance of the riser is dominated by this factor. Based on the initial geometric profile of the carcass, the bending stiffness can be calculated as (Fergestad & Ltveit, 2017)

$$E_c I_{eq} = \zeta n_t \frac{E_c I_{Gmin,c}}{L_c} \tag{3.1}$$

Where n_t is the number of tendons in the carcass layer, L is the pitch and I_{Gmin} is the smallest inertia moment, ζ is a factor that depends on the laying angle of the carcass tendons and the moment of inertia in the section, items with subscript 'eq' represents the parameters related to the equivalent layer while the items with subscript 'c' refer to the properties of the carcass.

Although Eq.(3.1) provides the bending stiffness of the carcass based on its initial geometric profile, it is much larger than the actual bending stiffness due to the neglect of geometric nonlinearities (de Sousa et al., 2018). In order to solve this problem, the absorbed strain energy is chosen to reflect the actual structural stiffness by subjecting the carcass to radial compression loads. This loading case is referred to the experimental set-up of carcass radial compression tests presented in the work of (Tang et al., 2016), which is shown in Figure 3.1.

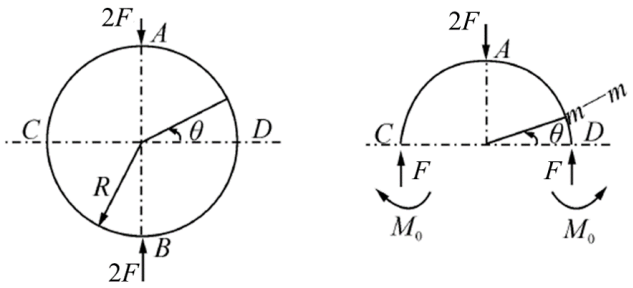

Figure 3.1: Schematic diagram of a ring compressed in the radial direction (Tang et al., 2016)

As the carcass is a complex interlocked structure, there is no formulae can be used directly to calculate its strain energy under a given compression load. Therefore, numerical approaches are used as an alternative to extract the strain energy of the carcass in such a loading case, which will be elaborated in the following section. For an equivalent ring model under the radial compression, the loading force F (at the cross section A) on its one quarter model can be resolved into component forces F_{r} and F_{θ} on any cross section, as shown in Figure 3.2. Therefore, its strain energy is made up of three parts

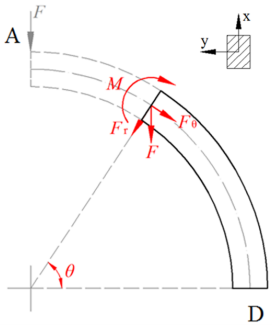

Figure 3.2: Schematic diagram of a ring compressed in the radial direction

$$\begin{aligned}
&\text{a) Due to hoop force } F_{\theta} && U_1 = \int \frac{F_{\theta}^2 R(1-\upsilon^2)}{2AE}\mathrm{d}\theta \\
&\text{b) Due to radial force } F_r && U_2 = \int \frac{CF_r^2 R}{2AG}\mathrm{d}\theta \\
&\text{c) Due to bending moment } M && U_3 = \int \frac{M^2 R(1-\upsilon^2)}{2EI}\mathrm{d}\theta
\end{aligned} \tag{3.2}$$

And the total strain energy of the one quarter ring model is given as

$$U_{\mathrm{eq}} = \int_0^{\frac{\pi}{4}} [\frac{F_{\theta}^2 R_{\mathrm{c}}(1-\upsilon_{\mathrm{c}}^2)}{2EA_{\mathrm{eq}}} + \frac{CF_r^2 R_{\mathrm{c}}}{2G_{\mathrm{c}}A_{\mathrm{eq}}} + \frac{M^2 R_{\mathrm{c}}(1-\upsilon_{\mathrm{c}}^2)}{2EI_{\mathrm{eq}}}]\mathrm{d}\theta \tag{3.3}$$

Where U_{eq} is the strain energy absorbed by the one-quarter equivalent ring under the radial compression load F, υ is Poisson's ratio, G is material shear modulus, A is the cross-sectional area of the ring, R is the mean radius of the ring, θ is the angular quantity. The parameter C in Eq.(3.3) is the correction factor for a rectangular cross-section in shear that takes form (Langhaar, 1962)

$$C = \frac{A}{I^2}\int_A \frac{S^2}{b^2}\mathrm{d}A \tag{3.4}$$

Where S is the first moment of area of the infinitesimal area element about neutral axis, b is the width of the cross section. The component forces and bending moment can be expressed as

$$\begin{cases} F_\theta = F\cos\theta \\ F_r = F\sin\theta \\ M = M_0 + FR(1-\cos\theta) \end{cases} \tag{3.5}$$

Where

$$M_0 = FR(\frac{2}{\pi} - 1) \tag{3.6}$$

Which is the bending moment on cross section D in Figure 3.2 and can be obtained by Castigliano's theorem (Timoshenko, 1930). Substituting Eqs.(3.5) into Eq.(3.3), then the strain energy of that one quarter ring can be calculated as

$$U_{\mathrm{eq}} = \frac{F^2 R_{\mathrm{c}}(1-\upsilon_{\mathrm{c}}{}^2)}{8}[\frac{\pi}{EA_{\mathrm{eq}}} + \frac{C\pi}{G_{\mathrm{c}}A_{\mathrm{eq}}} + \frac{R_{\mathrm{c}}^2(\pi^2-8)}{EI_{\mathrm{eq}}\pi}] \tag{3.7}$$

For the carcass collapses within the pressure armor, its collapse pressure is influenced by both bending stiffness and membrane stiffness (Tong, 2005). In order to capture the collapse behavior of the carcass, two kinds of equivalence should be constructed between those two structures, which are given as

$$\begin{cases} (EI)_{\mathrm{c}} = (EI)_{\mathrm{eq}} \\ (EA)_{\mathrm{c}} = (EA)_{\mathrm{eq}} \end{cases} \tag{3.8}$$

Since the bending stiffness equivalence is replaced by strain energy equivalence, then the equation set Eqs.(3.8) can be expressed as

$$\begin{cases} U_{\mathrm{c}} = U_{\mathrm{eq}} = \dfrac{F^2 R_{\mathrm{c}}(1-\upsilon_{\mathrm{c}}{}^2)}{8}[\dfrac{\pi}{E_{\mathrm{c}}A_{\mathrm{eq}}} + \dfrac{C\pi}{G_{\mathrm{c}}A_{\mathrm{eq}}} + \dfrac{12R_{\mathrm{c}}^2(\pi^2-8)}{E_{\mathrm{c}}t_{\mathrm{eq}}^3 L_{\mathrm{c}}\pi}] \\ E_{\mathrm{c}}A_{\mathrm{c}} = E_{\mathrm{c}}t_{\mathrm{eq}}L_{\mathrm{c}} \end{cases} \tag{3.9}$$

However, solving the above equation set is a hard task since it is not possible to find an equivalent thickness to satisfy both of the two equations in Eqs.(3.9). In view of that, the material Young's Modulus of the

equivalent ring is chosen as an additional unknown parameter. Similar concepts are could be found in the work of Cruz and Dias as well as Clinedinst (Clinedinst, 1939; Cruz & Dias, 1997). Therefore, two unknown parameters, the equivalent thickness t_{eq} and equivalent Young's Modulus E_{eq} of the equivalent ring, can be determined through the equation set Eqs.(3.10) as below

$$\begin{cases} U_{\mathrm{c}} = U_{\mathrm{eq}} = \dfrac{F^2 R_{\mathrm{c}}(1-{\upsilon_{\mathrm{c}}}^2)}{8}[\dfrac{\pi}{E_{\mathrm{eq}}A_{\mathrm{eq}}} + \dfrac{C\pi}{G_{\mathrm{c}}A_{\mathrm{eq}}} + \dfrac{12R_{\mathrm{c}}^2(\pi^2-8)}{E_{\mathrm{eq}}t_{\mathrm{eq}}^3 L_{\mathrm{c}}\pi}] \\ E_{\mathrm{c}}\dfrac{A_{\mathrm{c}}}{L_{\mathrm{c}}} = E_{\mathrm{eq}}t_{\mathrm{eq}} \end{cases} \tag{3.10}$$

Noting that the material constitutive relationship is changed when the equivalent Young's Modulus is adopted to construct the equivalent layer. This may have an impact on the strain energy equivalence between two structures when elastoplastic collapse failure occurs. Since the elastoplastic collapse is a yielding-based problem as given by Eq.(2.7) (Timoshenko & Gere, 1961), the material yield stress $\sigma_{\mathrm{Y,eq}}$ of the equivalent layer should also be regarded as a parameter awaiting solution.

The basic-cell energy-equivalence concept is used to determine value of material yield stress for the equivalent ring (Nemeth, 2011; Danzi et al., 2017). Assuming that the materials for the carcass and equivalent layer are both linear and elastic, obeying Hooke's law, up to the yield stress, then the structural strain energy density can be expressed as

$$u_{\varepsilon} = \frac{1}{2}(\sigma_{\theta}\varepsilon_{\theta} + \sigma_r\varepsilon_r + \sigma_y\varepsilon_y) \tag{3.11}$$

Where σ_{θ}, σ_r, σ_y and ε_{θ}, ε_r, ε_y are the stresses and strains generated in hoop, radial and longitudinal directions separately. Since the strain energy equivalence is used, then it can be reformulated by the structural strain energy density as

$$\int_{V_{\mathrm{c}}} u_{\varepsilon,\mathrm{c}}\mathrm{d}V = \int_{V_{\mathrm{eq}}} u_{\varepsilon,\mathrm{eq}}\mathrm{d}V \tag{3.12}$$

Where the V is the volume of the structure. The yield stress of the equivalent layer can be obtained by equating the strain energy between two structures when both of them reach their material yield stress. However, the strain of each direction on the carcass cross section is not distributed uniformly

due to the interlocked profile. To simplify this equation, two assumptions are made herein:

a) Assume that the strains in radial and longitudinal directions are negligible;

b) Assume the carcass and the equivalent layer have the same distribution of hoop strains along their wall thickness.

With those two assumptions, Eq.(3.12) can be rewritten as

$$\int_{V_c} \frac{1}{2} \frac{\sigma_{\theta,c}^2}{E_c} dV = \int_{V_{eq}} \frac{1}{2} \frac{\sigma_{\theta,eq}^2}{E_{eq}} dV \tag{3.13}$$

If taking the hoop stress of the outermost fiber at point A (see Figure 3.2) as σ_A, then the hoop stress at arbitrary section can be expressed as

$$\sigma_\theta(x,\theta) = \frac{x}{t}\sigma_A f(\theta) \tag{3.14}$$

Where $f(\theta)$ is a function regarding the distribution of hoop stress at the section of angle θ; x is the distance from the point of interest to the neutral axis of the cross section. The corresponding strain energy density therefore takes form as

$$u_\varepsilon(x,\theta) = \frac{\sigma_A^2}{2Et^2} x^2 f(\theta)^2 \tag{3.15}$$

and the strain energy for the one-quarter equivalent ring can be calculated as

$$\int_{V_{eq}} u_{\varepsilon,eq} dV = \int_0^{\pi/2} \int_{-t_{eq}/2}^{t_{eq}/2} u_{\varepsilon,eq}(R_c + x) L_c dx d\theta \tag{3.16}$$

Similarly, the strain energy of the one-quarter carcass is

$$\int_{V_c} u_{\varepsilon,c} dV = \int_0^{\pi/2} \int_{-t_c/2}^{t_c/2} u_{\varepsilon,c}(R_c + x) L_c \eta dx d\theta \tag{3.17}$$

Where η is the fraction fill coefficient of the cross-sectional area of the carcass. By substituting Eqs.(3.16) and (3.17) into Eq.(3.13), it has

$$\frac{\sigma_{A,eq}^2 L_c t_{eq}}{E_{eq}} = \frac{\sigma_{A,c}^2 A_c}{E_c} \tag{3.18}$$

When the hoop stress $\sigma_{A,c}$ at the point A of the carcass reaches the material yield stress $\sigma_{Y,c}$, then the yield stress of the equivalent layer can be calculated as

$$\sigma_{Y,eq} = \sqrt{\frac{E_{eq}\sigma_{Y,c}^2}{E_c}\frac{A_c}{L_c t_{eq}}} \tag{3.19}$$

With the values of equivalent thickness t_{eq} and equivalent Young's modulus E_{eq} obtained from Eqs.(3.10), the yield stress $\sigma_{Y,eq}$ of the equivalent layer can be calculated by Eq.(3.19). Finally, the geometric and material properties for the equivalent layer are both determined.

A brief step-by-step methodology is presented as follow to give a clear clarification of the proposed method:

Step 1, calculating the strain energy U_c of the carcass with a given radial compression load F numerically (A feasible numerical simulation is presented in Section 3.2 to show how to provide a reliable strain energy for the proposed method).

Step 2, determining equivalent layer properties t_{eq} and E_{eq} by substituting the values of U_c and F into Eqs.(3.10).

Step 3, determining the equivalent yield stress $\sigma_{Y,eq}$ with the above t_{eq} and E_{eq} by using Eq.(3.19).

With all the above-mentioned equivalent properties, t_{eq}, E_{eq} and $\sigma_{Y,eq}$, have been solved, an equivalent layer model can be built for collapse studies.

3.2 Numerical simulation for strain energy calculation

As above-mentioned, the strain energy U_c of the carcass was required as an input in Eqs.(3.10) to calculate the equivalent properties for the homogeneous layer, therefore, this section is mainly focused on how to provide such a strain energy with FE simulation. In this section, a feasible FE simulation is presented to show how to calculate the strain energy of the carcass. This FE simulation was referred to the experimental tests conducted by Tang et al. (Tang et al., 2016), as shown in Figure 3.3. In their work, the compression tests were performed on three kinds of carcass samples with inner diameters of 6 in., 7 in. and 8 in. The geometric and material properties of the samples

Table 3.1: Geometric and material properties of the carcass samples (Tang et al., 2016)

Sample ID (in.)	6	7	8	Sample ID (in.)	6	7	8
Pitch length L_c (mm)	14.88	17.00	12.55	L_5 (mm)	1.80	2.61	2.41
Carcass strip thickness $t_{s,c}$ (mm)	0.90	0.96	1.30	L_6 (mm)	0.00	2.02	0.00
L_1 (mm)	26.20	31.42	23.43	L_7 (mm)	1.77	2.67	2.12
L_2 (mm)	10.36	10.40	7.44	R_1 (mm)	4.18	3.75	4.18
L_3 (mm)	8.96	10.91	7.47	E_c (GPa)	206	206	206
L_4 (mm)	5.90	8.01	4.39	υ_c	0.3	0.3	0.3

are summarized in Table 3.1. The test data presented in Tang's work are used to validate the proposed numerical model.

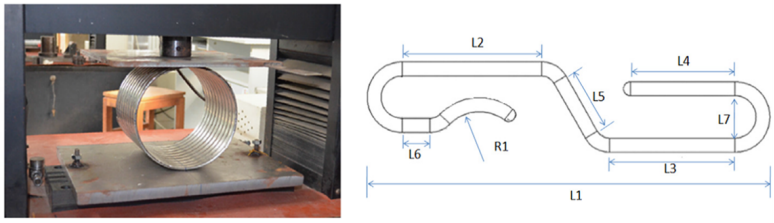

Figure 3.3: Experimental set-up (left) and Schematic diagram of the carcass profile (right) (Tang et al., 2016)

3.2.1 Radial compressed carcass model

A 3D model of the interlocked carcass was constructed using Abaqus 6.13 software. Two pitches of the carcass were considered as a representative length and solid elements were adopted in this 3D model, as shown in Figure 3.4. The lay angle of the carcass strips was neglected since it is not responsible for the important effects in collapse prediction according to the study of Gay Neto and Martins.(Gay Neto & Martins, 2012). Due to the symmetry of the carcass structure, only half of the carcass ring was modeled. A rigid plate was also modeled to support the carcass model.

The boundary conditions considered in the half carcass model were imposed as: (a) symmetry condition on the carcass cross sections, (b) the displacements of the portion of the carcass contacted with the bottom rigid plate are constrained in all directions and (c) the displacements of the side cutting sections are constrained in longitudinal direction. The supported rigid plate was fully fixed. Those applied boundary conditions are shown in Figure 3.5.

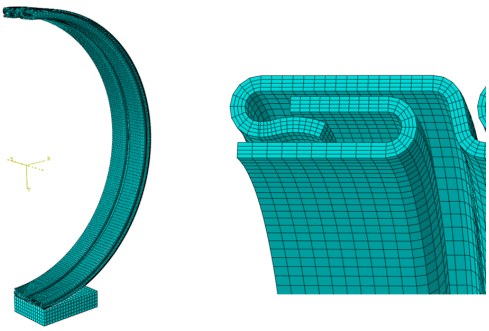

Figure 3.4: Radial compressed carcass model, (a) whole view and (b) detailed view

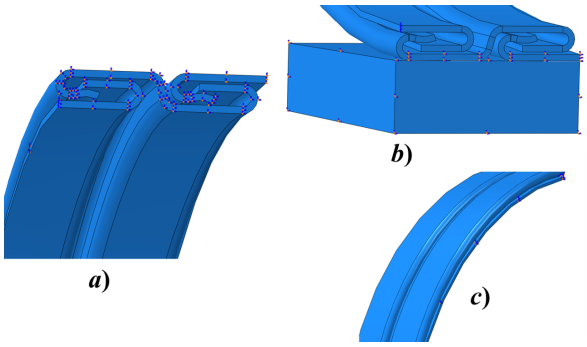

Figure 3.5: Boundary conditions applied onto the model (a) symmetry condition, (b) displacement constraints of the portion contacted with the rigid plate (c) displacement constraints of the side cutting section

Displacement couplings were set on the carcass profile to simulate a carcass layer with infinite pitches. MPC constraints were imposed on the cutting regions since there were only two pitches presented in this model, as shown in Figure 3.6. The loading force was applied on four top points of the carcass evenly, which is shown in Figure 3.7. This loading type was chosen due to two reasons: one was that the contact issue between the top loading plate and carcass could be eliminated; the other was the computational results from the FE models with and without the top loading plate were almost the same. Since the carcass was compressed within the elastic range (according to the test data of (Tang et al., 2016)), the stress concentration at those four points had little impact on the calculation results.

The penalty method was used to deal with the contact issues. A surface-

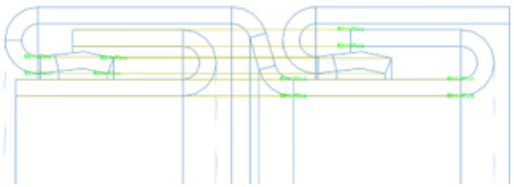

Figure 3.6: Coupling details considered in the compressed carcass model

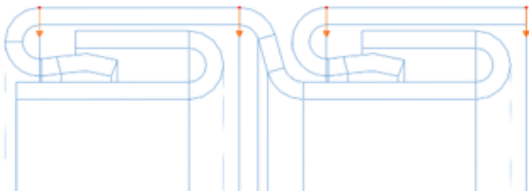

Figure 3.7: Compression force applied to the carcass model

to-surface formulation was used for the contact between the carcass strips and the normal penalty stiffness factor was defined as 0.1. Friction was also considered in the models to account for the related energy dissipation. The friction factor was defined as 0.13 at the self-contact regions. The values of those factors were referred to (Tang et al., 2016).

3.2.2 Model validation

The curves of radial deformation versus compression load of each carcass samples were recorded as Figure 3.8 (Tang et al., 2016). The maximum loading displacement was controlled to make sure that the maximum ovalization of all the samples lower than 3%. It can be seen from Figure 3.8 that the radial compression stiffness of the carcass samples become stable after the compression loads reach certain values. This represents that the space within the carcass layers were diminished with the increased compression loads. Finally, the samples were compressed into compact structures. In order to reflect the structural stiffness of a compact carcass, the compression loads applied to the numerical models were 2 kN and 3 kN for the 6 in. and 7 in. carcass and 4 kN and 6 kN for the 8 in. carcass. The mean value of the displacements at the loading nodes were obtained and compared to the test results.

The comparison results are listed in Table 3.2 and it can be seen that the radial displacements provided by numerical models agree well with the

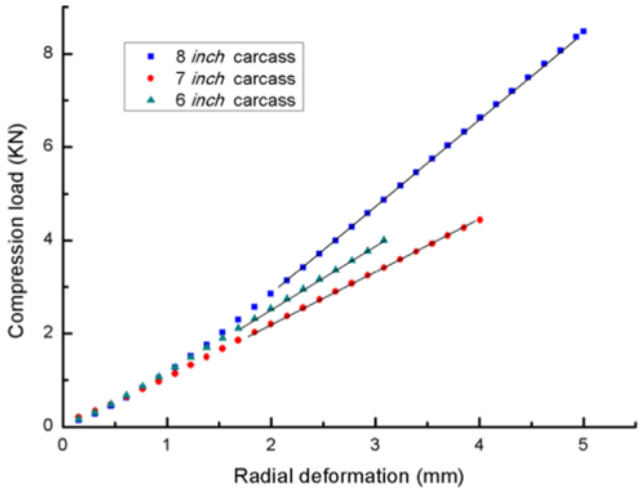

Figure 3.8: Test results of the radial compression of the carcass test pieces (Tang et al., 2016)

test results for each loading case. The maximum error that given by the numerical models is just around 10%, showing that those numerical models can be a reliable approach to extract the strain energy of the carcass.

3.3 Verification of the proposed equivalent method

With the methodology presented in the previous two sections, an equivalent layer model of the carcass can be constructed. In this section, the prediction accuracy of that equivalent layer model was verified by a full 3D carcass model presented in the work of Gay Neto and Martins (Gay Neto &

Table 3.2: Load-displacement results comparison for each case

Sample ID	Compression loads (kN)		2	3	4	6
6”	Radial displacements (mm)	Experimental	1.60	2.35	-	-
		numerical	1.43	2.16	-	-
7”		Experimental	1.90	2.80	-	-
		Numerical	2.07	3.10	-	-
8”		Experimental	-	-	2.60	3.70
		Numerical	-	-	2.66	3.99

865 Martins, 2012). This model has been widely used by many researchers and was recreated to provide a collapse pressure for comparison purpose. In the meanwhile, some other equivalent layer models based on the existing equivalent methods were also built in order to give a comprehensive comparison.

3.3.1 Full 3D model for the comparison purpose

870 To examine the effectiveness of the proposed equivalent method in collapse analysis, an example presented by Gay Neto and Martins (Gay Neto & Martins, 2012) was adopted. In that example, two layers, the carcass and the polymeric inner liner were considered. This inner liner only acted as a load transmitter during the loading process. The carcass profile is sketched in 875 Figure 3.9, and its geometrical and material are given in Table 3.3.

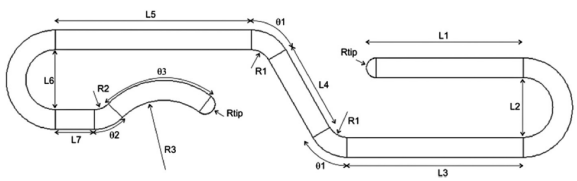

Figure 3.9: Schematic diagram of the carcass profile in Gay Neto's model (Gay Neto & Martins, 2012)

Table 3.3: Geometrical and material properties of Gay Neto's carcass model (Gay Neto & Martins, 2012)

Carcass ID (in.)	4	θ_1 (deg)	60
Pitch length L_c (mm)	16	θ_2 (deg)	45
Carcass strip thickness t (mm)	1.00	θ_3 (deg)	90
L_1 (mm)	8.00	R_1 (mm)	1.00
L_2 (mm)	3.00	R_2 (mm)	1.00
L_3 (mm)	9.00	R_3 (mm)	3.00
L_4 (mm)	4.50	E_c (GPa)	200
L_5 (mm)	10.00	υ_c	0.3
L_6 (mm)	3.00	Yield stress $\sigma_{Y,c}$ (MPa)	600
L_7 (mm)	2.00	Tangent modulus $E_{t,c}$ (after yielding) (MPa)	2000
R_{tip} (mm)	0.50		

A bi-linear constitutive model was adopted to describe the elastoplastic property of the carcass material. The carcass material behaves linearly and

elastically before reaching its yield stress. Once the yield stress is reached, another linear behavior is assumed with a slope given by the material tangent modulus. For the inner liner, a multi-linear elastic material constitutive model was used to describe its material property. The material stress-strain curves for both carcass and inner liner (Gay Neto & Martins, 2012) are plotted in Figure 3.10 and Figure 3.11 separately.

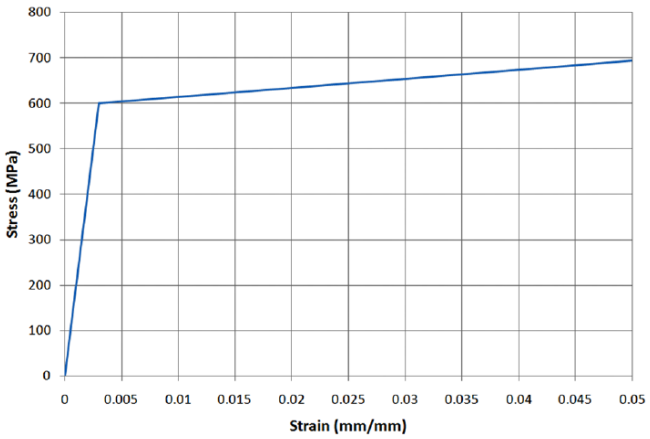

Figure 3.10: Stress-strain curve of the material used in carcass (Gay Neto & Martins, 2012)

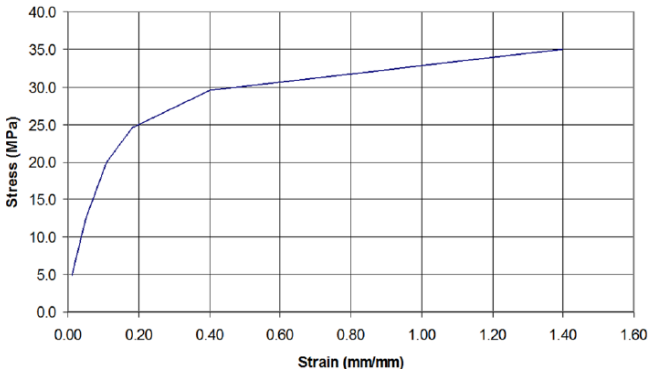

Figure 3.11: Stress-strain curve of the material of the inner liner (Gay Neto & Martins, 2012)

Considering that the collapse of the carcass was an axisymmetric issue, only half of the carcass was modeled in order to speed the computation up. Figure 3.12 shows the whole model and its applied boundary condition. The

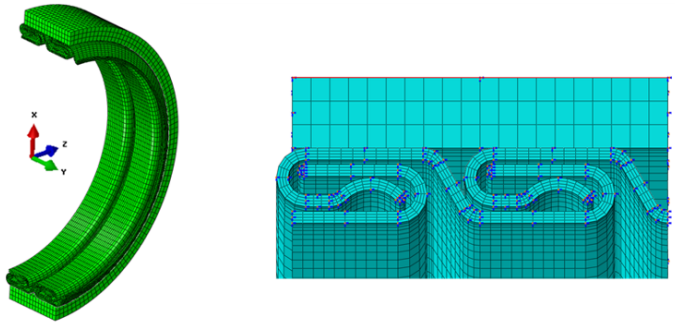

Figure 3.12: a) numerical model for collapse simulation and b) the imposed boundary conditions

boundary conditions were imposed as follows: a) symmetry conditions in plane of XY and b) a fully fixed external edge of the inner liner (the red line displayed in Figure 3.12b. The pressure applied onto the external surface of the inner liner was the only load considered in the models. To capture the collapse pressure of the carcass, the Riks method was used in the numerical models. The collapse pressure given by this 3D full FE model was regarded as a reference value for judging the predictive accuracy of the equivalent layer models.

3.3.2 Equivalent layer models

With the equivalent properties determined by the proposed method, a finite element model of the equivalent layer (Model A) was constructed, which is shown in Figure 3.13. The external pressure was applied onto the inner liner to compress to trigger the collapse. The collapse pressure of the equivalent model was read through its result files and then compared to the one from the 3D full model.

To give a comprehensive comparison, some other ring models based on the existing equivalent methods were constructed. Those methods are proposed based on different structural property equivalences, which are given as follows:

a) Area equivalence (Model B)

This method obtains the thickness of the equivalent layer by equating the cross-sectional areas between the carcass and the equivalent layer, which can

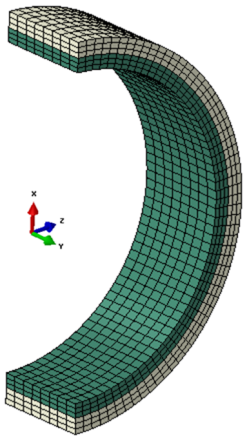

Figure 3.13: Whole view of the equivalent layer model

be expressed as (Zhang et al., 2003)

$$t_{\mathrm{eq},1} = \frac{A_{\mathrm{c}}}{L_{\mathrm{c}}} \tag{3.20}$$

b) Bending stiffness equivalence per area (Model C)

This method calculates the thickness by equating sectional bending stiffness between two structures (de Sousa et al., 2001). The equation takes the form

$$t_{\mathrm{eq},2} = \sqrt{\frac{12 I_{\mathrm{Gmin,c}}}{A_{\mathrm{c}}}} \tag{3.21}$$

c) Bending stiffness equivalence per length (Model D)

This method is similar to the second one but builds the bending stiffness equivalence based on unit length (Martins et al., 2003). Therefore, the equivalent thickness can be calculated as

$$t_{\mathrm{eq},3} = \sqrt[3]{\frac{12(1+\psi) I_{\mathrm{Gmin,c}}}{L_{\mathrm{c}}}} \tag{3.22}$$

where ψ is the rate of superposition of the carcass profiles. The value of the ψ depends on the profile geometry and the pitch considered, which could be calculated by using the superposed length L_{super} between two profiles in a pitch (Gay Neto & Martins, 2012)

$$\psi = \frac{L_{\text{super}}}{L_{\text{c}}} \tag{3.23}$$

d) Circumferential strain energy equivalence (Model E)

This method is proposed by Tang et al.(Tang et al., 2016), who built a strain energy equivalence between two structures that with a specific structural strain condition: uniform hoop strain was the only strain type that allowed to be generated. In the carcass, this strain condition was achieved by applying a displacement load u_θ onto its profile, which is linearly proportional to the radial length

$$u_\theta = \frac{\pi}{2} r_{\text{x}} \varepsilon_\theta \tag{3.24}$$

where r_{x} is the radial length of the carcass. By means of numerical simulation, the strain energy U_{c} of the carcass under that strain condition was obtained. The strain energy of the equivalent layer that with the same uniform hoop strain ε_θ can be calculated as

$$U_{\text{eq}} = \int \frac{1}{2} \sigma_\theta \varepsilon_\theta \mathrm{d}V = \frac{\pi}{4} \Psi \varepsilon_\theta^2 R_{\text{c}} L_{\text{c}} t_{\text{eq}} \tag{3.25}$$

The parameter Ψ within Eq.(3.25) takes the form

$$\Psi = E \frac{1 - \upsilon_{\text{c}}}{(1 + \upsilon_{\text{c}})(1 - 2\upsilon_{\text{c}})} \tag{3.26}$$

and thus the equivalent thickness is given as

$$t_{\text{eq},4} = \frac{U_{\text{c}}}{\frac{\pi}{4} \Psi \varepsilon_\theta^2 R L} \tag{3.27}$$

The geometric and material properties of those the equivalent layer models are presented in Table 3.4. The mean radius and longitudinal length of all the equivalent layer models were identical with the 4 in. carcass full model.

3.3.3 Prediction comparison

The Riks method was employed to capture the snap-through occurrence of each finite element model. It was necessary to choose a representative radial displacement value for each cross section in the numerical models since each point had a different displacement value. A reference line was chosen from

Table 3.4: Geometrical and material properties of the equivalent layer

Model	Thickness (mm)	Young's modulus (GPa)	Yield stress (MPa)
Model A	4.50	158	473
Model B	3.49	200	600
Model C	6.32	200	600
Model D	5.18	200	600
Model E	2.59	200	600

the internal surface of the carcass (full 3D model as well as equivalent models) that identified in Figure 3.14. The mean value of the radial displacement of the nodes on that reference line was regarded as the radial displacements of the models subjected to external pressure.

Figure 3.14: Reference line for measuring the radial displacement of FE models

The collapse pressure and the corresponding radial displacement from each model are summarized in Table 3.5. The curves of radial displacement versus external pressure are plotted in Figure 3.15. According to the black solid line plotted in Figure 3.15, a stiffness reduction of the full carcass model appears when the external pressure reaches 13 MPa approximately. Due to geometric nonlinearities of the carcass profile, the radial stiffness of the carcass reduces with the increase of external pressure, in which the space between the metallic strips is being eliminated gradually. Model C and D built the equivalent layer based on the moment of inertia of the initial carcass profile, therefore, they exhibited close stiffnesses to the full model before the external pressure reaches 13 MPa. As these two equivalent models did not take the geometric nonlinearities-induced stiffness reduction into account, the results came from them deviated considerably from that of the full model. Similarly, Model B also failed to capture the collapse behavior of the full carcass model due to area equivalence it used.

By contrast, the collapse pressure provided by Model A and Model E were relatively conservative. As stated above, the thickness of Model E

Table 3.5: Collapse pressure and radial displacement comparison between full and equivalent models

Model	Collapse pressure (MPa)	Radial displacement (mm)	Error in collapse pressure (%)
Full 3D model	16.40	0.88	-
Model A (the proposed method)	15.99	1.15	-2.50
Model B (area equivalence)	20.37	1.30	24.21
Model C (bending stiffness equivalence per area)	47.87	0.75	191.89
Model D (bending stiffness equivalence per length)	35.46	0.96	116.22
Model E (circumferential strain energy equivalence)	14.39	1.43	-12.26

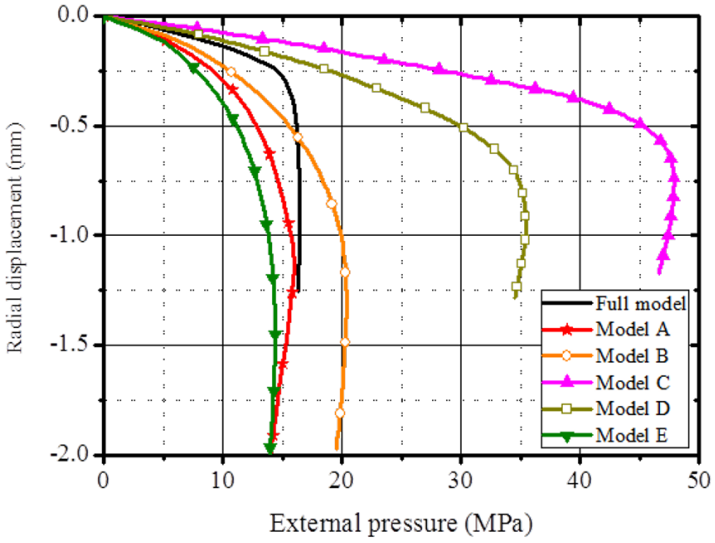

Figure 3.15: Comparison of the curves of external pressure versus radial displacement

was determined based on structural strain energy that generated by uniform
965 hoop deformation of the carcass. In other word, this model was constructed

based on membrane stiffness equivalence only and therefore underestimates the overall structural stiffness of the carcass. As a result, it gave an over-conservative prediction on the collapse pressure of the carcass. Among those equivalent models, Model A provided a much closer prediction to the collapse pressure of the carcass according to Figure 3.15. The predictive error on collapse pressure between the Full model and Model A was just around -2.5%, which showed that model built with both geometric and material equivalences can provide a better prediction of the collapse pressure of the carcass.

3.4 Summary

Predicting the collapse collapse of flexible risers accurately is a difficult task; therefore, efficient calculation methods are always demanded. Dealing the complex carcass structure with an equivalent layer is the first and foremost step in collapse analyses of the flexible risers. Up till now, various equivalent methods are developed for constructing such an equivalent layer. However, most of them are proposed based on the equivalence of one certain property, and the layer thickness has always been the only output. As a result, considerable errors occur in their predictions of the collapse pressure.

Considering that, an equivalent layer method is proposed in this chapter by considering the equivalence on strain energy and membrane stiffness simultaneously. As strain energy is required as an input in this equivalent method, 3D FE models was used to compute its value. Using such a 3D FE carcass model is due to the fact that there is no available mathematical model for the strain energy calculation of interlocked layer structures. Although there is a limitation of the proposed equivalent layer method, it offers an approach to involve the geometric nonlinearities of the carcass into the determination of equivalent properties.

A set of models were built to examine the reliability of the proposed method as well as other existing methods. From the comparison results, the model constructed based on the proposed method gave the closest prediction on the critical collapse pressure of the carcass, only with an error of -2.5%. It indicates that this proposed method is able to capture the actual structural stiffness of the carcass, which can be an effective tool for the collapse studies of flexible risers.

Chapter 4

Geometric imperfections

As the flexible riser is a multi-layered pipe structure, its wet collapse pressure is mainly affected by two geometric imperfections: initial ovalization of the carcass, and inter-layer gap between the carcass/liner and pressure armor. To date, most collapse analyses of flexible pipes on initial imperfections were conducted numerically. This is less feasible for the design stage of flexible risers.

In view of this, an analytical model is presented in this chapter to address the geometric imperfections in wet collapse prediction. This answers the 4th research question. The analytical model is developed based on the stability theories of ring and arched structures, which could take the initial ovalization and inter-layer gap into account. Additionally, this model is able to consider "heart" and "eight" collapse modes based on the imposed initial ovalization type.

The content of this chapter is organized as follows: Section 4.1 presents an analytical approach to assess the collapse strength for the flexible pipes with initial imperfections. In Section 4.2, numerical simulation is employed to check the reliability of the proposed analytical approach with case studies. Section 4.3 gives the summary of the research work presented in this chapter.

This chapter is published as a journal article: Li, X., Jiang, X., Hopman, H. (2020). Predicting the wet collapse pressure for flexible risers with initial ovalization and gap: an analytical solution, *Mar Struct*, 77, 102732.

4.1 Analytical model for initial imperfections

For conventional steel pipes, their plastic collapse pressure could be determined based on the assumption given by Timoshenko and Gere (Timoshenko & Gere, 1961), which has a definition as: pipe collapses when its maximum hoop compressive stress reaches the material yield stress. This assumption is also adopted in our model development for the wet collapse of flexible risers. The wet collapse pressure can be solved by equating the maximum hoop compressive stress of the carcass to its material yield stress.

Such a wet collapse pressure is not easy to be determined for flexible pipes, especially for the ones with geometric imperfections. For a carcass confined by the pressure armor, it would go through two different collapse phases if there is an inter-layer gap in-between. Depending on whether the gap closes or not, the whole collapse process can be divided as: pre-contact and post-contact phases, as depicted in Figure 4.1. During the pre-contact phase, the carcass and inner liner are deformed together as a buckled single layer ring. The pressure armor provides no constraints on the radial deformation of the carcass/liner in this period. Once the contact occurs, the carcass starts to be divided into two portions: attached and detached portions. During this post-contact phase, the wet collapse pressure of the carcass is dominated by the buckling strength of the detached portion.

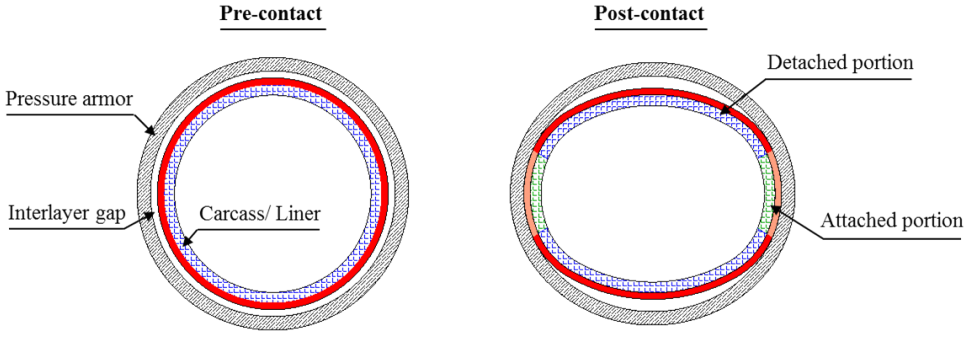

Figure 4.1: Progressive buckling process of an encased carcass

The presented analytical approach adopts different sub-models to describe those two phases, respectively. For the pre-contact phase, formulae of the ring buckling are used to solve the external pressure P_{con} that making

the contact occurs. For the post-contact phase, formulae of the arch buckling are employed to determine the elastoplastic buckling pressure P_{arch} of the detached portion. With those two sub-models, the wet collapse pressure of a flexible riser with initial imperfections is the sum of P_{con} and P_{arch}.

4.1.1 Pre-contact phase

For a flexible pipe with all layers are perfectly circular, the layer gap is the radial gap span between the liner and the pressure armor. If the carcass and the liner were in an ovalized shape initially, then the gap is minimum radial gap span ω_g between the layers, as shown in Figure 4.2. The carcass encased in the pressure armor may experience two different buckling situations, depending on the value of the inter-layer gap. If the gap width is large enough, the inner carcass collapses as a single ring without any support from the pressure armor; otherwise, layer contact occurs, followed by the post-contact phase.

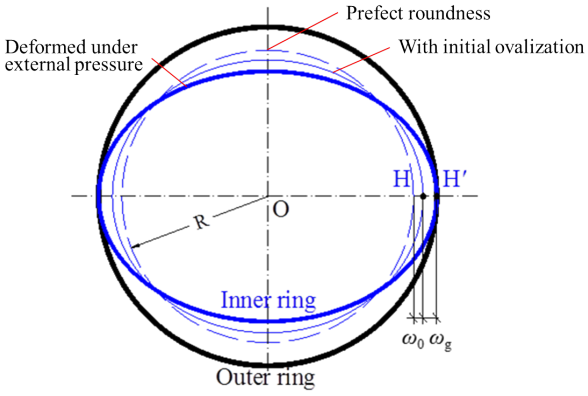

Figure 4.2: Contact moment of a concentric ring structure

Due to the initial ovality from the manufacturing process, the carcass always deviates from a perfect circularity (the dash line in Figure 4.2) with a small deflection ω_0. This initial deflection can be calculated according to the definition of ovalization given in API 17B (API17B Fifth Edition, 2014). For the above-mentioned first situation, the plastic collapse P_Y of such an ovalized carcass can be calculated by Eq.(2.7) (Timoshenko & Gere, 1961). At this plastic collapse pressure, the maximum horizontal displacement ω_{max}

of the point H (see in Figure 4.2) on the carcass is obtained as (Timoshenko & Gere, 1961)

$$\omega_{\max} = \frac{\omega_0 P_{\mathrm{Y}}}{P_{\mathrm{cr}} - P_{\mathrm{Y}}} \tag{4.1}$$

Where P_{cr} is the elastic collapse pressure of the pipe, which can be calculated by Eq.(2.2); $\omega_{\max}$ is the maximum radial deformation of the carcass. If the gap width ω_{g} is smaller than $\omega_{\max}$, then the radial deformation of the inner carcass is restrained after the closure of gaps. In this situation, the external pressure at the contact moment can be determined by the gap width ω_{g}, which is given as

$$P_{\mathrm{con}} = \frac{\omega_{\mathrm{g}} P_{\mathrm{cr}}}{\omega_{\mathrm{g}} + \omega_0} \tag{4.2}$$

Where P_{con} is the external pressure at the moment in which the carcass start to contact the pressure armor. However, it should be noted that the external pressure could cause a reduction on the wall thickness of the inner liner due to its elastic deformation. This reduction requires larger external pressure to close the gap span. Thus, Eq.(4.2) should be improved as

$$\begin{cases} P_{\mathrm{con}} = \dfrac{(\omega_{\mathrm{g}} + t_{\mathrm{l,r}}) P_{\mathrm{cr}}}{\omega_{\mathrm{g}} + \omega_0 + t_{\mathrm{l,r}}} \\ t_{\mathrm{l,r}} = t_{\mathrm{l,r}}(P_{\mathrm{con}}) \end{cases} \tag{4.3}$$

Where $t_{\mathrm{l,r}}$ is the reduction of wall thickness of the liner. Both the P_{con} and $t_{\mathrm{l,r}}$ can be determined by substituting the material constitutive equation of the liner into Eqs.(4.3). Moreover, the maximum hoop compressive stress at the crown point of the carcass under the external pressure P_{con} is

$$\sigma_{\mathrm{con}} = \frac{P_{\mathrm{con}} R_{\mathrm{c}}}{t_{\mathrm{c}}} + \frac{6 P_{\mathrm{con}} R_{\mathrm{c}}}{t_{\mathrm{c}}^2} \frac{\omega_0}{1 - P_{\mathrm{con}}/P_{\mathrm{cr}}} \tag{4.4}$$

After obtaining this maximum compressive stress, the following task is to work out how much additional external pressure is demanded in the post-contact phase for reaching the material yield stress of the carcass.

4.1.2 Post-contact phase

Once the carcass/liner contact the surrounded pressure armor, the attached portion starts to extend in the hoop direction until the critical pressure is

reached (Lo & Zhang, 1994), as shown in Figure 4.3. The initial ovalization and inter-layer gap guide the carcass to deform in either symmetrical or bi-symmetrical shape, leading to the "heart" or "eight" mode.

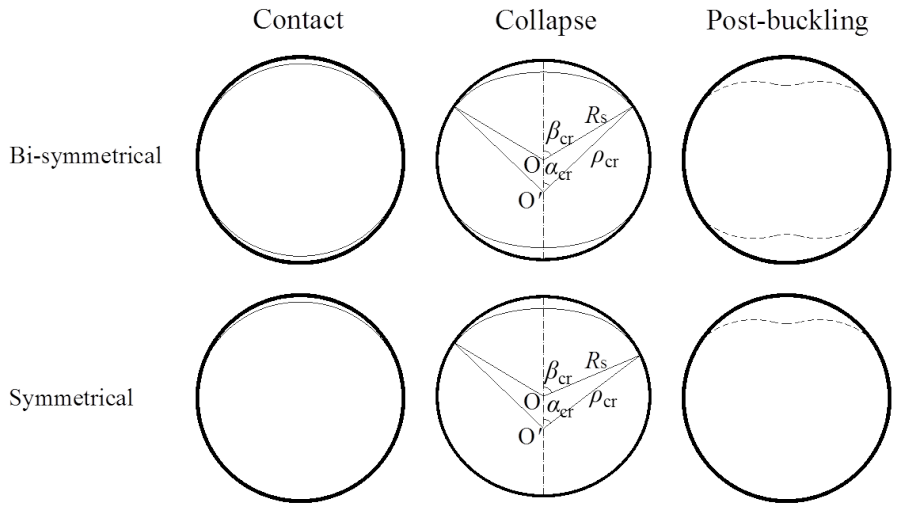

Figure 4.3: Progressive buckling process during the post-contact phase

The detached portion can be regarded as a circular arch with a new center O'. The geometry of this arch is determined by initial imperfections together with the collapse shapes. When the point where the carcass/liner separates from the pressure armor at the moment of collapse is determined, the geometry of this circular arch can be calculated for the carcass in either symmetrical or bi-symmetrical shapes:

$$\text{Bi}-\text{symmetrical} \quad \begin{cases} 2\pi R_c - 2R_s(\pi - 2\beta) = 4\alpha\rho \\ \rho \sin\alpha = R_s \sin\beta \end{cases} \tag{4.5}$$

$$\text{Symmetrical} \quad \begin{cases} 2\pi R_c - 2R_s(\pi - \beta) = 2\alpha\rho \\ \rho \sin\alpha = R_s \sin\beta \end{cases} \tag{4.6}$$

Where R_s is the distance from the separation point to the ring center at the collapse moment; ρ is the arch radius referred to the new center O'; α and β are the angular quantities displayed in Figure 4.3; subscript 'cr' represents the parameters at the moment of collapse.

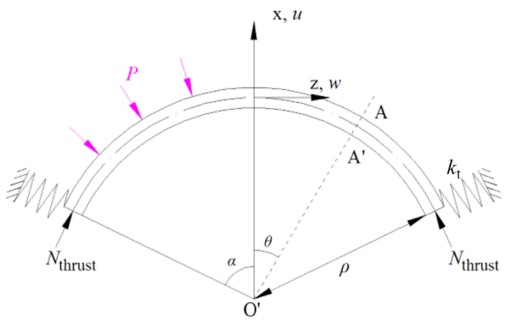

Figure 4.4: A spring-supported arch model for the post-contact phase

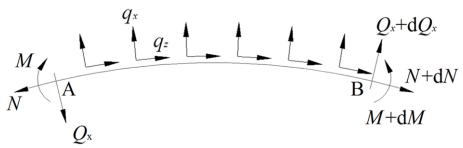

Figure 4.5: Equilibrium of a differential element of the arch (Tong, 2005)

Although this arch is detached from the surrounded pressure armor, the radial deformation of the arch ends is still restrained. Since the pressure armor confines the carcass as an elastic medium, it is treated as springs that support at the arch ends. Therefore, a spring-supported arch model is proposed for this collapse issue, as shown in Figure 4.4. The general linear equilibrium equation set for the differential element of a circular arch is expressed as (Tong, 2005)

$$\begin{cases} Q_x^{'} - N + q_x \rho = 0 \\ N^{'} + Q_x + q_z \rho = 0 \\ M^{'} + Q_x \rho = 0 \end{cases} \tag{4.7}$$

Where M, N, and Q_x are the bending moment, hoop force and radial shear force on the differential element; superscript $'$ represents $\frac{\partial}{\partial \theta}$; θ is the angle for an arbitrary cross section of the arch; q_x and q_z are the uniform loads along the radial and circumferential directions, as shown in Figure 4.5. In the wet collapse situation, values of the external loads are given by

$$\begin{cases} q_x = -q = -(P - P_{\text{con}}) \\ q_z = 0 \end{cases} \tag{4.8}$$

Where q is the differential pressure between the external pressure P and the pressure P_{con} at the contact moment. Using displacements to reformulate Eqs.(4.7), then

$$\begin{cases} E_{\text{eq}}A_{\text{eq}}\dfrac{w''+u'}{\rho}=0 \\ E_{\text{eq}}A_{\text{eq}}\dfrac{w'+u}{\rho}+\dfrac{E_{\text{eq}}I_{\text{eq}}}{\rho^3}(u^{\text{IV}}+2u''+u)=-\rho q \end{cases} \tag{4.9}$$

Where u and w are displacements of the differential element along the radial and circumferential directions, separately; A denotes the cross-sectional area; the items with subscript 'c' refer to the parameters of the carcass. If taking K as

$$K=-\frac{\rho^3}{E_{\text{eq}}I_{\text{eq}}}(\rho q+E_{\text{eq}}A_{\text{eq}}\frac{w'+u}{\rho}) \tag{4.10}$$

Then the general solution of Eqs.(4.9) can be written as

$$\begin{cases} u=KC_1\cos\theta+KC_2\theta\sin\theta+K \\ w=-KC_1\sin\theta-KC_2(\sin\theta-\theta\cos\theta)+KC_3\theta \end{cases} \tag{4.11}$$

Where $C_1 \sim C_3$ are constants that determined by the boundary conditions, and therefore, the forces at any cross section, defined by the angle θ, are

$$\begin{cases} N=\dfrac{E_{\text{eq}}A_{\text{eq}}K}{\rho}(1+C_3)+\dfrac{E_{\text{eq}}I_{\text{eq}}K}{\rho^3}(1+2C_2\cos\theta) \\ M=\dfrac{E_{\text{eq}}I_{\text{eq}}K}{\rho^2}(2C_2\cos\theta+1) \\ Q_x=\dfrac{E_{\text{eq}}I_{\text{eq}}K}{\rho^3}(2C_2\sin\theta) \end{cases} \tag{4.12}$$

For a spring-supported arch model as depicted in Figure 4.4, it has boundary conditions at its arch ends as

$$\begin{cases} w|_{\theta=\alpha}=0, & \text{No hoop displacement} \\ N|_{\theta=\alpha}=N_{\text{thrust}}, & \text{Force equilibrium in hoop direction} \\ (Q_x+k_{\text{t}}u)|_{\theta=\alpha}=0, & \text{Force equilibrium in radial direction} \end{cases} \tag{4.13}$$

Where N_{thrust} is the hoop thrust force at the arch end; k_{t} is the elastic stiffness of the pressure armor together with the liner. The liner between the carcass and pressure armor reduces the support effect of the pressure armor due to its low stiffness. According to the work of Chen et al. (Chen et al., 2015), the liner and pressure armor should be considered as two series of springs that supporting the carcass. Therefore, the value of k_{t} takes form as

$$k_{\text{t}} = \frac{k_{\text{p}} k_{\text{l}}}{k_{\text{p}} + k_{\text{l}}} \tag{4.14}$$

Where k_{p} and k_{l} are the elastic stiffness of the pressure and the liner, separately. They can be calculated by referring to the equations in (Chen et al., 2015). The formula for calculating the thrust force N_{thrust} at the arch ends is given as

$$N_{\text{thrust}} = [0.65 \frac{E_{\text{eq}} I_{\text{eq}}}{R_{\text{c}}^2} (\frac{\pi}{\beta})^2](1 - \frac{\omega_{\text{g}} + t_{\text{l,r}}}{\omega_{\max}})^{\phi_k^{-0.7}} (1 - \frac{\omega_0 + \omega_{\text{g}} + t_{\text{l,r}}}{R_{\text{c}}}) \tag{4.15}$$

Which is improved from the formula given by Glock (Glock, 1977) with non-linear regression analysis. Where ϕ_k is the bending stiffness ratio of the liner/pressure armor to the inner carcass, which is given as (Bai et al., 2016)

$$\phi_k = \frac{k_{\text{t}}}{k_{\text{c}}} \tag{4.16}$$

With the above boundary conditions, the formulae of $C_1 \sim C_3$ can be derived

$$\begin{cases} C_1 = \dfrac{D_5}{D_6} - \dfrac{D_4}{D_3 D_6} k_{\text{t}} \\ C_2 = (1 + C_1 \cos\alpha) \dfrac{k_{\text{t}}}{D_3} \\ C_3 = \dfrac{C_1 \sin\alpha + C_2(\sin\alpha - \alpha\cos\alpha)}{\alpha} \end{cases} \tag{4.17}$$

And the coefficients in Eqs.(4.17) can be calculated as

$$\begin{cases} D_1 = \dfrac{E_{\mathrm{eq}}A_{\mathrm{eq}}}{\rho}, D_2 = \dfrac{E_{\mathrm{eq}}I_{\mathrm{eq}}}{\rho^3} \\ D_3 = (2D_2 - k_{\mathrm{t}}\alpha)\sin\alpha, D_4 = D_1\dfrac{\sin\alpha - \alpha\cos\alpha}{\alpha} + 2D_2\cos\alpha \\ D_5 = -(\dfrac{N_{\mathrm{thrust}}}{K} + D_1 + D_2) \\ D_6 = D_1\dfrac{\sin\alpha}{\alpha} + \dfrac{D_4}{D_3}k_{\mathrm{t}}\cos\alpha \\ D_7 = \dfrac{\sin\alpha}{\alpha D_6} + k_{\mathrm{t}}\dfrac{\cos\alpha}{D_3 D_6}\dfrac{\sin\alpha - \alpha\cos\alpha}{\alpha} \\ D_8 = -\dfrac{k_{\mathrm{t}}}{D_3}[\dfrac{D_4}{D_6}\dfrac{\sin\alpha}{\alpha} - (1 - \dfrac{D_4 k_{\mathrm{t}}\cos\alpha}{D_3 D_6})\dfrac{\sin\alpha - \alpha\cos\alpha}{\alpha}] \\ K = \dfrac{\rho q - N_{\mathrm{thrust}}D_1 D_7}{(D_1 + D_2)(D_1 D_7 - 1) - D_1 D_8} \end{cases} \tag{4.18}$$

By substituting those coefficients into Eqs.(4.12), the maximum compressive stress at the crown point of the arch can be written as a function of the external pressure. Since the plastic collapse is defined by material yielding, therefore, the buckling pressure P_{arch} of the arch in the post-contact phase can be worked out by

$$\frac{6M_{\mathrm{cr}}}{t_{\mathrm{eq}}^2} - \frac{N_{\mathrm{cr}}}{t_{\mathrm{eq}}} = \sigma_{\mathrm{Y,eq}} - \sigma_{\mathrm{con}} \tag{4.19}$$

By substituting Eqs.(4.4) and (4.12) into Eq.(4.19), the buckling pressure P_{arch} can be calculated. Finally, the elasto-plastic collapse pressure $P_{\mathrm{Y,cr}}$ of the flexible risers with initial imperfections is obtained by

$$P_{\mathrm{Y,cr}} = P_{\mathrm{con}} + P_{\mathrm{arch}} \tag{4.20}$$

4.1.3 Separation point at the moment of collapse

If the position, i.e. R_{s} and β_{cr}, of the separation point at the moment of collapse is determined, the arch geometry can also be determined with Eqs.(4.5) or (4.6), followed by the calculation of the critical pressure with the above-mentioned approach. However, the position of the point where the carcass separates from the pressure armor is not easy to be determined since it is affected by initial ovalization and gap, and the bending stiffness ratio between the outer and the inner layers as well.

In order to tackle this problem, a formula is needed to estimate the R_s at the collapse moment. Since this separation point always lies on the inner surface of the pressure armor, then the value of R_s is mainly decided by the internal radius of the pressure armor, influenced by the stiffness of the armor wall. Considering two extreme conditions: (1) the surrounded pressure armor is rigidity; (2) the stiffness of the pressure armor is close to zero, or the inner surface of the pressure armor is too far away from the liner to provide supports before the collapse of the carcass. The actual value of R_s is bounded by the two extreme values from these two conditions, which should have $R_{p.i} < R_s < R_{c,H'}$, as shown in Figure 4.6. Where $R_{p.i}$ is the internal radius of the pressure armor in condition (1) while $R_{c,H'}$ is the semi-major axis of the elliptical carcass at the collapse moment in condition (2).

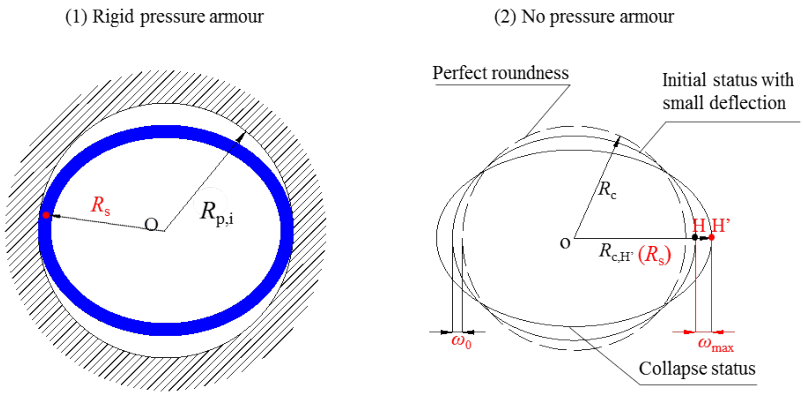

Figure 4.6: Two extreme conditions regarding the stiffness of pressure armor

After taking the factors such as initial deflection ω_0 and gap ω_g, wall thickness reduction of the liner $t_{l,r}$ into account, such a formula is proposed

$$R_s = R_c + \omega_0 + \omega_g + t_{l,r} + (\omega_{max} - \omega_g - t_{l,r})(\frac{\omega_0 + \omega_g + t_{l,r}}{\omega_{max} + \omega_0})^{\phi_k}, \qquad (4.21)$$
$$0 \leqslant \omega_g + t_{l,r} < \omega_{max}$$

With the value of R_s that estimated from Eq.(4.21), the buckling pressure P_{arch} can be determined by decreasing β_{cr} (from $\pi/2$ to 0) continually until the bending moments of the attached and detached portions at the separation point equal to each other, as shown in Figure 4.7. The bending moment

M_s for the detached arch ends can be calculated by Eq.(4.12). For the attached portion, the bending moment at the separation point is obtained by (Timoshenko & Gere, 1961)

$$M_1 = E_{eq} I_{eq} \left(\frac{1}{\rho_{cr}} - \frac{1}{R_s} \right) \tag{4.22}$$

Once M_s and M_1 are equal, the angle β_{cr} can be determined as well as the buckling pressure P_{arch} of the arch. A flowchart that shows the whole procedure is given as Figure 4.8.

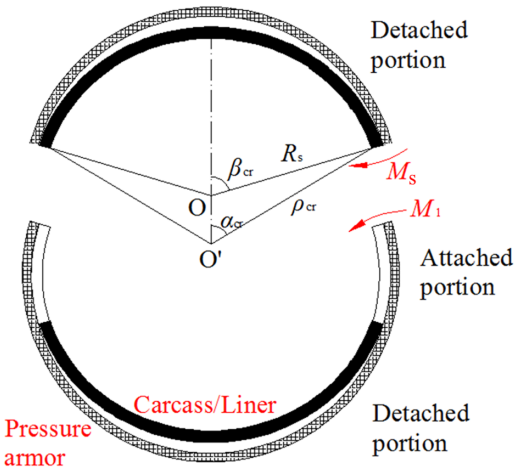

Figure 4.7: Bending moments at the separation point

4.2 Verification of the proposed analytical model

The above sections clarify the development of the proposed analytical model for predicting the wet collapse pressure of flexible pipes with initial ovalization and gap. To verify its reliability, numerical simulation is employed as a tool to examine this developed model on collapse prediction. The case study is explained in subsection 4.2.1 while in subsection 4.2.2, discussion is given based on the results from the studied case.

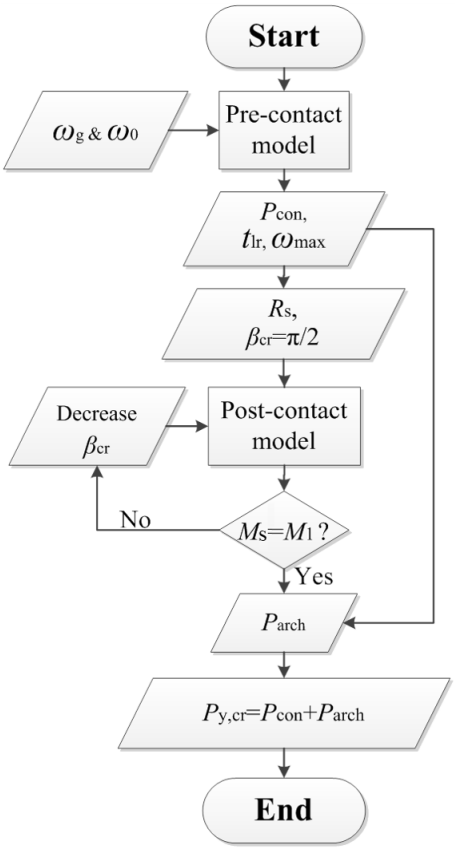

Figure 4.8: Flowchart of the whole analytical scheme

4.2.1 Case description

For verification purposes, a 2D FE equivalent ring model with variable initial ovalization and gap was constructed, as shown in Figure 4.9. Half of the cross section with symmetric boundary conditions was built with Abaqus 6.13. With this half cross-section 2D model, the initial ovalization could be introduced onto the carcass in either singly or doubly way for triggering the corresponding symmetrical or bi-symmetrical collapse shape.

This 2D FE model was developed from a prototype model that presented by Gay Neto and Martins (Gay Neto & Martins, 2014), which is a 3D FE model of a 4" flexible pipe with three layers, i.e., the carcass, the inner liner and the pressure armor. In the prototype model, the carcass was built with a detailed profile while the liner and pressure armor were represented as two homogeneous equivalent layers, as shown in Figure 4.10. With the material

properties presented in their previous work (Gay Neto & Martins, 2012), the equivalent layer method could be employed to determine the equivalent properties of the carcass for this 2D FE model. The reliability of the 2D FE model on predicting the collapse pressure was examined before using it for the verification of the analytical model.

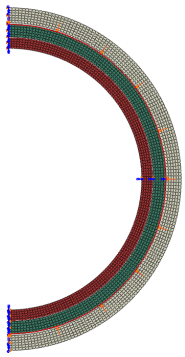

Figure 4.9: 2D FE ring model for verification

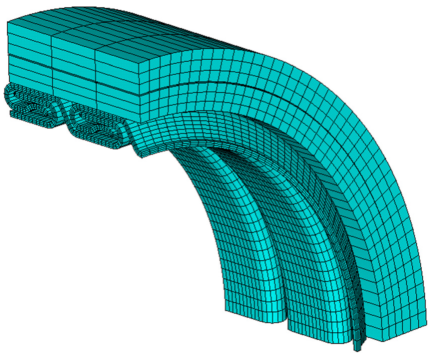

Figure 4.10: 3D FE model of a 4" flexible pipe (Gay Neto & Martins, 2014)

Table 4.1 lists the geometric and material data of the prototype model (Gay Neto & Martins, 2014, 2012). Geometric details of the carcass profile are given in the source references. The material stress-strain curves of the liner is given in Figure 3.11. With those data, the strain energy-based equivalent layer method was employed to determine the equivalent properties of the carcass. The equivalent thickness, Young's Modulus and yield stress for ring models are 4.5 mm, 158 GPa and 473 GPa, respectively. Those equivalent properties along with other layer data were used to construct the 2D FE ring model.

Table 4.1: Geometric and material properties (Gay Neto & Martins, 2014, 2012)

Model	Carcass	Liner	Pressure armor
Internal diameter (mm)	101.6	114.40	var.
Layer thickness (mm)	6.40	5.00	5.86
Young's Modulus (GPa)	200	-	207
Poisson's Ratio	0.3	0.45	0.3
Tangent Modulus (GPa)	2.02	-	50.00
Yield stress (MPa)	600	-	650

The reliability of this 2D FE model for critical pressure prediction were examined by the 3D FE model that given by Gay Neto (Gay Neto & Martins, 2014). That 3D FE model gave a critical pressure of 24.90 MPa for the case "B1", which only considered a 0.5% initial ovalization on its carcass. The critical pressure predicted by the equivalent 2D FE model was 23.43 MPa, with a 5.9% difference from the result in Ref.(Gay Neto & Martins, 2014). It should be noted that the collapse in 2D FEA is a plane-stress issue while the 3D FE model studied the collapse in a plane-strain state. For a better comparison, the above result was transferred to 25.75 MPa to consider a plane-strain state by including Poisson's ratio. Therefore, the errors was further reduced to -3.4%. It indicated that the 2D FE model is trustworthy for the following verification.

Parametric studies were done to examine the reliability of the analytical approach for different level of initial ovalization and inter-layer gap. Firstly, three levels of initial ovalization were considered as 0.5%, 1.0%, and 2.0%. The ovality were imposed to the carcass and the liner in either singly or doubly type in order to trigger corresponding "heart" or "eight" modes. The surrounded pressure armor remains a perfectly circular cross section. Secondly, an initial gap was introduced between the pressure armor and the liner while the initial ovalization of the carcass and the liner was fixed to 0.5%. According to the numerical analysis, the ultimate gap width for the carcass collapses with layer contacts is 0.36 mm; therefore, the gap width considered in the cases has a range that varies from 0 to 0.3 mm. The calculated wet collapse pressure of the 4" flexible pipe with initial imperfections were collected and listed with tables in subsection 4.2.2.

4.2.2 Results and discussion

The predictions given by the proposed analytical model were compared against the corresponding numerical results. Table 4.2 shows the critical pressure that calculated analytically or numerically for varied singly/doubly initial ovalization. The wet collapse pressure predicted by the analytical model correlates quite well with the numerical results, with a difference below 10%. From the results, it can be seen that the confined carcass collapses with a bi-symmetrical shape yields a higher critical pressure than the one with symmetrical shape. This phenomenon is probably caused by the definition of initial ovalization that given by API 17B (API17B Fifth Edition, 2014), which imposes a larger initial deflection on the singly ovalized carcass for the same level of initial ovalization.

Table 4.2: Comparison of collapse pressure between FE and analytical models for singly and doubly initial ovality

Initial ovalization	Critical pressure (MPa)					
	singly			doubly		
	FEA	Analyt.	Diff. (%)	FEA	Analyt.	Diff. (%)
0.5%	22.68	20.48	9.72	23.43	23.21	0.94
1.0%	20.63	18.73	9.19	21.97	21.95	0.11
2.0%	17.60	17.39	1.17	19.71	20.42	-3.63

In addition, the numerical simulation shows a one-side ovalization could also trigger the detachment on the other side of the carcass, as displayed in Figure 4.11. For a carcass with initial ovalization, there is a length shortage in its circumference comparing with the one in a perfect roundness. In the numerical simulation, the length shortage is spread over two detached portions rather than one. As a result, the carcass in numerical simulation has a smaller degree of ovalization than that in analytical models and hence performs a higher critical pressure. This explains why the analytical model gives much lower prediction for the singly ovality cases, since it assumes the singly ovalized carcass always collapses with a symmetrical shape.

It should be noted that a singly initial ovalization would still lead to a “heart mode”, regardless of whether “symmetrical” or “bi-symmetrical” shape develops. This is because the snap-through can only occur at a single point if the cross section is not in a perfect symmetric shape. Once the snap-through takes place, the release of strain energy will stabilize any other

possible failure points of the carcass immediately. This may explain why the "heart" mode is a typical mode shape that usually found in wet collapse tests (Paumier et al., 2009).

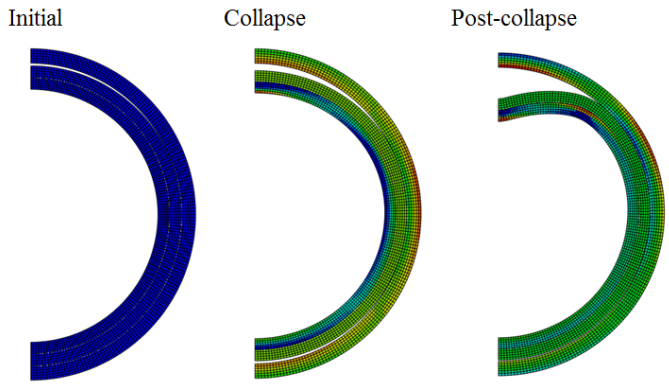

Figure 4.11: Collapse process of the singly ovalized pipe in 2D FEA

The comparison of critical pressure regarding initial gap is given in Table 4.3. According to the results listed in the Table 4.3, the proposed analytical model provides conservative estimation of the collapse pressure with comparison to numerical results. Notable differences occur between the numerical and analytical predictions, especially for the large gap cases. This is because the proposed analytical model treats the pressure armor as springs which could only provide the constraints on the radial deformation of the carcass from their contact regions. In the numerical simulation, however, the surrounded pressure armor restrains not only the radial deformation but also the rotation of the carcass. Therefore, the bending stiffness of the carcass was largely enhanced after getting in contact with the pressure armor.

For the flexible pipes, its wet collapse pressure is mainly decided by the bending and membrane stiffness of the carcass (Tong, 2005; Karnovsky, 2011). When the encased carcass is deformed from a perfect roundness to an ovalized shape under the external pressure, the dominated stiffness of the carcass for collapse resistance is gradually switched from the hoop membrane stiffness to the bending stiffness. With the increase of the initial gap width, the carcass is more oval-shaped when the contact occurs. Therefore, the bending stiffness of the carcass plays an important role in those large gap cases. Since the analytical model neglects the rotational restraints from the pressure armor, it underestimates the bending stiffness of the carcass in the post-contact phase. As a result, much conservative predictions are given by

the analytical solution.

Table 4.3: Comparison of collapse pressure between FE and analytical models for inter-layer gap

Initial gap (mm)	Critical pressure (MPa)					
	singly ovality			doubly ovality		
	FEA	Analyt.	Diff. (%)	FEA	Analyt.	Diff. (%)
0.05	22.41	19.44	13.27	23.09	20.40	11.64
0.1	22.14	18.33	17.18	22.83	18.92	17.10
0.2	21.61	15.38	28.82	22.26	16.83	24.39
0.3	21.11	14.12	33.13	21.72	16.68	23.21

4.3 Summary

In this chapter, an analytical approach is presented to predict the wet collapse pressure for the flexible risers with initial ovality and gap. Stability theories of ring and arched structures are employed to address the collapse behaviors of the encased carcass subjected to wet collapse. With those theories, the plastic wet collapse pressure of the imperfect flexible pipes can be determined.

Numerical simulation was adopted as a tool in the case studies to verify this proposed analytical model. The verification shows the analytical model has a good performance on predicting the wet collapse pressure for flexible pipes regarding the initial ovalization. By contrast, the performance of the analytical approach on inter-layer gap was not as good as that in ovality cases. The collapse strength of the carcass in the analytical model was underestimated due to the neglect of rotational restraints imposed by pressure armor. As a result, the analytical approach gives much conservative prediction on wet collapse pressure for the flexible risers with initial gaps.

Additionally, one noticeable phenomenon from the case study is the comparison differences displayed in the singly ovality cases are relatively larger than those in doubly ones. To trigger different collapse modes of the carcass, the initial ovalization was imposed as singly and doubly type respectively in all the cases. For the analytical model, it assumes the singly ovalized carcass always collapses with an "symmetrical" shape. However, the simulation shows that a singly initial ovalization could also trigger a approximate "bi-symmetrical shape" of the carcass when coming to collapse. This results in

a smaller maximum ovalization level of the carcass and hence increases the collapse pressure of the FE models.

Up to now, analytical models that developed for collapse prediction of flexible pipes are limited, especially for the risers with geometric imperfections. Wet collapse pressure of an actual flexible riser is not easy to be predicted since it is affected by those imperfections. In this regard, this chapter presents an analytical model which can take initial ovalization and inter-layer gap into account, aiming to facilitate the collapse analysis of flexible risers in its design stage. The verification given by numerical simulation indicates that this analytical model can be a good choice for ovalization issue. As for inter-layer gap, this model needs to be further improved to enhance its prediction accuracy.

Chapter 5

Pipe curvature

Owing to the structural flexibility, flexible risers are curved naturally in the touchdown zone (TDZ) and buoyed regions (Anderson & O'Connor, 2012). The influence of pipe curvature on the collapse strength is negligible if the outer sheaths of flexible risers remain intact (Gay Neto et al., 2016). Once the outer sheaths are breached, however, the collapse strength of the curved flexible risers can be largely reduced.

Due to the structural complexity of flexible risers, the way in which the pipe curvature affects the wet collapse strength is still not fully understood (Clevelario et al., 2010; Loureiro & Pasqualino, 2012; Edmans, 2014a). The main difficulties lie in the development of analytical models come from two aspects: one is the dominant factors of curvature effect for triggering the reduction of wet collapse resistance are still unclear, and the other is how to address the global curvature effect with a two-dimensional ring model.

In order to address the curvature effect analytically, this chapter first presents mechanism study to gain insights into collapse behaviors of curved flexible risers. With the mechanism study, an analytical model for curved collapse is established afterwards based on the spring-supported arch model from last chapter. This chapter answers the 5 & 6th research questions, which is an edited version of the following two journal articles:

Li, X., Jiang, X., Hopman, H. (2020). Curvature effect on wet collapse behaviours of flexible risers subjected to hydro-static pressure, *Ships and Offshore Structures*, 1861705.

Li, X., Jiang, X., Hopman, H. Development of an analytical model for predicting the wet collapse pressure of curved flexible risers, *Ocean Engineering*. (under review)

5.1 Numerical investigation on curvature effect

In this section, three dimensional finite element models were presented to gain insights into collapse mechanisms of curved flexible risers. The finite element studies were established to reveal the dominant factors of curvature effect, paving the way for the development of analytical approaches in collapse analyses. This section is made up of three subsections. Subsection 5.1.1 gives a description of the 3D full FE models adopted in this investigation. In subsection 5.1.2, case studies are carried out to investigate the effect of pipe curvature on the wet collapse behaviors of flexible risers. The results of case studies are analyzed in subsection 5.1.3 to identify the dominant factors in this curvature effect.

5.1.1 Finite element modeling

Model description

To investigate the wet collapse mechanism of curved flexible risers, a 3D full FE model of 4" internal diameter (ID) was constructed using the commercial finite element software Abaqus 6.14 (Abaqus 6.14, 2014), as illustrated in Figure 5.1. This FE model was developed from a prototype given by Gay Neto et al (Gay Neto & Martins, 2012, 2014), which consists of three layers, the innermost carcass, the inner liner and the pressure armor. In what follows, this three-layered 3D full FE model is referred as "Model-A".

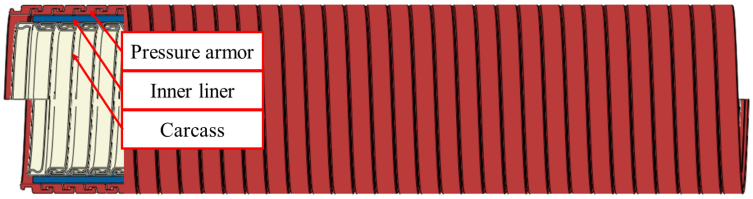

Figure 5.1: Model-A for investigating the wet collapse mechanism of curved flexible risers

The prototype of Model-A, as shown in Figure 5.2, was a one quarter model of flexible pipe section that developed in ANSYS 12.0 (ANSYS, 2011), which had a length of two carcass pitches (Gay Neto & Martins, 2014). An initial ovalization of 0.5% was imposed on the carcass in the prototype, which is defined as Eq.(2.8) (API17B Fifth Edition, 2014). With this

initial ovalization, the cross section of the entire carcass as well as the liner was ovalized in the direction of Z-axis, as shown in Figure 5.3. Table 5.1 lists the basic geometric and material data of the layers within the prototype. Geometric details of interlocking layer profiles and stress-strain curve of the
1390 inner liner are given in the source references mentioned above.

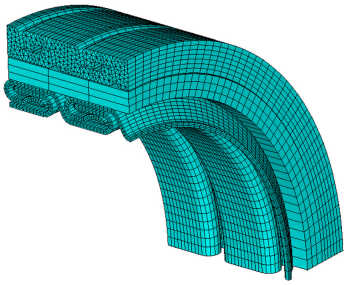

Figure 5.2: Prototype presented in the work of Gay Neto and Martins (Gay Neto & Martins, 2014)

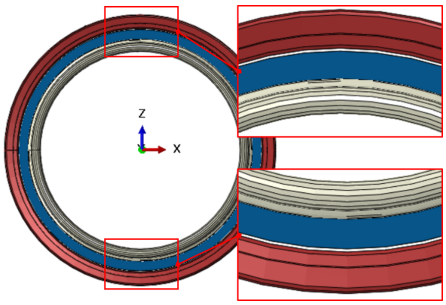

Figure 5.3: Initial ovalization imposed to the entire carcass and liner

Table 5.1: Geometric and material properties (Gay Neto & Martins, 2014, 2012)

Model	Carcass	Liner	Pressure armor
Internal diameter (mm)	101.6	114.4	124.4
Layer thickness (mm)	6.4	5.0	7.0
Young's Modulus (GPa)	200	-	207
Poisson's Ratio	0.3	0.45	0.3
Tangent Modulus (GPa)	2.02	-	50.00
Yield stress (MPa)	600	-	650

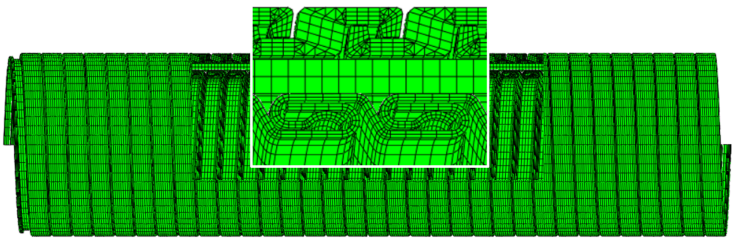

Figure 5.4: Mesh of Model-A

Layer contact occurs during the loading process as the flexible riser is a multi-layered pipe structure. This was addressed by using a surface-based penalty method. According to the work of Gay Neto and Martins (Gay Neto & Martins, 2014), and Caleyron et al. (Caleyron et al., 2014), a Coulomb friction coefficient of 0.15 was adopted for the tangent sliding between layers while a penalty stiffness factor of 0.1 was used in normal contact. By using the sweep meshing technique, Model-A was meshed as Figure 5.4. An 8-node linear brick element, C3D8R, was employed as the main element type in the meshing process of all the layers. A small amount of C3D6 elements were adopted to mesh the irregular corners of the pressure armor, which were the 6-node wedge elements.

Loads and boundary conditions were applied to Model-A as follows. This FE model was first bent to a specified curvature. The external pressure was then applied to the outer surface of the liner to compress the carcass into collapse. The tips of the model were constrained as two rigid regions to simulate the clamped ends. This was done by creating two reference points (RP) on the model center line to constrain the tip nodes with MPC constraints. These two RPs were fully fixed in the collapse analysis of straight models. In the curved collapse studies, one RP was allowed to move within YZ plane only in order to introduce the specified curvature, as shown in Figure 5.5. This RP was fully fixed after bending while the other RP was always fully fixed.

To maintain the specified curvature in the collapse process, two lines from the outer surface of the liner, lying on the neutral plane, were also fixed after bending, as illustrated in Figure 5.6. The nodes on these two lines were only allowed to move along X-axis direction within the neutral plane. This is due to the fact that the external pressure applied onto a curved pipe always restores it to a straight configuration (Gay Neto et al., 2012), as shown in

Figure 5.7. Therefore, such a line-fixed boundary condition was defined, which is referred as "BC1" in the following. The Riks method was adopted in the collapse analysis to capture the collapse pressure.

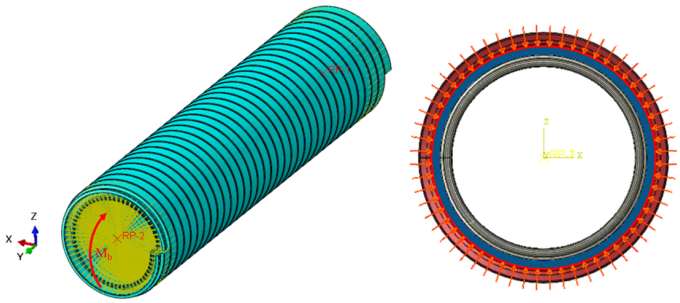

Figure 5.5: Constraints at the ends (left) and the applied pressure (right)

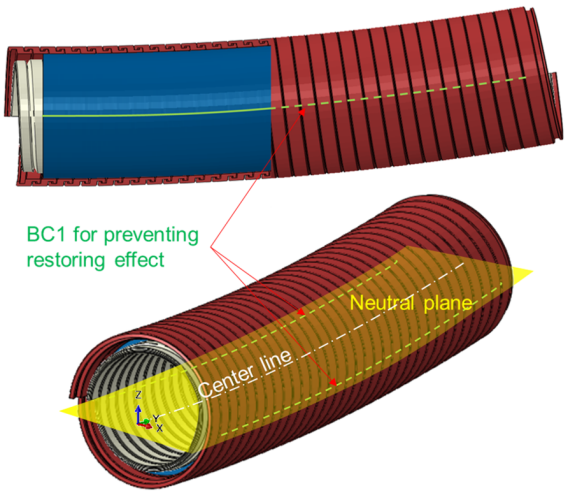

Figure 5.6: BC1 – fixed lines on the outer surface of the inner liner for preventing restoring effect in Model-A

Length determination

To achieve the balance between computational cost and accuracy, a suitable pipe length should be determined in the numerical simulation to eliminate the end effects. In this respect, a set of sample models with the same layers were built, in which their lengths were extended from 10 to 40 carcass

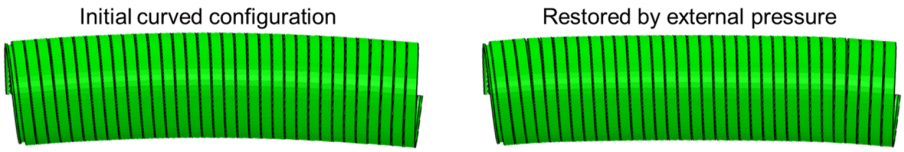

Figure 5.7: Curved pipe is restored to straight configuration

pitches (the pitches at two ends for clamped boundary conditions were not included), as shown in Figure 5.8. Those sample models were kept in straight configuration for collapse analyses, where the two RPs at their ends were fully fixed.

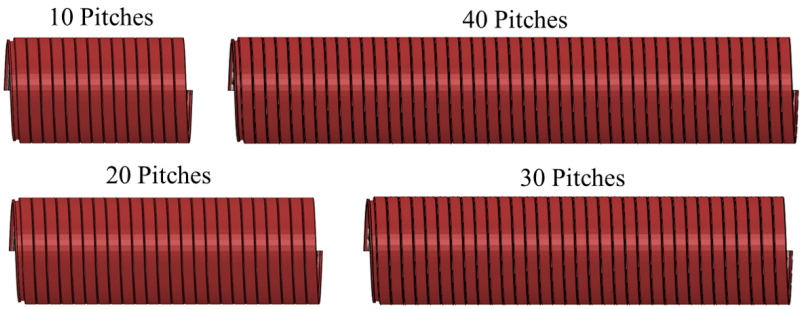

Figure 5.8: Sample models built in different length

The wet collapse pressures of those sample models were plotted in Figure 5.9, which were used to identify a suitable pipe length for eliminating the end effects in numerical simulation. It can be seen that the wet collapse pressure becomes stable when the sample length was increased to 30 carcass pitches. This indicates that the end effects were almost eliminated for the sample model with a length of 30 carcass pitches. Therefore, this length was used for all the 3D full FE models presented in this work.

Model verification

Based on the pipe length studies, Model-A was constructed into 30 carcass pitches' long. To ensure the reliability of Model-A in the wet collapse studies of curved risers, a verification process, as illustrated in Figure 5.10, was carried out. First, the prototype was reproduced using Abaqus 6.14. After the reproduced model was verified by the prototype, it was then extended to 30 pitches' long with full pipe section. If there was not much difference among

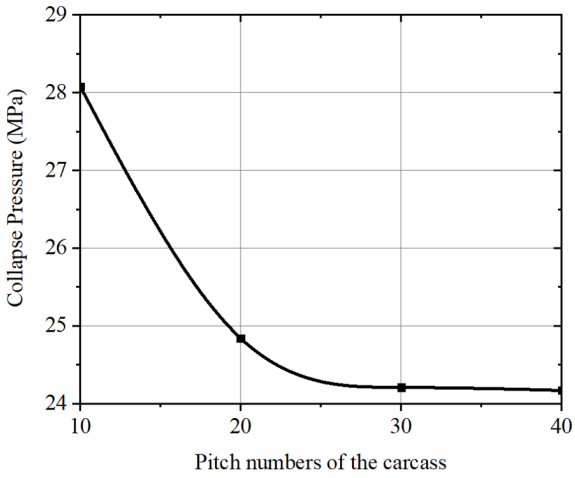

Figure 5.9: Collapse pressure vs. Number of carcass pitches

the collapse pressures given by these three FE models, then the reliability of Model-A was verified.

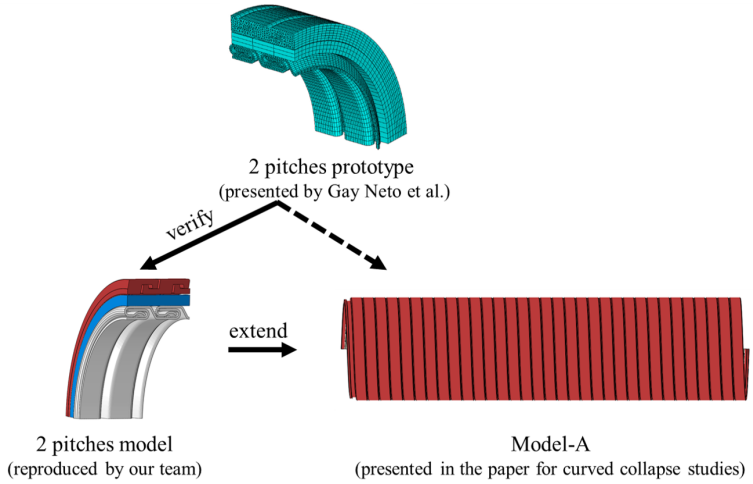

Figure 5.10: Verification procedure of Model-A

Table 5.2 lists the wet collapse pressure predicted by the above-mentioned three FE models for a straight riser. The collapse pressure given by reproduced model agrees well with that of the prototype, which performs a difference less than 4%. It indicates that the prototype model was well reproduced in Abaqus. Model-A extended from the reproduced model also shows a good agreement with the prototype and the reproduced model in respect of the col-

lapse pressure prediction. Therefore, this Model-A could be a reliable tool for the following investigation.

Table 5.2: Verification of Model-A

Model	Pitch number	Collapse pressure (MPa)	Diff (%)
Prototype (Gay Neto and Martins 2014)	2	25.36	–
Reproduced model	2	24.36	3.94
Model-A	30	24.21	4.53

5.1.2 Case study

Case studies were carried out to investigate the wet collapse behaviors of curved flexible risers. This subsection presents a detailed description of how those case studies were conducted, and what results were obtained from this investigation.

Study of curvature effect

Based on the design criteria given by API 17J (2014) (API17J Fourth Edition, 2014), the minimum bending radius (MBR) of the riser models presented in this work was calculated (Sævik & Ye, 2016), which was 3 meters. Therefore, the minimum radius of curvature in case studies was set to 3 meters. By applying bending moments to the RP at one end of Model-A, a set of radius of curvature was imposed, which were 7, 5 and 3 meters. The bending moments for each specified radius of curvature were determined by a bending response study prior to this curved collapse investigation.

The curves of external pressure vs. pipe ovalization given by Model-A for curved and straight risers are plotted as Figure 5.11. According to the results plotted in Figure 5.11, it seems that the curvature has little influence on the wet collapse behaviors of the curved riser. However, we noted that the cross-sectional shape from the collapse region of the carcass at the collapse moment, as shown in Figure 5.12, still remained an approximate bi-symmetric shape even for the pipe was bent to its MBR. On the side of pipe intrados, there was an obvious unclosed gap between the layers. This is

abnormal since the curvature creates a dis-symmetry between the carcass intrados and extrados, making its extrados less stiff and easier to be deformed (Gay Neto et al., 2012; Clevelario et al., 2010). As a result, the external pressure forces the cross section of the carcass to form a symmetric shape rather than a bi-symmetric one. Considering BC1 in Model-A might interfere the collapse behavior of the carcass, a better boundary condition for preventing the restoring effect was carried out in the following.

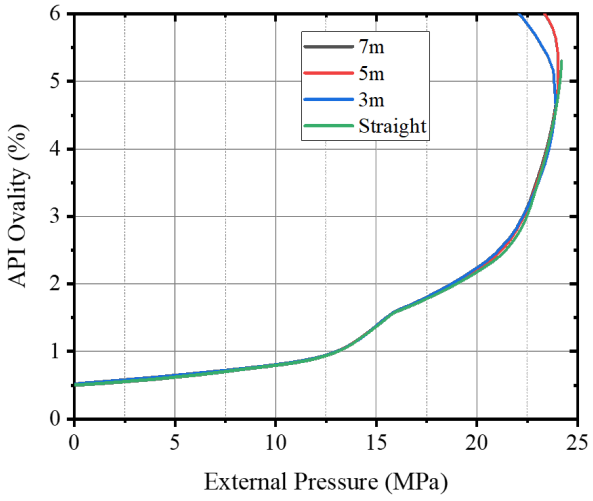

Figure 5.11: External pressure vs. API ovalization for Model-A with different pipe curvature

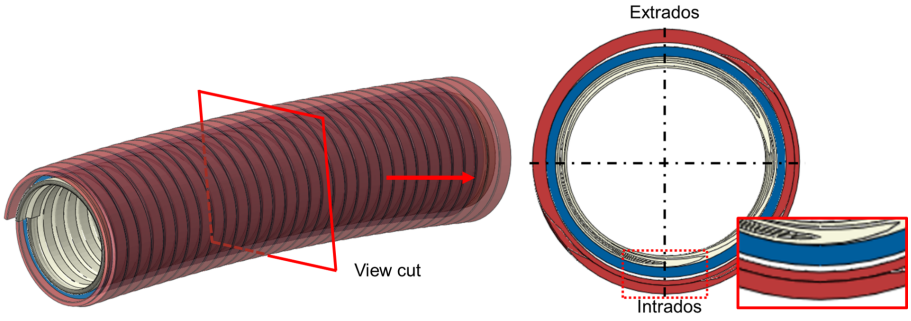

Figure 5.12: View cut – cross-sectional shape of Model-A with MBR at collapse moment

Improved boundary condition for preventing restoring effect

By referring to the work of Gay Neto et al.(Gay Neto et al., 2012), a four layers' model called Model-B was built, as shown in Figure 5.13. This model was improved from Model-A by adding an additional outer sheath. The function of the outer sheath in Model-B was only to maintain the pipe curvature in the collapse process, preventing the pipe model from being restored to straight configuration. BC1 was abandoned in Model-B. Instead, a boundary condition called BC2 was adopted as follows: two middle lines from the outer surface of the outer sheath, lying on the neutral plane, were only allowed to move along X-axis direction while one bottom line on the pipe intrados was fully fixed.

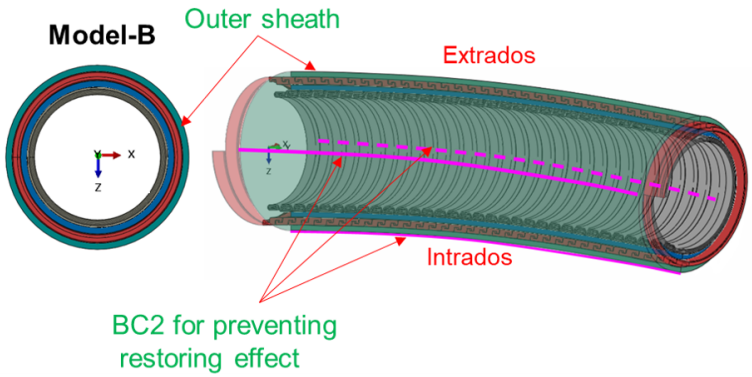

Figure 5.13: BC2 – fixed lines on the outer surface of the outer sheath for preventing restoring effect in Model-B

Table 5.3 lists the wet collapse pressure predicted Model-A and Model-B for each radius of curvature (∞ represents the straight riser). Since the wet collapse is a snap-through buckling issue, the carcass becomes extremely unstable when the external pressure close to its collapse pressure. Self-termination of the calculation were therefore caused in some cases due to the non-convergence issue. For those cases, the critical pressures were read from their last analytical step. The results from Model-A and Model-B are very close for a straight riser, which indicated the newly-added outer sheath has little influence on the wet collapse pressure. Figure 5.14 plots the curves of external pressure vs. pipe ovalization given by Model-B for each radius of curvature. Discussion of those results are given in the following subsection.

Table 5.3: Wet collapse pressure predicted by Model-A and Model-B for each radius of curvature

Curvature radius(m)		∞	7	5	3
Collapse pressure (MPa)	Model-A	24.21	24.07	24.04	23.92
	Model-B	24.23	23.06	22.82	22.07

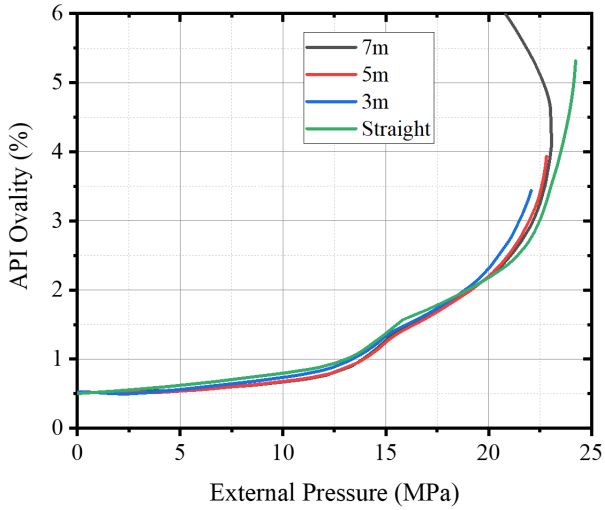

Figure 5.14: External pressure vs. API ovalization for Model-B with different pipe curvature

5.1.3 Result discussion

In the subsection of case study, two FE models, Model-A and Model-B, were established. Model-A was a three-layer model with the carcass, the inner liner and the pressure armor. A boundary condition called BC1 was adopted in Model-A to prevent the restoring effect in curved collapse analyses, which was the nodes on the two lines of inner liner (see Figure 5.6) that were only allowed to move along X-axis direction after bending. However, it was noted that BC1 had an interference on the collapse behaviors of the carcass since the liner it was applied onto was a layer for transferring external pressure to the carcass. Therefore, Model-B was developed with an additional outer sheath, and BC2 replaced BC1 by moving the fixed lines to the outer surface of the outer sheath (see Figure 5.13).

Both Model-A and Model-B were employed to predict the wet collapse pressure of a 4" ID flexible riser with an increased radius of curvature from ∞, i.e. straight, to 3 meters, as listed in Table 5.3. For the straight riser, the predictions from these two models agree quite well with each other, indicating that the outer sheath in Model-B has little influence on wet collapse pressure. However, they performed different in the curved collapse analyses. This difference between the results from those two models was analyzed to identify the curvature-induced factors for triggering the decrease of wet collapse pressure.

Investigation of the factors listed in literature

According to the literature review presented in chapter 2, two possible factors were given by researchers to explain the reduction of wet collapse resistance in curved flexible pipes. One is the squeeze effect from the bent liner, which could introduce an additional ovalization to the cross section of the carcass (Loureiro & Pasqualino, 2012). The other is the pitch elongation due to bending (Gay Neto et al., 2012), which reduces the superposed area between two carcass profiles within one pitch (Gay Neto & Martins, 2012), leading to a decreased radial stiffness on the carcass extrados. The influence of these two factors on the wet collapse pressure of curved risers were investigated by bending both Model-A and Model-B to their MBR (3m).

To observe the squeeze effect, the ovalization of the carcass were calculated by measuring the internal maximum and minimum pipe diameters, $D_{\text{I\_max}}$ and $D_{\text{I\_min}}$, of the carcass before and after bending. With Eq.(2.8), the ovalization of the carcass could be determined. The pitch of the carcass was also measured to reflect its change due to the bending. Those measurement were performed as illustrated in Figure 5.15, and the results are listed in Table 5.4.

Table 5.4: Changes of ovalization and pitch of the carcass before and after bending

Model Name	Status	Ovalization (%)	Carcass pitch (mm)
Model-A	Before bending	0.500	16.00
	After bending	0.524	16.32
Model-B	Before bending	0.500	16.00
	After bending	0.523	16.32

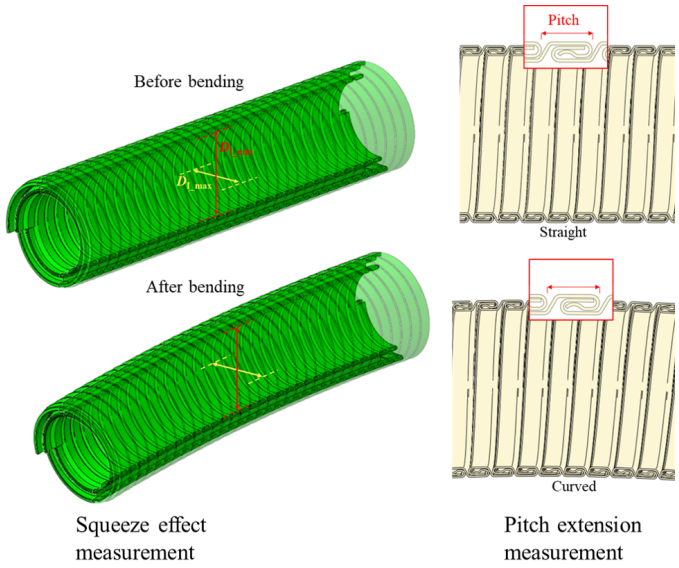

Figure 5.15: Measurement of the additional ovalization (left) and the pitch elongation (right) of the carcass before and after bending

According to Table 5.3, Model-A and Model-B have different performances on their curved wet collapse resistances. Compared to the straight one, there is a 8.9% drop of wet collapse pressure when Model-B is bent to MBR. In the same case study of Model-A, this drop is only 1.2%. However, the curvature-induced additional ovalization and pitch elongation in two models are almost the same. The additional ovalizations of the carcass caused by squeeze effect are quite close in both two models, which are around 0.023%, while the carcass pitches perform the exact same elongation. It indicates that the squeeze effect and pitch elongation can cause slight decrease of wet collapse pressure, but they are not the major factors for reducing the wet collapse resistance of the curved flexible risers.

Dominant factor in curvature effect

As stated above, the application of BC1 in Model-A interfered the layer interaction during the collapse process, leading to incorrect prediction results. Therefore, Model-B was adopted to study the collapse behaviors of curved flexible risers. According to the results listed in Table 5.3, a significant reduction on the wet collapse pressure occurred after Model-B was bent to MBR. By observing the collapse behaviors of the curved Model-B,

it was found that the carcass presented a symmetrical cross-sectional shape at its collapse region, as shown in Figure 5.16. This differs from the ones of Model-A, see Figure 5.12, which performed an approximate bi-symmetrical oval-shaped cross section even for MBR.

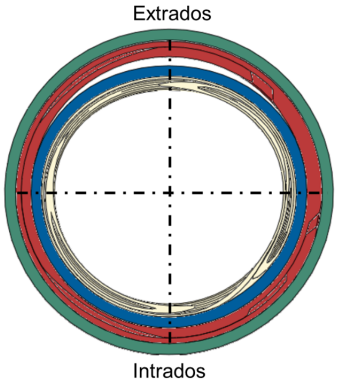

Figure 5.16: View cut – cross-sectional shape of Model-B with MBR at collapse moment

Figure 5.17 gives an illustration of these two oval-shaped cross sections by treating them as concentric rings. When the external pressure goes up, it forces parts of the carcass to detach from the inner surface of the pressure armor. Those detached portions of the carcass can be regarded as a circular arch with a new center O', which has a rise f, the vertical distance between the separation points and crown, and a span l, the horizontal distance between its two separation points (Karnovsky, 2011). The bi-symmetrical cross section of the carcass has two identical detached portion at its top and bottom while the symmetrical shape only has one detached portion. If the circumferential length of the carcass is assumed to remain unchanged during the collapse process, its detached arched portion performs a smaller rise-span ratio f/l in the symmetrical oval-shaped cross section. For the arch with a smaller rise-span ratio, a greater circumferential thrust can be triggered by the uniform radial external pressure, making the arch material easier to be plasticized (Timoshenko & Gere, 1961; Coccia et al., 2015). As a result, a greater decrease of the collapse resistance occurs for the carcass in a symmetrical cross-sectional shape.

Since the curvature-induced pitch change causes a dis-symmetry of the radial stiffness on the carcass extrados and intrados, the cross-sectional shape of the carcass is then more close to a symmetrical one at the collapse mo-

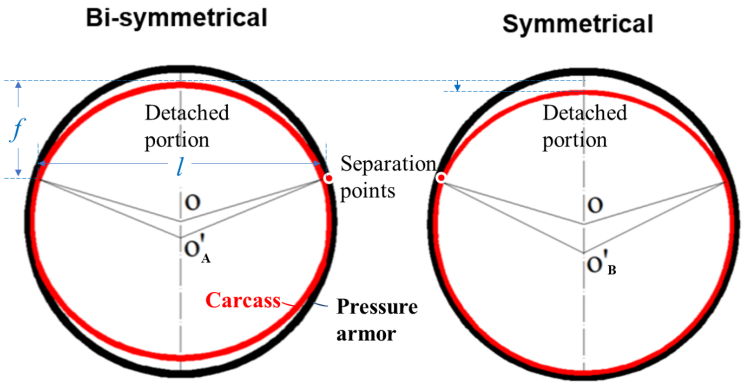

Figure 5.17: Bi-symmetrical and symmetrical shapes of the pipe cross section at the collapse moment

ment. For the curved flexible riser, its wet collapse capacity is dominated by the buckling strength of the detached portion of the carcass extrados, as shown in Figure 5.18. Therefore, the rise-span ratio f/l of this detached portion plays an important role in the collapse resistance. Figure 5.19 shows the cross-sectional shape of the carcass at the collapse moment for each radius of curvature, indicating that the rise-span ratio f/l of the detached portion decreases with the increase of pipe curvature. As a result, the wet collapse pressure of the flexible riser is heavily reduced when there is a large pipe curvature.

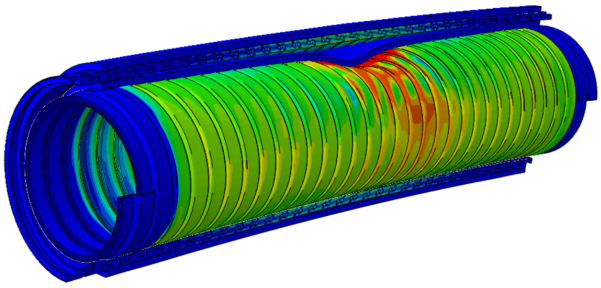

Figure 5.18: Wet collapse occurs on the carcass extrados of the curved riser

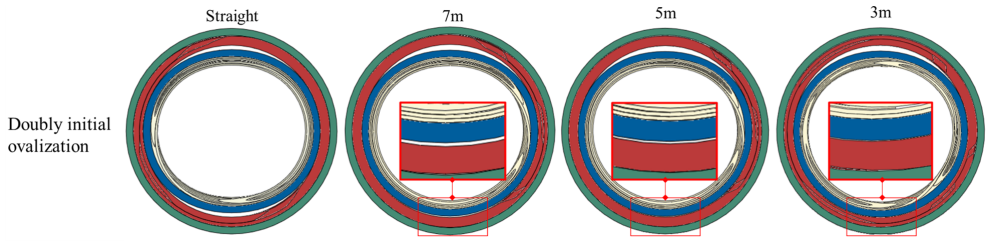

Figure 5.19: View cut – cross-sectional shapes of the doubly initial ovalized-carcass at collapse moment for different radius of curvature

5.2 Analytical model for curved wet collapse

In the last section, the numerical investigation reveals the curvature effect for reducing the wet collapse resistance of flexible risers is the result of three factors: the squeeze-induced additional ovalization, the pitch elongation and the deformed cross-sectional shape of the carcass. Among them, the deformed cross-sectional shape of the carcass is the major contributing factor in this issue. Following this mechanism study, an analytical model is developed in this section to predict the wet collapse pressure of curved risers, which is able to take these three factors into account.

In our previous chapter 4, a spring-supported arch model is proposed to predict the wet collapse pressure for straight flexible risers with initial ovalization and layer gap. This arched model is taken as a theoretical framework to incorporate the curvature effect. The development process of this analytical model is going to be presented with three subsections: subsection 5.2.1 clarifies how to introduce the above-mentioned three factors into the spring-supported arch model. In subsection 5.2.2, the verification of the analytical model is presented, in which the 3D full FE models from section 5.1 are employed. Discussions based on the results from both the analytical and numerical models are given in subsection 5.2.3.

5.2.1 Model development

As mentioned above, three factors induced by pipe curvature can lead to the decrease of wet collapse resistance, which are the deformed cross-sectional shape and the pitch elongation of the carcass, and the squeeze effect of the liner. In what follows, these factors are introduced to the spring-support arch model step by step.

Cross-sectional shape of the carcass

The geometry of the circular arch is directly related to the deformed cross-sectional shape of the carcass under external pressure. Depending on the initial ovalization types and pipe curvature of flexible pipes, the carcass could collapse into symmetrical, bi-symmetrical or transitional shapes. Compared to the bi-symmetrical oval-shaped carcass, a symmetrical one leads to a circular arch with a smaller rise-span ratio, providing less collapse resistance to the hydro-static pressure. In this work, the carcass with singly and doubly initial ovalization is studied respectively, as depicted by the section CC' in Figure 5.20. In order to provide a conservative prediction of the wet collapse, the singly ovalization in this study is always introduced to the side of the carcass where pitch elongation occurs during the bending.

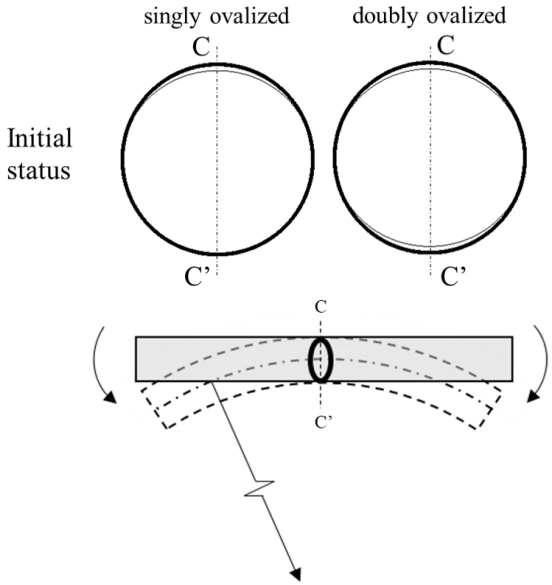

Figure 5.20: Singly and doubly initial ovalization

Considering a carcass with a doubly initial ovalization first, as shown in Figure 5.21. The cross section of this initial doubly-ovalized carcass at the collapse moment gradually turns from a bi-symmetrical shape to a symmetrical one with the increase of pipe curvature. Assuming the circumference of the carcass remains unchanged during the collapse process, then the arch radius ρ and included angle 2α can be determined with Eqs.(4.5) & (4.6) based on the cross-sectional shapes.

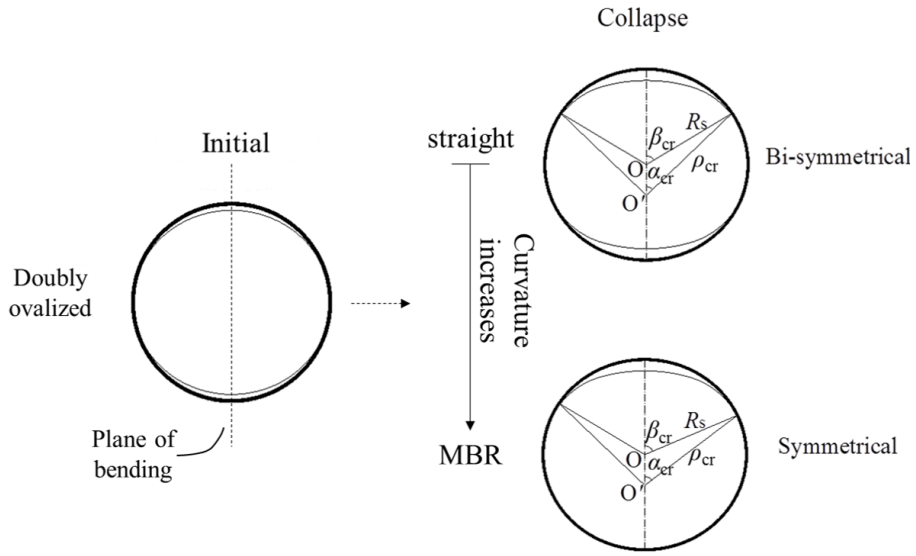

Figure 5.21: Cross-sectional shape of the carcass affected by the curvature

In this doubly initial ovalized case, the bi-symmetrical shape is adopted in the wet collapse prediction of straight risers while the symmetric one is used for the risers bent to their MBR. The collapse pressures from these two pipe configurations are regarded as upper and lower bounds in the wet collapse analysis. Based on these two bounds, the wet collapse pressure of risers with a curvature in-between can be predicted by interpolation.

For the carcass with a singly initial ovalization, its cross section is assumed to perform a symmetrical shape at the collapse moment, no matter the pipe is in a straight or curved configuration. Therefore, the formulas of the symmetrical shape can be used to determine the arch geometry for the riser with a singly initial-ovalized carcass. By substituting the arch radius and angle into the corresponding equations listed in the theoretical framework, this curvature-induced shape effect is included.

Pitch elongation

During the bending, the pitch of the carcass extrados is elongated. This pitch elongation reduces the superposed areas between two carcass profiles within one pitch, making the carcass extrados less stiff and easier to be collapsed. In our theoretical framework, the carcass extrados is treated as an equivalent arch. By determining the equivalent properties of the carcass extrados, the

reduced radial stiffness caused by the pitch elongation is introduced into the arch model.

For the flexible riser bent with a curvature of κ, the elongated pitch of the carcass extrados is given as (Sævik & Ye, 2016).

$$L_{c,ex} = L_c(R_c\kappa + 1) \tag{5.1}$$

Where $L_{c,ex}$ is the elongated pitch of the carcass extrados; L_c is the carcass pitch of a straight riser without any external loads; κ represents the pipe curvature. With the elongated pitch from Eq.(5.1), equivalent properties of the carcass extrados can be determined for the arch model. The strain energy-based equivalent method presented in chapter 3 is adopted in this arch model, which builds the equivalences between the carcass and its equivalent layer with their membrane stiffness, and the absorbed strain energy. The strain energy is obtained by subjecting the carcass and its equivalent layer to a radial compression force that could cause the onset of material yielding of the carcass. With this strain energy-based method, the equivalent thickness and Young's Modulus of the carcass can be determined by

$$\begin{cases} U_c = U_{eq} = \dfrac{F^2 R_c(1-\upsilon_c{}^2)}{8}\left[\dfrac{\pi}{E_{eq}A_{eq}} + \dfrac{C\pi}{G_c A_{eq}} + \dfrac{12R_c^2(\pi^2-8)}{E_{eq}t_{eq}^3 L_{c,ex}\pi}\right] \\ E_c\dfrac{A_c}{L_{c,ex}} = E_{eq}t_{eq} \end{cases} \tag{5.2}$$

The equivalent yield stress can be also worked out as

$$\sigma_{Y,eq} = \sqrt{\frac{E_{eq}\sigma_{Y,c}^2}{E_c}\frac{A_c}{L_{c,ex}t_{eq}}} \tag{5.3}$$

With Eqs.(5.2) & (5.3), the equivalent properties of the carcass extrados are determined for the arch. It should be noted that the strain energy-based equivalent layer method used here is just one way to involve the reduction effect of radial stiffness caused by the pitch elongation. Other equivalent methods such as bending stiffness equivalence per length (Martins et al., 2003) or per area (de Sousa et al., 2001) could also be used as alternatives.

Squeeze effect of the liner

Owing to the large lay angle and interlocked nature of the carcass, the flexural stress introduced by bending can be neglected. However, the flexural

stresses in the polymeric liner can generate a flattening load P_s to squeeze the cross section of the carcass (Sævik & Ye, 2016), as depicted in Figure 5.22(a) (Gresnigt, 1986). For the flexible riser bent with a curvature of κ, the squeeze pressure generated by the liner can be calculated as (Brazier, 1927; Guarracino, 2003)

$$P_s(\xi) = \kappa^2 E_l t_l R_l \sin\xi \tag{5.4}$$

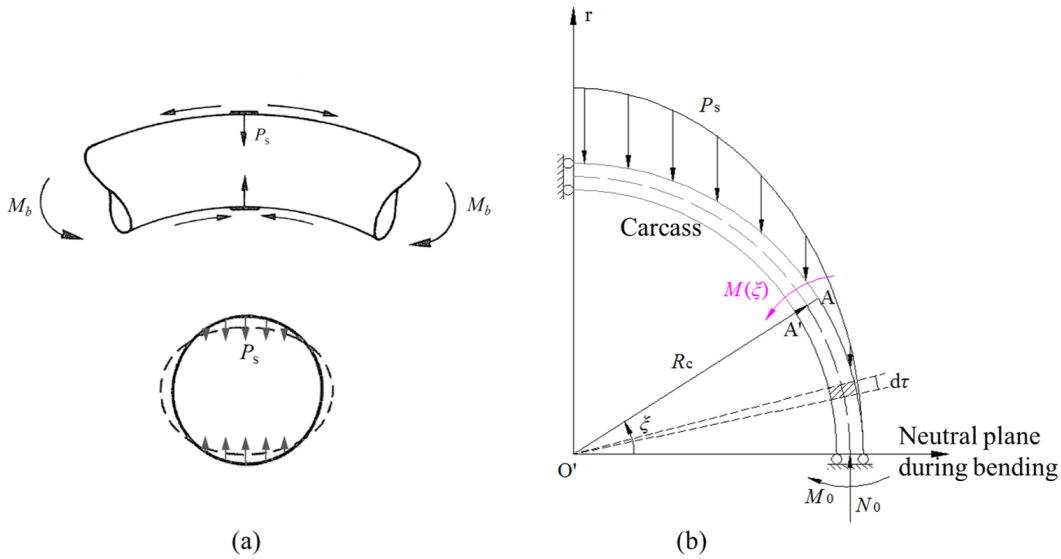

Figure 5.22: (a) Squeeze load generated from the bent liner (Gresnigt, 1986) (b) Carcass ovalized under the squeeze load

Where P_s is the harmonic squeeze load; the items with subscript 'l' refer to the properties of the liner; ξ is the angle measured from neutral plane to section AA', as illustrated in Figure 5.22(b). Under this squeeze load, the moment equilibrium at the section AA' of the carcass gives

$$M(\xi) = M_0 - N_0 R_c(1-\cos\xi) + R_c^2 \int_0^{\xi} P_s(\xi)(\cos\tau - \cos\xi)d\tau \tag{5.5}$$

Where $d\tau$ denotes the angle enclosed by the differential element; M_0 and N_0 are the bending moment and reaction force at the section that on the neutral plane, respectively. The reaction force N_0 can be derived as

$$\begin{aligned} N_0 &= \int_0^{\frac{\pi}{2}} P_s(\xi) R_c \sin\xi d\xi \\ &= \frac{\pi}{4}\kappa^2 E_l t_l R_l R_c \end{aligned} \tag{5.6}$$

The bending moment M_0 can be also derived based on the Moment-area theorem

$$\int_0^{\frac{\pi}{2}} \frac{M(\xi)}{E_c I_c} R_c d\xi = 0 \tag{5.7}$$

$$M_0 = (\frac{2}{\pi} + \frac{\pi - 5}{4})\kappa^2 E_l t_l R_l R_c^2 \tag{5.8}$$

Thus, Eq.(5.5) can be written as

$$M(\xi) = \frac{1}{4}[\cos 2\xi + (\pi - 4)\cos\xi + \frac{8}{\pi} - 2]\kappa^2 E_l t_l R_l R_c^2 \tag{5.9}$$

Since the differential equation of radial deflection of the carcass is ex-
1700 pressed as

$$\frac{d^2\omega}{d\xi^2} + \omega = -\frac{M(\xi)R_c^2}{E_{eq} I_{eq}} \tag{5.10}$$

Where ω is the radial deflection caused by squeeze load P_s. With the conditions given below,

$$\frac{d\omega}{d\xi}\Big|_{\xi=0} = \frac{d\omega}{d\xi}\Big|_{\xi=\frac{\pi}{2}} = 0 \tag{5.11}$$

the radial deflection at the arbitrary section of the carcass takes form as

$$\omega(\xi) = \frac{\kappa^2 E_l t_l R_l R_c^4}{4 E_{eq} I_{eq}}[2 - \frac{8}{\pi} + \frac{\cos 2\xi}{3} + \frac{(4-\pi)(\xi\sin\xi + \cos\xi)}{2}] \tag{5.12}$$

Considering the pipe collapse is a plane strain issue, then the radial de-
1705 flection of the carcass at ξ=0 and $\frac{\pi}{2}$ can be obtained as

$$\omega(0) = (1 + \frac{3\pi}{2} - \frac{24}{\pi})\frac{\kappa^2 E_l t_l R_l R_c^4}{E_{eq} t_{eq}^3}\frac{1 - \upsilon_c^2}{1 - \upsilon_l^2} \tag{5.13}$$

$$\omega(\frac{\pi}{2}) = (5 - \frac{3\pi^2}{4} + 3\pi - \frac{24}{\pi})\frac{\kappa^2 E_l t_l R_l R_c^4}{E_{eq} t_{eq}^3}\frac{1-\upsilon_c^2}{1-\upsilon_l^2} \tag{5.14}$$

Therefore, the additional ovalization caused by squeeze load is work out as

$$\Delta_{ad} = \frac{\omega(\frac{\pi}{2}) - \omega(0)}{2R_c + \omega(\frac{\pi}{2}) + \omega(0)} \tag{5.15}$$

Where Δ_{ad} is the additional ovalization due to the squeeze effect. For the straight riser with an initial ovalization Δ_0, it performs an ovalization for its curved configuration as

$$\Delta_0^c = \Delta_0 + \Delta_{ad} \tag{5.16}$$

Where Δ_0 is the initial ovalization of the straight riser; Δ_0^c is the ovalization after bending. Δ_0^c can be regarded as a new initial ovalization for the spring-supported arch model (Loureiro & Pasqualino, 2012). Once the new initial ovalization Δ_0^c is obtained, the curvature-induced squeeze effect is then included in this arch model.

With these three factors involved in the theoretical framework, the curvature effect is therefore considered in the wet collapse analysis. Below is a flowchart which shows the whole procedure of predicting the wet collapse pressure of a curved riser with this arch model. In the next subsection, case studies are conducted to verify this analytical model.

5.2.2 Model verification

The above subsection clarifies the development of the analytical model for incorporating the curvature effect. To verify this analytical model, the finite element models presented in the numerical investigation were employed. Case studies regarding various pipe curvature were carried out in this verification, in which the wet collapse pressures were predicted for the carcass with singly and doubly initial ovalization, respectively.

Doubly initial ovalization

In section 5.1, two FE models, Model-A and Model-B, were established to study the wet collapse resistance of a 4" ID bent flexible pipe that with a 0.5% doubly initial ovalization, as shown in Figure 5.6 & Figure 5.13,

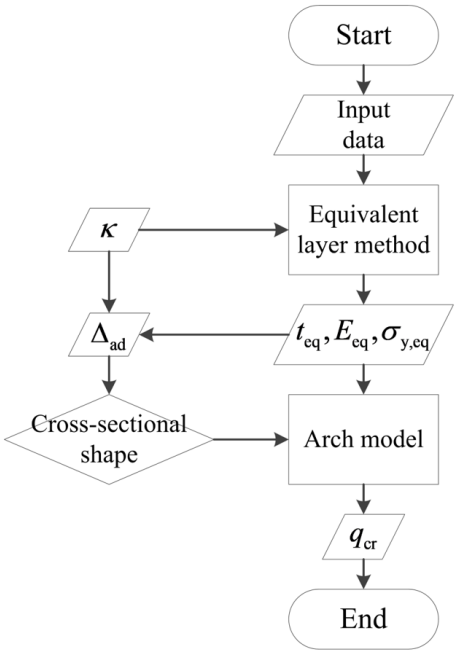

Figure 5.23: Flowchart for the curved collapse analysis with the spring-supported arch model

respectively. Model-A was a three-layer model with the carcass, the inner liner and the pressure armor. A boundary condition called BC1 was adopted in Model-A to prevent the restoring effect in curved collapse analyses, which was the nodes on the two lines of inner liner that were only allowed to move along X-axis direction after bending.

The BC1 was found that had an interference on the collapse behaviors of the carcass during the finite element studies. Therefore, Model-B was developed with an additional outer sheath, and BC2 replaced BC1 by moving the fixed lines to the outer surface of the outer sheath. The difference between these two FE models is the cross-sectional shape effect is excluded in Model-A due to the improper condition BC1 it adopted for preventing pipe restoration. Both these FE models were employed to verify the analytical model. Model-B was used to examine the reliability of the arch model in predicting the wet collapse pressure of curved risers. With the aid of Model-A, whether those curvature-induced factor were correctly considered in the arch model can be also examined.

The case studies were conducted with a set of radius of curvature, which

were 3m (MBR), 4m, 5m, 6m, 7m, and ∞ (straight). By using the strain energy-based equivalent method, the equivalent properties of the carcass and the pressure armor were work out. Table 5.5 lists the equivalent properties of the carcass extrados in each curved case for the analytical model. The equivalent thickness and Young's Modulus of the pressure armor are 6.2mm and 207.7GPa, respectively. Before the curved collapse analysis, a comparison was made between the analytical and numerical calculations regarding the pitch elongation and additional ovalization, which was given in Table 5.6. It can be seen that both numerical and analytical calculations perform an increase of the same magnitude for each factor when the curvature goes up. Therefore, the analytical calculations of these two curvature-induced factors can be reliable inputs for the following curved collapse analysis.

Table 5.5: Equivalent properties of the carcass extrados for each radius of curvature

Curvature radius (m)	Equivalent thickness (mm)	Equivalent Young's Modulus (GPa)	Equivalent yield stress (MPa)
∞	4.5	158.0	473.0
7	4.5	156.8	470.5
6	4.5	156.6	469.9
5	4.5	156.4	469.1
4	4.5	156.0	467.9
3	4.5	155.3	465.8

Table 5.6: Numerical and analytical results of pitch elongation and additional ovalization for each radius of curvature

Curvature radius (m)		∞	7	6	5	4	3
Carcass pitch (m)	FEA	16.00	16.14	16.16	16.20	16.25	16.32
	Analyt.	16.00	16.12	16.14	16.17	16.21	16.29
Additional ovalization (%)	FEA	0.000	0.009	0.010	0.011	0.015	0.023
	Analyt.	0.000	0.002	0.003	0.005	0.007	0.013

With the equivalent properties and additional ovalization, the wet collapse pressures for different curvature were predicted by the analytical model. Although multiple factors were involved in the curvature effect, the cross-sectional shape of the carcass was identified by the finite element studies as a major contributing factor to reduce the wet collapse strength. This

should also be reflected by the analytical model. In this respect, Model-A and Model-B were used separately to verify the arch model with and without the incorporation of the shape factor. As the carcass within Model-A always performed an approximate bi-symmetrical cross section due to BC1, therefore, the bi-symmetrical shape was adopted in the corresponding arch model. Table 5.7 gives the wet collapse pressures predicted by Model-A and the arch model for no shape effect incorporated, which are in good agreement.

Table 5.7: Comparison of wet collapse pressure between Model-A and the analytical model for no shape effect included

Radius of curvature (m)		∞	7	6	5	4	3
Collapse pressure (MPa)	Model-A	24.21	24.07	24.05	24.04	24.01	23.92
	Analyt.	23.44	23.26	23.22	23.18	23.12	23.01
Error (%)		3.20	3.39	3.44	3.57	3.71	3.80

Model-B was employed to verify the arch model that incorporated all the curvature-induced factors. As stated in section 5.2.1, the riser curved with a curvature less than MBR^{-1} presents a transition shape between the bi-symmetrical and symmetrical ones. This brings barriers to the prediction of the wet collapse pressure for those risers which are not heavily bent. To tackle this problem, a solution is proposed as follow. During the analytical prediction, the bi-symmetrical shape is adopted in the wet collapse prediction of straight risers while the symmetric one is used for the risers in MBR. Based on the pressures from these two pipe configurations, the wet collapse pressures for the risers with transitions shape can be interpolated linearly according to their curvature.

Figure 5.24 plots the collapse pressure given by Model-B and the analytical model for each curvature. With the above-mentioned solution, the wet collapse pressure for cases with a radius of curvature from 4 – 7m were interpolated. Those data are listed in Table 5.8, which show a good correlation between the analytical and numerical predictions.

Singly initial ovalization

The analytical model was further verified for predicting the wet collapse pressure of the curved risers which were singly initial ovalized. For comparative purposes, a singly initial ovalization of 0.5% was imposed to the carcass extrados side of Model-B, as shown in Figure 5.25. By conducting

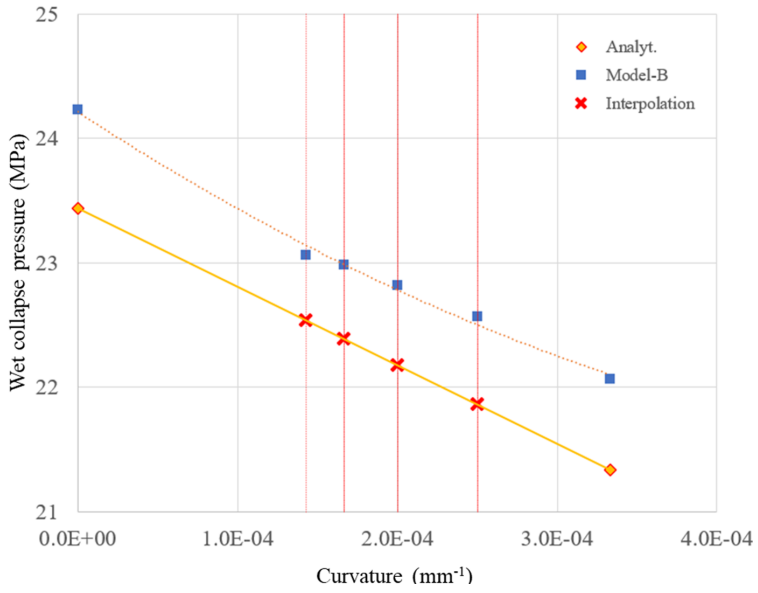

Figure 5.24: Wet collapse pressure predicted by Model-B and the arch model for the risers with doubly initial ovalization

Table 5.8: Comparison of wet collapse pressure between Model-B and the analytical model for doubly initial ovalization

Radius of curvature (m)		∞	7	6	5	4	3
Collapse pressure (MPa)	Model-B	24.23	23.06	22.98	22.82	22.57	22.07
	Analyt.	23.44	22.54	22.39	22.18	21.86	21.34
Error (%)		3.26	2.26	2.57	2.81	3.13	3.31

the same curvature cases, this verification was made. For the riser with such a singly initial ovalization, the arch model assumes that it always triggers a symmetrical shape of the carcass at the collapse moment. Therefore, wet collapse pressures of all the cases predicted by the arch model were performed based on this symmetrical shape assumption, regardless of the pipe curvature. The predictions from the singly initial-ovalized Model-B and the arch model are listed in Table 5.9. It can be seen that the result from the arch model for each pipe curvature is in good agreement with numerical one, which shows a maximum error that less than 8%.

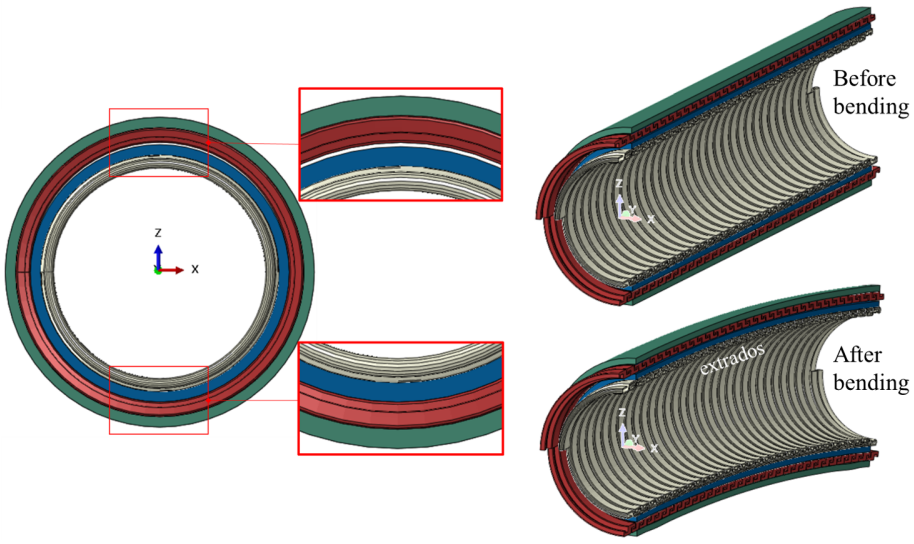

Figure 5.25: Model-B with singly initial ovalization on its carcass extrados

Table 5.9: Comparison of wet collapse pressure between Model-B and the analytical model for singly initial ovalization

Radius of curvature (m)		∞	7	6	5	4	3
Collapse pressure (MPa)	Model-B	22.50	21.49	21.40	21.15	20.93	20.92
	Analyt.	20.81	20.68	20.65	20.62	20.56	20.46
Error (%)		7.50	3.77	3.49	2.52	1.74	2.16

5.2.3 Result analysis and discussions

In subsection 5.2.2, the analytical model is verified by the 3D full finite element models for both singly and doubly initial ovalization. As stated in section 5.1, multiple factors such as pitch elongation and squeeze-induced ovalization are involved in the curvature effect. Among them, the cross-sectional shape of the carcass is the one which contributes the most to the reduction of curved wet collapse resistance. To make sure whether this phenomenon could also be reflected by the analytical model, both Model-A and Model-B were employed in the verification.

Model-A was used to verify the analytical model which only incorporates the pitch elongation and the squeeze effect. Before compressing the models into collapse, comparisons regarding pitch elongation and squeeze effect between two models were made, as given in Table 5.6. It can be seen

that the pitch elongation calculated by the analytical model for each curvature agrees well with the numerical results. As the 4" ID flexible pipe adopted in this verification has a large stiffness ratio from the carcass to the liner, the squeeze-induced additional ovalization was negligible even for the 3m (MBR) case. Thereby, the data measured in the FE models might be influenced by the measurement errors. Despite this, the magnitude levels of those analytical and numerical data are correlated well.

The effects of pitch elongation and squeeze-induced ovalization on the wet collapse resistance were studied by both Model-A and the analytical model. According to Table 5.7, the analytical prediction of wet collapse pressure for each curvature case gives an error around 3.5% by comparing to the results of Model-A, indicating that these two factors are well considered in the analytical model. Furthermore, both the analytical and numerical results perform insignificant reduction of the wet collapse pressure with the increase of curvature radius from ∞ to 3 meters, which are 1.83% and 1.2%, respectively. It implies that the effects of pitch elongation and squeeze-induced ovalization on the reduction of wet collapse resistance are limited.

By including the shape effect, the analytical model was then verified by Model-B for different initial ovalization types. For the doubly initial ovalization, the analytical model gives predictions of wet collapse pressure that match well with the numerical ones, with an error of 3% on average. This comparison shows that the analytical model is capable of predicting the wet collapse pressure of curved risers with doubly initial ovalization. Moreover, significant decreases of the wet collapse pressure occur in both two kinds of model, which go up to 9% in the 3m case. This indicates that the shape effect does play an important role in the curved collapse resistance of flexible risers.

For the singly initial ovalization, the predictions from the analytical model also agree well with the numerical results. In the curved cases, the differences between two kinds of prediction are less than 4%. However, the analytical model gives a much conservative prediction for the straight riser by comparing to Model-B. This is due to the fact that the applied external pressure can trigger a radial deflection of not only the (initial) ovalized portion but also the (initial) unovalized one, as shown in Figure 5.26. Since ovalized and unovalized portions of the carcass have the closest radial stiffnesses for the riser in a straight configuration, a small deflection on the unovalized side could also be caused by the external pressure before the collapse of the oval-

ized portion. As a result, the straight case performs a transition shape rather than a symmetrical shape.

With the increase of curvature, the difference of radial stiffness between these two portions goes up. The external pressure is unable to cause a significant radial deflection of the unovalized portion before the final collapse. From the 7m case displayed in Figure 5.26, an unclosed gap on the pipe intrados at the collapse moment could still be observed. When the radius of curvature goes above 5 meters, there is no gap any more on the pipe intrados for the collapse moment. Since a symmetrical shape assumption is adopted in the analytical model for the singly initial-ovalized carcass, the wet collapse pressure is therefore conservatively predicted for the straight riser.

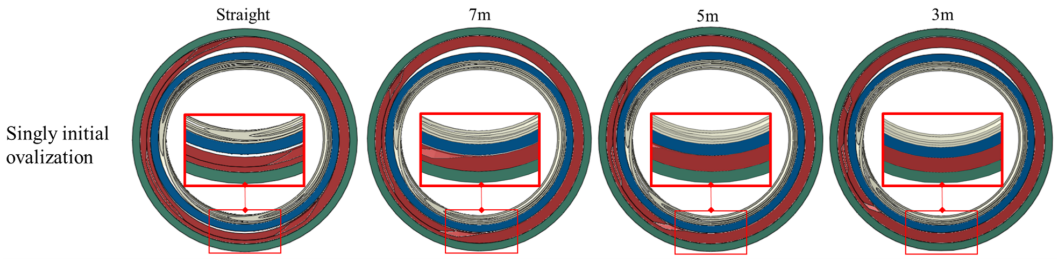

Figure 5.26: View cut – cross-sectional shapes of the singly initial-ovalized carcass at the collapse moment for different radius of curvature

5.3 Summary

In this chapter, an analytical model is established for the curved collapse issue of flexible risers. This establishment consist of two parts of work: one is the mechanism study for determining the dominant factors of curvature effect; the other is the model development which introduces those curvature-induced factors into our spring-supported arch model. Based on the whole curved collapse studies presented in this chapter, several conclusions can be drawn as follows:

(1) Curvature has a significant reduction effect on the wet collapse pressure of flexible risers. When the riser was bent to its MBR, there was a 9% drop of wet collapse pressure in comparison with the straight one according to the results from Model-B.

(2) Both analytical and numerical studies reveal that the deformed cross-sectional shape of the carcass is the major contributing factor in curvature effect. For the models includes the pitch elongation and squeeze effect only, their results show that the pipe curvature could only trigger a slight decrease of the wet collapse pressure. Once the shape effect is introduced to those models, significant drop of the wet collapse pressure occurs with the increase of pipe curvature.

(3) The proposed analytical model has a good performance on predicting the wet collapse pressure of curved flexible pipes. This analytical model was used to predict the wet collapse pressure for a 4" ID flexible pipe with different curvature and initial ovalization types. By comparing analytical predictions to the numerical ones, the proposed analytical model is verified, in which the maximum error is 7.5%.

With the study of curvature effect, this chapter adds some information into the understanding of the curved collapse mechanism of flexible risers. Moreover, the analytical model developed in this chapter can be an efficient tool for the collapse analysis in pipe design stage. The numerical simulation in our case studies consumes 2$\sim$3 days on average to finish one job. By contrast, the computational time required by the proposed analytical model is less than one minute, which could provide a rapid feedback to the designers for their cross-sectional design.

Chapter 6

Integrated analytical model

In the previous chapters, factors like geometric imperfections and pipe curvature are addressed individually in the analytical model. Chapter 3 addresses the interlocked metallic layers while Chapter 4 focuses on the initial ovalization and inter-layer gap of flexible risers. In Chapter 5, the attention is paid to the curvature effect in the wet collapse of the risers. Naturally, it gives rise to the following question (7th research question): how to formulate an integrated analytical model by involving all those factors in one wet collapse prediction?

To answer this question, the studies presented in Chapter 3, 4 and 5 are recalled to formulate such an integrated analytical model. The verification of this analytical model is conducted using the 3D full FE models presented in Chapter 5, which answers the last research question listed in Chapter 1. This chapter is arranged as follows: based on the previous work, an integrated analytical model is presented in Section 6.1 to incorporate the geometric imperfection and curvature factors. Case studies are conducted both numerically and analytically in Section 6.2 for the model verification. Discussions are given in Section 6.3 while Section 6.4 summarizes the whole work.

6.1 Integrated analytical model

By integrating the analytical approaches presented in the previous chapters, an integrated model can be formed to incorporate the coupling effect of geometric imperfections and pipe curvature. Figure 6.1 gives the overview of such an integrated analytical model, and a step-by-step explanation is given as below to show how it works.

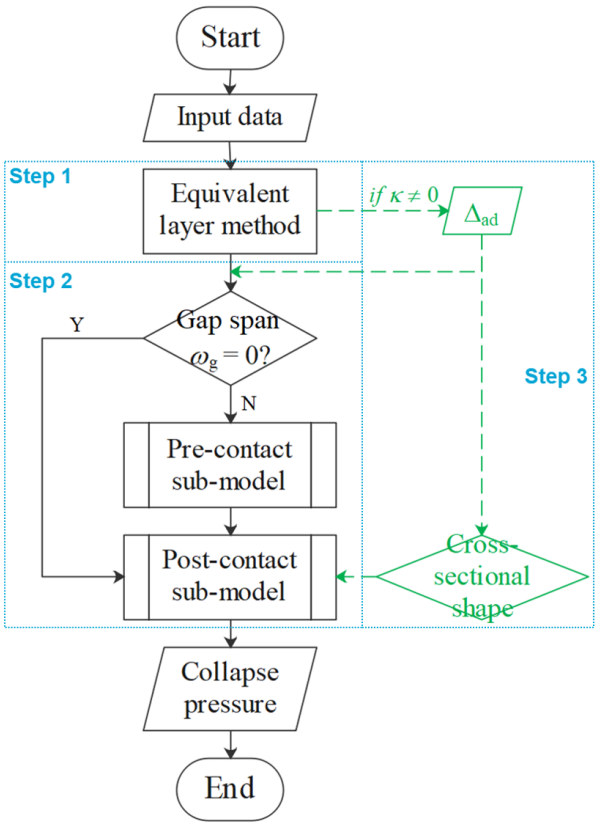

Figure 6.1: Flowchart for the integrated analytical model

Step 1 Equivalent treatment of metallic interlocked layers.

Once the cross-section dimensions and materials of the flexible riser have been selected, the equivalent properties of the carcass and pressure armor could then be determined. With the strain energy-based equivalent layer method that presented in Chapter 3, the equivalent Young's Modulus, thickness and yield stress of the interlocked lay-

ers are solved. Other equivalent layer methods could also be used as alternatives for this step.

Step 2 Predicting the wet collapse pressure for straight risers with initial geometric imperfections.

The designers can input an assumed initial ovality into the analytical model on the basis of manufacturing tolerance limits and residual ovalization from the installation process. A minimum ovality of 0.2% can be used when there is no other data provided by the manufacturers (API17B Fifth Edition, 2014).

For the cross-section configuration design without considering interlayer gap, the layer properties are imported to post-contact sub-model directly for the wet collapse prediction. If an initial gap span is assumed, the pre-contact and post-contact sub-models should be employed in sequence. The work from Curstódio and Vaz (Custódio & Vaz, 2002), and Shen et al. (Shen et al., 2011, 2012) could be referred for determining such an initial gap span. By finishing this step, the wet collapse pressure of straight flexible risers can be solved.

Step 3 Introducing the curvature effect into the wet collapse analysis

For the curved wet collapse analysis, the equivalent properties of interlocked layers should be updated first based on the curvature κ. With those updated equivalent properties, an additional ovalization of the carcass caused by curvature-induced layer squeeze is then calculated. This additional ovalization should be imported into the analytical model along with the initial ovality. After determining the cross-sectional shape of the carcass for the post-contact sub-model based on the initial ovalization type and the pipe curvature, the wet collapse pressure of curved flexible risers is predicted.

With this integrated analytical model, the coupling effect of geometric imperfection and pipe curvature could therefore be taken into account. To verify this integrated analytical model, 3D full FE models from Chapter 5 were adopted. In what follows, case studies are performed with both analytical and numerical models.

6.2 Case studies

In order to verify this integrated analytical model, the 3D full FE models presented in Chapter 5 were employed. A set of case studies were performed with both analytical and numerical models to study the coupling effect of the initial geometric ovalization and gap, and the pipe curvature on wet collapse pressure of flexible riser. The 3D full FE models were constructed with those three factor at two levels each, which are 0.5% and 1% for the initial ovalization, 0 mm and 0.1 mm for the inter-layer gap span, and ∞ (straight) and 3 m (RMB) for the radius of curvature, as shown in Figure 6.2. Details of each case are summarized in Table 6.1. The verification is done by comparing the predictions provided by the integrated analytical model with numerical results.

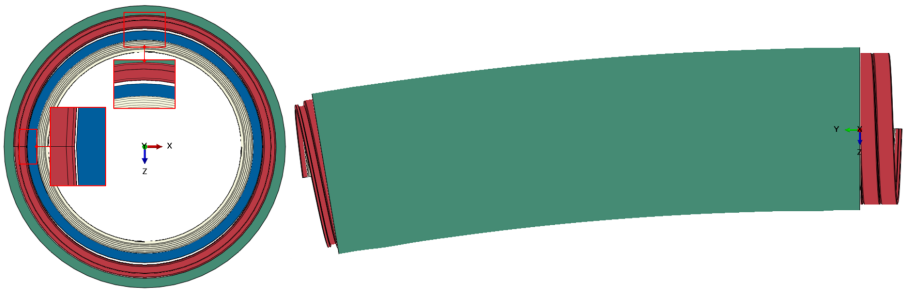

Figure 6.2: Numerical simulations for the riser with combined initial geometric imperfections and curvature

Table 6.1: Factor combinations for each case

Case No.	Initial ovality (%)	Gap span (mm)	Radius of curvature (mm)
1	0.5	0	∞
2	0.5	0	3000
3	0.5	0.1	∞
4	0.5	0.1	3000
5	1.0	0	∞
6	1.0	0	3000
7	1.0	0.1	∞
8	1.0	0.1	3000

By using the strain energy-based equivalent layer methods, the equivalent properties of metallic interlocked layers could be determined. With

the equivalent data of the carcass and the pressure armor that given in Section 5.2.2, the wet collapse pressures for the 4" flexible riser in both straight and curved configurations were solved analytically. Table 6.2 presents the comparison of wet collapse pressure between the numerical and analytical predictions for all the case studies.

Table 6.2: Comparison of wet collapse pressure between the analytical and numerical predictions for each case

Case No.	Wet collapse pressure (MPa)		Diff. (%)
	FEA	Analyt.	
1	24.23	23.44	3.26
2	22.07	21.34	3.31
3	23.38	20.20	13.59
4	21.34	19.46	8.79
5	22.62	22.13	2.18
6	20.96	19.89	5.12
7	22.10	18.72	15.32
8	20.58	17.39	15.51

As mentioned in Chapter 5, the load increment becomes extremely small in numerical simulations when the carcass is coming to collapse. To reduce the computational cost, the jobs were terminated automatically when the minimum increment was reached. Therefore, the numerical results were read from the last analytical step of those cases, and their stress fields were extracted to evaluate whether they are close to collapse limits. The stress distribution of the carcass at (near) the collapse limits for case 1–4 and 5–8 are provided in Figure 6.3 and Figure 6.4, respectively. According to the stress fields of each case, it can be seen that the collapse of the carcass occurs when the maximum von Mises stress goes up around 650 MPa.

With those numerical results, comparison were made between the analytical and numerical predictions. According to the comparison given by the Table 6.2, the predictions given by the integrated analytical model correlate well with the numerical results. The maximum difference between those two kinds of prediction is around 15%. From the result comparison, it can be seen that the integrated analytical model has a good performance on predicting the wet collapse for the risers with initial ovality, curvature and the combinations thereof. More importantly, the predictions given by the analytical model are always on the safe side.

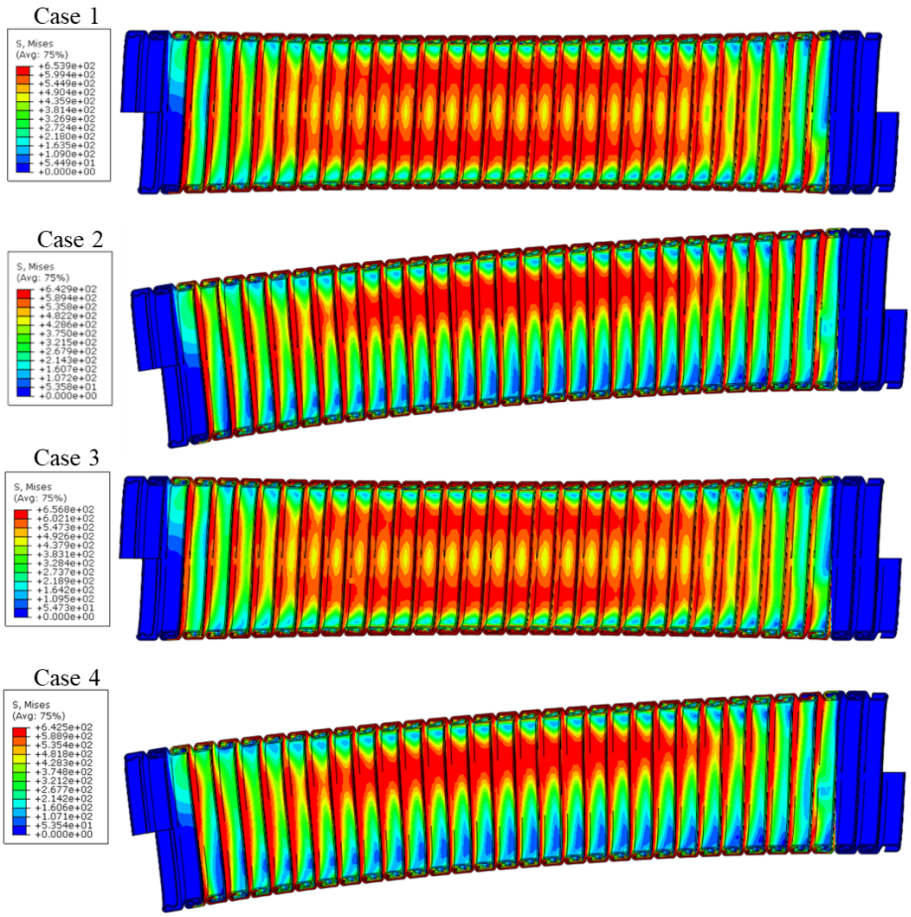

Figure 6.3: Stress distribution of the carcass at/ near the collapse limit for cases 1–4

6.3 Result discussions

In Section 6.2, the coupling effect of initial ovalization, inter-layer gap and pipe curvature is studied by both numerical and analytical approaches. For the cases 1, 2, 5 and 6 where the inter-layer gap is zero, the predictions given by the numerical and analytical approaches are in good agreement. The analytical predictions start to deviate from the numerical results after the gap span is introduced to the riser. This phenomenon comes from the treatment of the pressure armor in the analytical model, in which the springs are used as a replacement for this interlocked layer. As discussed in Chapter 4, the rotational restraints from the pressure armor that act on the contact

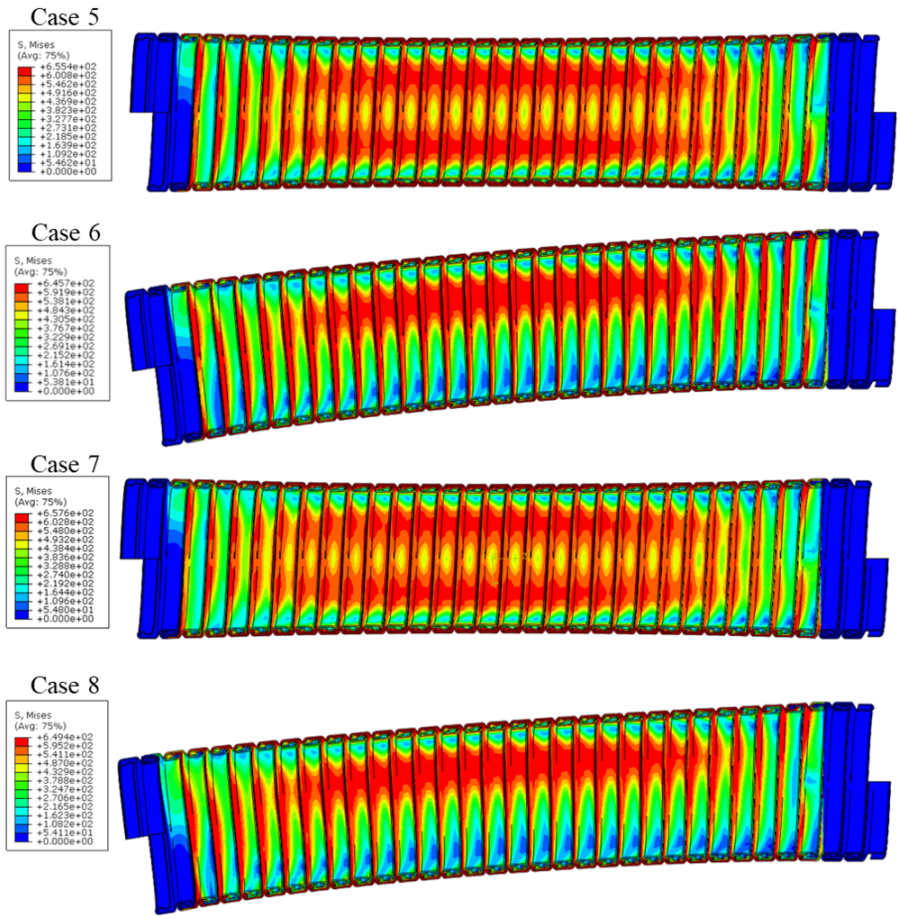

Figure 6.4: Stress distribution of the carcass at/ near the collapse limit for cases 5–8

region of the carcass is neglected by simplifying it into springs. Because of the neglect of this rotational restraints, the differences between the analytical and numerical predictions go up to 10% $\sim$ 15% for the cases which contain the inter-layer gap.

To visualize the effect of each factor and the combinations thereof on collapse behaviors of flexible risers, the curves of external pressure vs. pipe ovalization of the carcass are plotted in Figure 6.5 and Figure 6.6 based on the numerical data. From those curves, it can be observed that there is a significant decrease of radial stiffness of the carcass when the external pressure increases to 11$\sim$13 MPa. At this range of external pressure, the material of the carcass strip starts to be plasticized, which causes this softening behav-

ior. After that, a recovery of the radial stiffness occurs around the external pressure of 15 MPa owing to the self-contact of the carcass strips. With the external pressure is further increased, more and more regions of the carcass are plasticized. Finally, the radial stiffness of the carcass drops dramatically and the collapse limit is reached.

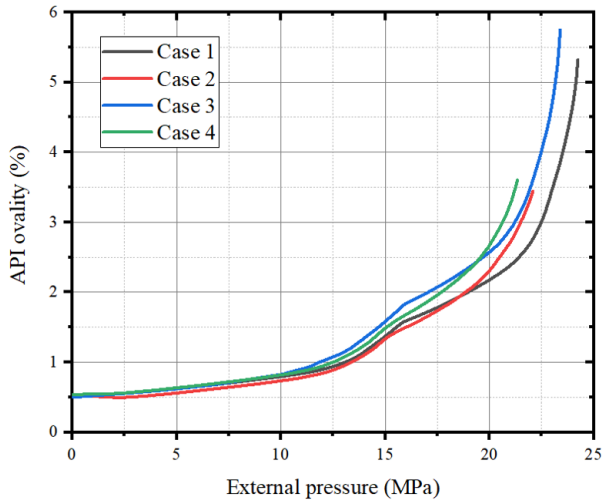

Figure 6.5: External pressure vs. API ovalization of the carcass from numerical simulations for cases 1–4

For riser with a larger inital ovalization, a premature material yielding of the carcass strip can be triggered. This phenomenon is reflected by comparing the curves between case 1 and 5, where the initial ovality is the only factor involved. In case 1 the softening behavior appears around the external pressure of 12.5 MPa while in case 5, this appears at 11 MPa. According to the stability theory of rings (Timoshenko & Gere, 1961), there is a positive correlation between the bending moment and the initial ovalization. For the ring with a larger initial ovalization, its section has to bear a greater bending moment under the same external pressure. As a result, the premature material yielding of the carcass strip is caused, followed by the softening of the radial stiffness.

This softening effect is further magnified after the inter-layer gap is involved. If there is an initial gap between the layers, the external pressure is first resisted by the carcass alone before the gap closure. In this situation, the larger initial ovalization the carcass has, the greater radial deformation the external pressure causes. As a result, the material of the carcass strips

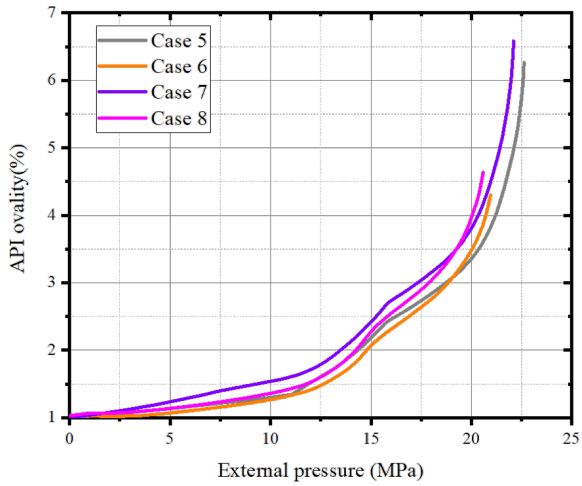

Figure 6.6: External pressure vs. API ovalization of the carcass from numerical simulations for cases 5–8

could be easily plasticized, leading to a much smaller collapse limit. This phenomenon can be observed by comparing the curves among cases 1, 3, 5, and 7. For the case 3 or 5 where only one initial geometric imperfection involved (taking case 1 as the base), the onset of stiffness reduction occurs around the external pressure of 10 MPa. By contrast, the occurrence of stiffness reduction in case 7 appears at 2 MPa merely, which shows the coupling effect of initial ovalization and gap on the collapse resistance of the carcass.

The wet collapse behaviors of flexible risers become more complex once the curvature is introduced. When the riser is bent, a restoring load is generated which forces the curved carcass back to straight. This restoring load is the resultant of pressure fields on the intrados and extrados of the curved carcass (Gay Neto et al., 2017b). In this restoring stage, the external pressure mainly contributes to the global displacement rather than the radial deformation of the carcass, which can be clearly seen by comparing the curves between case 7 and 8. Significant radial deformation of the carcass only occurs after it is fully supported by the pressure armor.

For the carcass supported by the pressure armor in a curved riser, the collapse resistance is dominated by the radial stiffness of its detached portion, as mentioned in Chapter 5. If regarding this detached portion as an arch, then the arch geometry is totally decided by the initial ovalization and inter-layer gap (at a given curvature). With the increase of inital ovalization

and inter-layer gap, the ratio of radius to wall thickness ρ/t_c of this arch goes up (El-Sawy & Sweedan, 2010, 2013; Watkins & Anderson, 1999). This radius-thickness ratio increases the pre-buckling hoop stresses in carcass extrados(Kyriakides & Corona, 2007) for the same external pressure, which hastens the softening of the radial stiffness in the post-contact phase, as shown in Figure 6.5 and Figure 6.6.

6.4 Summary

In this chapter, an integrated analytical model is established based on the theories from the previous chapters, which can predict the wet collapse of flexible risers by involving the geometric and curvature factors. To verify this integrated analytical model, the 3D full FE models in chapter 5 were adopted. A set of case studies were performed with both analytical and numerical models, in which each factor was considered with two levels. According to the comparison, the predictions given by the integrated analytical model correlate well with the numerical results for the risers with initial ovality, pipe curvature and the combinations thereof. For the riser with an inter-layer gap, the wet collapse pressure predicted by the analytical model is around $10\% \sim 15\%$ smaller than that of numerical simulations.

Chapter 7

Conclusions and recommendations

In this thesis, an integrated analytical model is presented to predict the collapse pressure of flexible risers, aiming to facilitate the collapse analysis in the design stage. With the establishment of such an analytical model, all the research questions listed in Chapter 1 have been answered. The conclusions towards the whole research work are provided in section 7.1, followed by the recommendations for future research in section 7.2.

7.1 Conclusions

The goal of this Ph.D project is to develop an analytical model for the collapse analysis of flexible risers in the design stage. This goal was achieved by solving the main research question proposed in Chapter 1:

- How to develop an integrated analytical model for predicting the wet collapse pressure of the flexible risers?

More specifically, this main question was addressed by answering the following sub-questions:

1. Are there any analytical models developed for the collapse studies of flexible risers?

2. What are the limitations of those analytical models in predicting the wet collapse pressure of flexible risers?

In essence, the collapse of flexible pipes is a structural stability problem. As the flexible pipe can be treated as an equivalent ring or tube, ring buckling theories are therefore used to develop the related analytical models. In Chapter 2, the existing analytical models for the collapse studies of flexible pipes have been listed, which can be summarized as follows.

Timoshenko's model: This model solves the elastic buckling pressure of a circular ring by considering the bending moment in the ring section. In dry collapse analysis of flexible pipes, the carcass and the pressure armor are regarded as equivalent rings (or tubes). With the Timoshenko approach, the dry collapse pressure could be determined as the sum of those interlocked layers.

Glock's model: An elastic solution for the restrained hydro-static buckling problem based on non-linear deformation theory and the principle of minimum potential energy. This model can be used to predict the wet collapse of flexible pipes. By using this model, the pressure armor is assumed a rigid tube that restrains the radial deformation of the carcass.

Bai's model: This model also provides an elastic solution of wet collapse pressure based on the principle of minimum potential energy. Unlike the Glock's model, the pressure armor in the approach is regarded as springs that support the carcass.

Although those analytical models have been used in the collapse design methodology of flexible pipes for years, there are still some limitations. Firstly, most of them only give the elastic solution of collapse pressure for the flexible riser. For the flexible risers used for ultra-deep production, they are designed with a small diameter-thickness rato ($\sim<35$). This makes them collapse in the elastic-plastic range and therefore, an elastoplastic solution for the wet collapse should be provided. Secondly, the influences of initial imperfections on the wet collapse resistance could not be reflected by those analytical models. Lastly, those models are unable to take into the curvature effect in the prediction of collapse pressure. In view of those limitations of the existing analytical models in the wet collapse analysis of flexible risers, this project was thereby carried out to develop a new analytical model.

3. How to address the complex interlocked layers of the flexible riser in the prediction model?

Based on the literature review, three layers, the carcass, the pressure armor and the inner liner, should be taken into account to develop the analytical

model. The innermost carcass is the main layer that withstands the hydro-
2140 static pressure in a wet collapse situation. The pressure armor increases the collapse resistance of the carcass by restraining its radial deformation. The plastic inner liner contributes little to the wet collapse resistance though, it reduces the restraining effects from the pressure armor through its own elastic deformation. Therefore, those three layers are the necessities for con-
2145 structing the new analytical model.

As the interlocked layers like the carcass cannot be addressed directly in the analytical model, they need to be treated as cylindrical tubes with equivalent properties. The work presented in Chapter 3 is to propose an equivalent layer method for such a treatment. Mostly, the equivalent properties of those
2150 interlocked layers are determined based on their bending stiffness since the collapse of ring-like structures is a bending-dominated problem. However, it is found such kind of equivalent methods might lead to overestimated predictions due to the neglect of geometric nonlinearities of the interlocked layers. During the collapse process, the hydro-static pressure gradually eliminates
2155 the space between the interlocked carcass strips, leading to the reduction of its bending stiffness. Considering the actual bending stiffness of the carcass was difficult to be evaluated, another property, the strain energy at the onset of material yielding, was used to replace it. Based on the equivalent concepts of strain energy and membrane stiffness, the equivalent properties of
2160 interlocked layers can be determined and imported to the analytical models.

4. How to take the initial ovalization and the inter-layer gap into account?

Once the riser annulus is flooded, the collapse is dominated by the detached portion of the carcass. In Chapter 4, this detached portion is regarded as a circular arch, and the stability theories of arched structures are adopted
2165 to solve its buckling pressure. The initial ovlization and the inter-layer gap decide the arch geometry. The arch radius and inclined angle are determined based on the initial gap span, the level and the types of the initial ovalization.

5. What is the buckling mechanism of curved risers subjected to wet collapse?

2170 6. How to incorporate the curvature effect into the analytical model?

In Chapter 5, 3D full FE models are employed to gain insights into the curvature effect in the wet collapse. According to the investigation, the deformed cross-sectional shape of the carcass during the collapse process is the

dominant factor of curvature effect. The geometry of the detached portion on carcass extrados is influenced by pipe curvature. Besides, two another factors induced by curvature can also influence the wet collapse resistance. One is the pitch elongation, which reduces the superposed areas between two carcass profiles within one pitch, making the carcass extrados less stiff and easier to be collapsed. The other is the squeeze effect from the bent liner, which imposes an additional ovalization to the carcass.

Those factors affect the radial stiffness of the detached portion of the carcass. Since this detached portion is regarded as an arch in the analytical model, its geometric and material properties are corrected based on those curvature-induced factors. The elongated pitch is used to update the equivalent properties for the arch. The additional ovalization caused by squeeze loads is added to the initial ovalization of the carcass. As for the shape effect, it is considered by selecting corresponding collapse modes on the basis of the curvature magnitude. The collapse mode together with the geometric imperfections is used to determine the arch geometry for the curved risers.

7. How to formulate an integrated analytical model by involving the geometric imperfections and pipe curvature in its wet collapse prediction?

8. How to verify the proposed integrated analytical model?

The aim of the integrated analytical model is to account for the coupling effects of those factors on wet collapse resistance of flexible risers. As the confined carcass is simplified as an spring-supported arch, those coupling effects can be introduced by adjusting the geometric and material properties of the equivalent arch. Depending on the geometric imperfections and pipe curvature, three steps are made to determine those arch properties. The first step is to obtain the equivalent properties of the interlocked layers for the equivalent arch, in which the riser is considered in the straight configuration. In the second step, the initial ovality and gap are introduced to help determine the arch radius and angle. The wet collapse of the straight riser can be predicted with this step. The third step is executed when a curved collapse analysis is required, which corrects the geometric and material properties of the arch based on the pipe curvature.

As the collapse tests of flexible risers are costly and require specialized hyperbaric chambers and end fitting equipment, it is not affordable by this Ph.D. project. Alternatively, numerical simulations were adopted to verify

this proposed integrated analytical model. 3D full FE models were constructed according to the practices established by Gay Neto and Martins. Comparison of wet collapse pressure is made between these two kinds of prediction, which were in good agreement. In this comparison, the FEA consumed 2∼3 days on average to give a prediction of wet collapse pressure by using the High Performance Computer (2 nodes / 32 cores). By contrast, the integrated analytical model took only few seconds (programmed by Matlab) to complete the prediction, which is much effective than the numerical simulations. For any future work related to the wet collapse of flexible risers, experimental comparisons are always welcome.

7.2 Recommendations

Following the work presented in this thesis, the future research can be expanded to several directions as below:

a. **Effect of carcass erosion on the collapse capacity of flexible pipes.**

During the oil and gas production, sand is an inevitable byproduct (Helgaker et al., 2017). Sand can cause erosion of the pipe bore, which has become an important concern in the design of carcass. The erosion rate of the carcass depends on a number of parameters (Out, 2012)

- bulk-flow velocity
- mass flow of sand
- pipe curvature
- carcass material
- size, sharpness of sand grains, etc.

which makes the erosion tests become a time-consuming, expensive process and in some cases does not reflect exactly the operating conditions (API17B Fifth Edition, 2014; Hosseini & Hosseini, 2016). In API 17J (API17J Fourth Edition, 2014), the manufacturers are required to demonstrate that the carcass has sufficient erosion resistance to meet the specified design requirements. To ensure the structural integrity of flexible risers, the future study can focus on quantifying the erosion effect on the collapse resistance of the carcass, especially for the high-curvature areas.

b. **Collapse of flexible pipes that caused by depressurization**

The barrier of flexible risers for high temperature service is designed in multiple layers (Chicheportiche & Demanze, 2011). Fluid or gas transported in the pipe bore can be trapped within the layer annular space by means of flow paths through the end-fittings, which builds up the pressure in the multi-layered barrier (Lambert et al., 2012). During the rapid depressurization of flexible pipes, carcass collapse might be caused due to this build-up pressure (Buchner et al., 2003). Such kind of collapse incidents have been found in Njord and Visund oilfields (4Subsea, 2013; Farnes et al., 2013). In the future, it is necessary to perform an investigation on this particular failure mode, gaining some insights into the effect of depressurization rate on collapse resistance of the carcass.

c. **Collapse failure under combined loads**

Operating in the ocean environment exposes the flexible pipes to various loads. In recent years, attentions are being paid to the collapse behaviors of the carcass under combined loads (Zhu & Lei, 2019). Flexible pipes are subjected to crushing and axial loads during installation and operations (Miyazaki et al., 2018; Caleyron et al., 2014). The effects brought by those loads to the collapse response of flexible pipes are still not fully clear. To ensure the safety of flexible risers in the ocean environment, future research towards the effect of axial compression/tension, torsion, crushing loads and the combinations thereof on collapse performance of flexible risers are demanded.

d. **Collapse performance of the flexible risers designed with composite materials**

Self-weight becomes an important factor that can limit the applications of flexible pipes in ultra-deep water fields (Melillo, 2015). To reduce the self-weight of flexible risers, the industry has engaged in two approaches (Murphy, 2000). A short-term approach is to optimize the riser design for the specified operating conditions. In a long run, a more general approach is to replace the traditional metallic layers like tensile or pressure armors with one made of much lighter composite materials. Such new design concepts have been proposed by industry in recent years (Jha et al., 2015; Anderson et al., 2016). For those new-generation flexible pipes, further studies are in demand to investigate their collapse performance in hostile offshore environments.

Bibliography

4Subsea (2013) Unbounded flexible risers - recent field experience and actions for increased robustness, Tech. rep., PSA Norway.

Abaqus 6.14 (2014) *Abaqus analysis user's guide*, SIMULIA.

Abbassian, F., S. H. L. Parfitt (1998) A simple model for collapse and post-collapse behavior of tubulars with application to perforated and slotted liners, in: *Society of Petroleum Engineer,* SPE-51188-PA.

Adams, A. J., A. V. R. Warren, P. C. Masson (1998) On the development of reliability-based design rules for casing collapse, in: *Society of Petroleum Engineer,* SPE-48331-MS, The Woodlands, Texas, USA.

Alavandimath, S. (2009) *Local plastic deformation in pressure & tensile armor layers of flexible risers*, Doctoral thesis, Sheffield Hallam University.

Allen, A. J., C. Andreani, M. T. Hutchings, C. G. Windsor (1981) Measurement of internal stress within buck materials using neutron diffraction, *NDT Int.*, 14(5), pp. 249–254.

Anderoglu, O. (2004) Residual stress measurement using X-ray diffraction.

Anderson, K., M. O'Connor (2012) The evolution of Lazy-S flexible riser configuration design for harsh environments, in: *Proc. 31st OMAE,* OMAE2012-83404, Rio de Janeiro, Brazil.

Anderson, T. A., B. Fang, M. Attia, V. Jha, N. Dodds, D. Finch, J. Latto (2016) Progress in the development of test methods and flexible composite risers for 3000 m water depths, in: *Proc. Offshore Technology Conference,* OTC-27260-MS, Houston, Texas, USA.

ANSYS (2011) *Ansys 13.0 help*, Canonsburg (PA): ANSYS, Inc.

API17B Fifth Edition (2014) Recommended practice for unbonded flexible pipe, Tech. rep., American Petroleum Institute.

API17J Fourth Edition (2014) Specification for unbonded flexible pipe, Tech. rep., American Petroleum Institute.

Axelsson, G., H. Skjerve (2014) Flexible riser carcass collapse analyses - sensitivity on raidal gaps and bending, in: *Proc. 33rd OMAE,* OMAE2014-23922, San Francisco, California, USA.

Bai, Q., Y. Bai, W. Ruan (2017) *Flexible pipes: advances in pipes and pipelines*, John Wiley & Sons.

Bai, Y., Q. Bai (2005) *Subsea pipelines and risers*, Elsevier Science.

Bai, Y., S. Yuan, P. Cheng, P. Han, W. Ruan, G. Tang (2016) Confined collapse of unbonded multi-layer pipe subjected to external pressure, *Compos. Struct.*, 158, pp. 1–10.

Bakeer, B. R. M., M. E. Barber, S. E. Pechon, J. E. Taylor, S. Chunduru (1999) Buckling of HDPE liners under external uniform pressure, *J. Mater. Civil Eng.*, 11, pp. 353–361.

Barnes, P. (2014) *An investigation into the corrosion fatigue behavior of high strength carbon steel armor wires*, Doctoral thesis, Faculty of Engineering and Physical Science, The University of Manchester.

Boot, J. C. (1998) Elastic buckling of cylindrical pipe linings with small imperfections subject to external pressure, *Trenchless Technol. Res.*, 12(1–2), pp. 3–15.

Boyer, H. E., T. L. E. Gall (1985) *Metals handbook: desk edition*, American Society for Metals.

Brazier, L. G. (1927) On the flexure of thin cylindrical shells and other "thin" sections, *Proc. Roy. Soc. A*, 116, pp. 104–114.

Buchner, S., J. Belcher, P. Williams, T. Sheldrake (2003) Pressure build-up in multi layer flexible pipe barrier during shut down, in: *Oilfield Engineering with Polymers 2003*, London, UK.

Caleyron, F., M. Guiton, J. Leroy, T. Perdrizet, D. Charliac, P. Estrier, L. Paumier (2014) A multi-purpose finite element model for flexible risers studies, in: *Proc. 33rd OMAE,* OMAE2014-23250, San Francisco, California, USA.

Callister, W. D. (1992) *Materials science and engineering: an introduction*, John Wiley & Sons, New York.

Chaperon, G. R., H. P. Boccaccio, M. J. Bouvard (1991) A new generation of flexible pipe, in: *Proc. Offshore Technology Conference,* OTC-6584, Houston, Texas, USA.

Chen, Y., J. Liu, L. Zhu, Z. Tan, G. Karabelas (2015) An analytical approach for assessing the collapse strength of an unbonded flexible pipe, *J. Mar. Sci. Appl.*, 14, pp. 196–201.

Chicheportiche, S., F. Demanze (2011) Development of a new, low plasticized, PVDF for monolayer dynamic applications in flexible pipes, in: *Proc. Offshore Technology Conference,* OTC-21477-MS, Houston, Texas, USA.

Clevelario, J., F. Pires, G. Falco, Z. Tan, J. Lu, T. Sheldrake (2010) Flexible pipe curved collapse behavior assessment for ultra deepwater developments for the Brazilian pre-salt area, in: *Proc. Offshore Technology Conference,* OTC-20636-MS, Houston, Texas, USA.

Clinedinst, W. O. (1939) A rational expression for the critical collapsing pressure of pipe under external pressure, in: *American Petroleum Institute, Drilling and Production Practice,* API-39-383, New York, USA.

Coccia, S., F. D. Carlo, Z. Rinaldi (2015) Collapse displacements for a mechanism of spreading-induced supports in a masonry arch, *Int. J. Adv. Struct. Eng.*, 7(3), pp. 307–320.

Cooke, N., S. Kenny (2014) Comparative study on the collapse response of flexible pipe using finite element methods, in: *Proc. 33rd OMAE,* OMAE2014-23306, San Francisco, California, USA.

Crome, T. (2013) Experiences from design and operation, learning and improvements, Tech. rep., Technip.

Cruz, F. T. L., C. A. N. Dias (1997) Structural analysis of flexible pipe using finite element method, in: *Proc. 7th ISOPE,* ISOPE-I-97-174, Honolulu, Hawaii, USA, pp. 137–143.

Cuamatzi-Melendez, R., O. Castillo-Hernández, A. O. Vázquez-Hernández, M. A. Vaz (2017) Finite element and theoretical analyses of bisymmetric collapses in flexible risers for deepwaters development, *Ocean Eng.*, 140, pp. 195–208.

Custódio, A. B., M. A. Vaz (2002) A nonlinear formulation for the axisymmetric response of umbilical cables and flexible pipes, *Appl. Ocean Res.*, 24(01), pp. 21–29.

Danzi, F., E. Cestino, G. Frulla, J. M. Gibert (2017) Equivalent plate model of curvilinear stiffened panels, in: *Proc. 7th M2D*, Albufeira, Portugal.

Davidson, M., U. S. Fernando, B. Donnell, A. Bell, A. Ramsay (2016) Prediction of extruded profile shape of polymer barrier in flexible pipes, in: *Proc. 26th ISOPE,* ISOPE-I-16-261, Rhodes, Greece.

de Sousa, J. R. M., E. C. P. Lima, G. B. Ellwanger, A. Papaleo (2001) Local mechanical behavior of flexible pipes subjected to installation loads, in: *Proc. 20th OMAE,* OMAE2001/PIPE-4102, Rio de Janeiro, Brazil.

de Sousa, J. R. M., C. Magluta, N. Roitman, G. B. Ellwanger, E. C. P. Lima, A. Papaleo (2009) On the response of flexible risers to loads imposed by hydraulic collars, *Appl. Ocean Res.*, 31, pp. 157–170.

de Sousa, J. R. M., M. K. Protasio, L. V. S. Sagrilo (2018) Equivalent layer approaches to predict the bisymmetric hydrostatic collapse strength of flexible pipes, in: *Proc. 37th OMAE,* OMAE2018-78146, Madrid, Spain.

DNV-OS-C501 (2010) Offshore Standard – Composite components, Tech. rep., Det Norske Veritas.

DNV-RP-A203 (2011) Qualification of new technology, Tech. rep., Det Norske Veritas AS.

Edmans, B. (2014a) Finite element studies for assessment of collapse modelling methodologies for unbonded flexible pipes, in: *Proc. Offshore Technology Conference,* OTC-24815-MS, Kuala Lumpur, Malaysia.

Edmans, B. (2014b) Studying the finite elements of flexible pipe, Tech. rep., Lloyd's Register Energy.

El-Sawy, K. M., A. M. I. Sweedan (2010) Elastic stability analysis of loosely fitted thin liner - a proposed simplified procedure and evaluation of existing solutions, *Tunn. Undergr. Sp. Tech.*, 25(6), pp. 689–701.

El-Sawy, K. M., A. M. I. Sweedan (2013) Inelastic stability of liners of cylindrical conduits with local imperfection under external pressure, *Tunn. Undergr. Sp. Tech.*, 33, pp. 98–110.

Eyssautier, S., J. Ryan, Y. Brouard, K. E. Roniawan, F. Germanetto (2018) Cost effective riser solutions for deepwater gas developments: steel lazy wave riser and tethered catenary riser, in: *Proc. Offshore Technology Conference,* OTC-28279-MS, Kuala Lumpur, Malaysia.

Farnes, K. A., C. Kristensen, S. Kristoffersen, J. Muren, N. Sødahl (2013) Carcass failures in multilayer PVDF risers, in: *Proc. 32rd OMAE,* OMAE2013-10210, Nantes, France.

Fergestad, D., S. A. Ltveit (2017) Handbook on design and operation of flexible pipes, Tech. rep., MARINTEK.

Fernando, U. S. (2015) Challenges and solutions in developing ultra-high pressure flexibles for ultra-deep water applications, Tech. rep., GE Oil & Gas.

Fernando, U. S. (2016) New decompression analysis for flexible pipes with multi-layer barrier, in: *Proc. 26th ISOPE,* ISOPE-I-16-185, Rhodes, Greece.

Fernando, U. S., M. Davidson, C. Simpson, T. Pirling, K. Yan, M. D. Callaghan, M. Roy, J. A. Francis, P. J. Withers (2015) Measurement of residual stress shakedown in pressure/ tensile armor wires of flexible pipes by neutron diffraction, in: *Proc. 34th OMAE,* OMAE2015-41328, St. John's, Newfoundland, Canada.

Fernando, U. S., D. M., K. Yan, M. J. Roy, T. Pirling, P. J. Withers, J. A. Francis (2017) Evolution of residual stress in tensile armor wires of flexible pipes during pipe manufacture, in: *Proc. 36th OMAE,* OMAE2017-61490, Trondheim, Norway.

Fernando, U. S., Z. Tan, T. Sheldrake, R. Clements (2004) The stress analysis and residual stress evaluation of pressure armor layers in flexible pipes using 3D finite element models, in: *Proc. 26th ISOPE,* ISOPE-I-16-185, Vancouver, British Columbia, Canada.

Fyrileiv, O., L. Collberg (2005) Influence of pressure in pipeline design: effective axial force, in: *Proc. 24th OMAE,* OMAE2005-67502, Halkidiki, Greece.

Gay Neto, A., C. A. Martins (2012) A comparative wet collapse buckling study for the carcass layer of flexible pipes, *J. Offshore Mech. Arct. Eng.*, 134, pp. 1–9.

Gay Neto, A., C. A. Martins (2014) Flexible pipes: influence of the pressure armor in the wet collapse resistance, *J. Offshore Mech. Arct. Eng.*, 136(3), p. 031401.

Gay Neto, A., C. A. Martins, E. R. Malta, C. A. F. Godinho, T. F. B. Neto, E. A. Lima (2012) Wet and dry collapse of straight and curved flexible pipes: a 3d fem modeling, in: *Proc. 22nd ISOPE,* ISOPE-I-12-309, Rhodes, Greece.

Gay Neto, A., C. A. Martins, E. R. Malta, R. L. Tanaka, C. A. F. Godinho (2016) Simplified finite element models to study the dry collapse of straight and curved flexible pipes, *J. Offshore Mech. Arct. Eng.*, 138(2), p. 021701.

Gay Neto, A., C. A. Martins, E. R. Malta, R. L. Tanaka, C. A. F. Godinho (2017a) Simplified finite element models to study the wet collapse of straight and curved flexible pipes, *J. Offshore Mech. Arct. Eng.*, 139(6), p. 061701.

Gay Neto, A., P. M. Pimenta, C. A. Martins (2017b) Hydrostatic pressure load in pipes modeled using beam finite elements: theoretical discussions and applications, *J. Offshore Mech. Arct. Eng.*, 143(4), p. 04017003.

Glock, D. (1977) überkritisches verhalten eines starr ummantelten kreisrohres bei wasserdruck von außen und temperaturdehnung, *Stahlbau*, 46, pp. 212–217.

Gresnigt, A. M. (1986) *Plastic design of buried steel pipelines in settlement areas*, Stevin-Laboratory of the Fac. of Civil Engeneering, Delft University of Technology; Rijswijk (ZH) : Inst. TNO for Building Materials and Structures.

Grognec, P. L., P. Casari, D. Choqueuse (2019) Influence of residual stresses and geometric imperfections on the elastoplastic collapse of cylindrical tubes under external pressure, *Mar. Struct.*, 22(4), pp. 836–854.

Guarracino, F. (2003) On the analysis of cylindrical tubes under flexure: theoretical formulations, experimental data and finite element analyses, *Thin-Walled Struct.*, 41, pp. 127–147.

Helgaker, J. F., S. IJzermans, T. J. Landheim, T. B. Eeg, S. M. Hverven, P. Piotrowski (2017) Large-scale erosion testing of an unbonded flexible pipe, *SPE J.*, 22(03), pp. 736–745.

Hosseini, S. M. K., S. M. H. Hosseini (2016) CFD simulation of sand erosion in multiphase flow flexible risers, in: *Eurocorr 2016*, Montpellier, France.

Huet, C. (1990) Application of variational concepts to size effects in elastic heterogeneous bodies, *J. Mech. Phys. Solids*, 38(6), pp. 813–841.

Jha, V., D. Finch, N. Dodds, J. Latto (2015) Optimized hybrid composite flexible pipe for ultra-deepwater applications, in: *Proc. 34th OMAE,* OMAE2015-41801, St.John's, Newfoundland, Canada.

Kalman, M., L. Yu, C. Durr (2014) Qualification of unbonded flexible pipe to API and DNV standards, in: *Proc. Offshore Technology Conference,* OTC-25092-MS, Houston, Texas, USA.

Karnovsky, I. A. (2011) *Theory of arched structures: strength, stability, vibration*, Springer Science & Business Media.

Kyriakides, S., E. Corona (2007) *Mechanics of offshore pipelines: volume 1 buckling and collapse*, Elsevier, London.

Lacerda, J. (2014) Development and experimental calibration of numerical model based on beam theory to estimate the collapse pressure of flexible pipes.

Lacerda, J., M. I. Lourenço, T. A. Netto (2015) Development and experimental calibration of numerical model based on beam theory to estimate the collapse pressure of flexible pipes, in: *Proc. 34th OMAE,* OMAE2015-41884, St. John's, Newfoundland, Canada.

Lambert, A., A. Felix-Henry, P. Gilbert, M. Gainvile (2012) Experimental and numerical study of a multi-layer flexible pipe depressurization, in: *Proc. 31st OMAE,* OMAE2012-83127, Rio de Janeiro, Brazil.

Langhaar, H. L. (1962) *Energy methods in applied mechanics*, Wiley, New York, USA.

Lo, K., J. Zhang (1994) *Collapse resistance modeling of encased pipes*, Buried Plastic Pipe Technology: 2nd Volume. ASTM STP 1222, ed. D. Eckstein.

Lohr, C., M. Pena (2017) Stones development: a pioneering management philosophy for enhancing project performance and safety field development, in: *Proc. Offshore Technology Conference,* OTC-27674-MS, Houston, Texas, USA.

Loureiro, W. C., I. P. Pasqualino (2012) Numerical-analytical prediction of the collapse of flexible pipes under bending and external pressure, in: *Proc. 31st OMAE,* OMAE2012-83476, Rio de Janeiro, Brazil.

Lu, J., F. Ma, Z. Tan, T. Sheldrake (2008) Bent collapse of an unbonded rough bore flexible pipe, in: *Proc. 27th OMAE,* OMAE2008-57063, Estoril, Portugal.

Machado, K. L., J. M. Dumay (1980) Dynamic production riser on Enchova Field Offshore Brazil, in: *Offshore Brazil Conference, Latin America Oil Show*, Rio de Janeiro, Brazil.

Malta, E. R., C. A. Martins, A. Gay Neto, F. G. Toni (2012) An investigation about the shape of the collapse mode of flexible pipes, in: *Proc. 22nd ISOPE,* ISOPE-I-12-280, Rhodes, Greece.

Martins, C. A., C. P. Pesce, J. A. P. Aranha (2003) Structural behavior of flexible pipe carcass during launching, in: *Proc. 22nd OMAE,* OMAE2003-37053, Cancun, Mexico.

Melillo, J. (2015) Industry advances deepwater production riser technology, Tech. rep., Wood Group Kenny.

Miyazaki, M., L. Paumier, F. Caleyron (2018) Effect of tension on collapse performance of flexible pipes, in: *Proc. 33rd OMAE,* OMAE2018-77286, Madrid, Spain.

Moore, B., A. Easton, J. Cabrera, C. Webb, B. George (2017) Stones development: Turritella FPSO - design and fabrication of the world's deepest producing unit, in: *Proc. Offshore Technology Conference,* OTC-27663-MS, Houston, Texas, USA.

Muren, J. (2007) Failure modes, inspection, testing and monitoring, Tech. rep., Seaflex.

Murphy, J. (2000) Flexible pipe becoming deepwater staple, Tech. rep., Oil and Gas Online.

Nemeth, M. (2011) A treatise on equivalent-plate stiffnesses for stiffened laminated-composite plates and plate-like lattices, Tech. rep., NASA, TP-2011-216882.

Nielsen, P. S. (2014) *Analysis and optimization of carcass production for flexible pipes*, Doctoral thesis, Department of Mechanical Engineering, Technical University of Denmark.

Nogueria, V. P. P., T. A. Netto (2010) A simple alternative method to estimate the collapse pressure of flexible pipes, in: *Proc. 29th OMAE,* OMAE2010-20692, Shanghai, China.

NOV (2014) Floating production systems: dynamic flexible risers, Tech. rep., National Oilwell Varco.

NOV (2015) Flexibles, Tech. rep., National Oilwell Varco.

Novitsky, A., F. Gray (2003) Flexible and rigid pipe solutions in the development of ultra-deep water fields, in: *Proc. 22nd OMAE,* OMAE2003-37401, Cancum, Mexico.

O'Brien, P., C. Overton, J. Picksley, K. Anderson, I. Macleod, E. Meldrum (2011) Outcomes from the SureFlex Joint Industry Project: an international initiative on flexible integrity assurance, in: *Proc. Offshore Technology Conference,* OTC-21524-MS, Houston, Texas, USA.

Out, J. M. M. (2012) Integrity management of flexible pipe: chasing failure mechanisms, in: *Proc. Offshore Technology Conference,* OTC-23670-MS, Houston, Texas, USA.

Paumier, L., D. Averbuch, A. Felix-Henry (2009) Flexible pipe curved collapse resistance calculation, in: *Proc. 28th OMAE,* OMAE2017-61490, Honolulu, Hawaii, USA.

Pavlina, E. J., C. J. Van Tyne (2008) Correlation of yield strength and tensile strength with hardness for steels, *J. Mater. Eng. Perform.*, 17, pp. 888–893.

Pesce, C. P., C. A. Martins, A. Gay Neto, A. L. C. Fujarra, F. C. M. Takafuji, G. R. Franzini, T. Barbosa, C. A. Godinho (2010) Crushing and wet collapse of flowline carcasses: a theoretical-experimental approach, in: *Proc. 29th OMAE,* OMAE2010-20423, Shanghai, China.

Provasi, R., F. G. Toni, C. A. Martins (2016) Equivalent model for interlocked carcass under axial loads, in: *Proc. 35th OMAE,* OMAE2016-54381, Busan, South Korea.

Pynn, R. (2009) *Neutron scattering – a non-destructive microscope for seeing inside matter. In: Liang L., Rinaldi, R., Schober, H. (eds). Neutron Applications in Earth, Energy and Environmental Sciences. Neutron Scattering Applications and Techniques.*, Springer, Boston, MA.

Rahmati, M. T., H. Bahai, G. Alfano (2016) An accurate and computationally efficient small-scale nonlinear FEA of flexible risers, *Ocean Eng.*, 121, pp. 382–391.

Ribeiro, E. J. B., J. R. M. Sousa, G. B. Ellwanger, E. C. P. Lima (2003) On the tension-compression behavior of flexible risers, in: *Proc. 13th ISOPE,* ISOPE-I-03-097, Honolulu, Hawaii, USA, pp. 105–112.

Rosas, M. A. P., A. P. F. Souza, M. V. Rodrigues, D. M. L. Silva (2014) Hydrostatic collapse pressure and radial collapse force comparisons for ultra-deepwater pipeline, in: *Proc. 33rd OMAE,* OMAE2014-24081, San Francisco, California, USA.

Sævik, S., N. Ye (2016) *Aspects of design and analysis of offshore pipelines and flexibles*, Southwest Jiao Tong University Press, Chengdu, China.

Santos, C. C. P., C. P. Pesce (2019) An alternative strategy for offshore flexible pipes finite element analysis, *Mar. Struct.*, 65, pp. 376–416.

Shen, Y., P. Jukes (2015) Techical challenges of unbonded flexible risers in HPHT and deepwater operations, in: *Proc. 25th ISOPE*, Kona, Big Island, Hawaii, US.

Shen, Y., J. Zhao, Z. Tan, Sheldrake (2012) Analysis of the creep behavior of the polymer barrier layer in unbonded flexible pipes under different fluid temperatures, in: *Proc. 31st OMAE,* OMAE2012-83164, Rio de Janeiro, Brazil.

Shen, Y., J. Zhao, Z. Tan, T. Sheldrake (2011) Influence of bore pressure on the creep behavior of polymer barrier layer inside an unbonded flexible pipe, in: *Proc. 30th OMAE,* OMAE2011-49392, Rotterdam, The Netherlands.

Simonen, F. A., R. J. Shippell (1982) Collapse of thick-walled cylinders under external pressure, *Exp. Mech.*, 22, pp. 41–48.

Simpson, P. J., A. J. Lima (2019) Deepwater riser systems – historical review and future projections, in: *Proc. Offshore Technology Conference,* OTC-29787-MS, Rio de Janeiro, Brazil.

Soki, C. A., L. M. B. Troina, W. C. Loureiro, J. R. M. de Sousa (2015) Effect of asymmetric boundary conditions on flexible pipes crushing, *Mar. Syst. Ocean Technol.*, 10, pp. 101–119.

Sousa, F. V. V., M. C. E. Bandeira, O. R. Mattos, C. J. B. M. Joia, F. Santos (2015) Laboratory test to evaluate service life extension of AISI 304 flexible pipe carcass at sour service, in: *NACE International*, Dallas, Texas, USA.

Souza, A. P. F. (2002) *Flexible pipes' collapse under external pressure*, Doctoral thesis, Department of Ocean Engineering, COPPE/UFRJ.

Steinzig, M., E. Ponslet (2003) Residual stress measurement using the hole dring method and laser speckle interferometry: Part I, *Exp. Tech.*, 27, pp. 45–48.

Tadjiev, D. (2016) Life extension assessment of dynamic risers – a case study, *Pipeline Technology Journal*, pp. 28–37.

Tang, M., Q. Lu, J. Yan, Q. Yue (2016) Buckling collapse study for the carcass layer of flexible pipes using a strain energy equivalence method, *Ocean Eng.*, 111, pp. 209–217.

Tang, M., J. Yan, J. Chen, Z. Yang, Q. Yue (2015) Residual stress evaluation and buckling analysis of carcass layers in flexible pipes using 3d finite element model, in: *Proc. 34th OMAE,* OMAE2015-41705, St. John's, Newfoundland, Canada.

Thépot, O. (2001) Structural design of oval-shaped sewer linings, *Thin-Walled Struct.*, 39, pp. 499–518.

Timoshenko, S. P. (1930) *Strength of materials. Part 1: elementary theory and problems*, McGraw-Hill, New York, USA.

Timoshenko, S. P., J. M. Gere (1961) *Theory of elastic stability*, McGraw Hill, New York.

Timoshenko, S. P., S. Woinowsky-Krieger (1959) *Theory of plates and shells, Second ed.*, McGraw Hill Kogakusha.

Tong, G. (2005) *In-plane stability of steel structures*, China Architecture & Building Press, Beijing, China.

Vidigal da Silva, J., A. Damiens (2016) 3000 m water depth flexible pipe configuration portfolio, in: *Offshore Technology Conference,* OTC-26933-MS, Houston, Texas, USA.

von Kármán, T. H. (1911) Uber die formänderung dünnwandiger rohre, insbesondere federnder ausgleichsrohre (in German), *Z. Ver. deut. Ing.*, 55, pp. 1889–1895.

Watkins, R. K., L. R. Anderson (1999) *Structural mechanics of buried pipes*, CRC Press.

Wolodko, J., D. DeGeer (2006) Critical local buckling conditions for deepwater pipelines, in: *Proc. 25th OMAE,* OMAE2006-92173, Hamburg, Germany.

Yue, Q., Q. Lu, J. Yan, A. Zheng, J. Palmer (2013) Tension behavior prediction of flexible pipelines in shallow water, *Ocean Eng.*, 58, pp. 201–207.

Zhang, P., S. X. Li, Z. F. Zhang (2011) General relationship between strength and hardness, *Mater. Sci. Eng.*, 529, pp. 62–73.

Zhang, Y., B. Chen, L. Qiu, T. Hill, M. Case (2003) State of the art analytical tools improve optimization of unbonded flexible pipes for deepwater environments, in: *Proc. Offshore Technology Conference,* OTC-15169-MS, Houston, Texas, USA.

Zhu, X., Q. Lei (2019) Effect of axial compression and wet collapse loads on torsional response of flexible pipe, *Arab. J. Sci. Eng.*, 44, pp. 10397–10408.

Summary

A flexible riser is a multi-layered pipe device which enables deep-water production by connecting seabed facilities to floating vessels. To withstand huge hydro-static pressure, it is required to have strong collapse capacities. At present, the collapse capacity of a flexible riser is designed based on a "wet collapse" concept, in which the outer sheath is damaged and the seawater has flooded the annulus. For a given water depth, the hydro-static collapse design of a flexible riser needs to be confirmed by a wet collapse calculation.

Calculating the wet collapse pressure of flexible risers is always challenging since the layers within risers are different in geometries and materials. Such a complex cross-sectional configuration makes the numerical simulation become the main approach for collapse analysis, which is quite time-consuming for the design stage. As the production is moving towards ultra-deep water fields, the design of new riser product is being required to achieve a balance between collapse resistance and self-weight. Therefore, there is a demand to develop an efficient tool to facilitate the collapse design.

This Ph.D. project aims to develop an analytical model to predict the wet collapse pressure for flexible risers in ultra-deep water applications. To determine the challenges in model development, a literature review on collapse studies of flexible pipes is conducted, which is presented in Chapter 2. This review indicates that three challenges should be faced with in order to proposed an analytical model. One is the self-interlocked metallic layers of flexible risers, which hinders the direct application of stability theories of ring and tubular structures. Another challenge for the model development relates to the initial geometric imperfections, which requires the initial ovality and layer gap to be involved in the wet collapse calculations. The pipe curvature brings the third challenge to the model development. The main difficulty lies in that is how to address the global curvature effect with a two-dimensional ring model.

Dealing with the self-interlocked metallic layers is always the first and

foremost step for the model development. Within the riser body, the interlocked carcass taking the external pressure are manufactured with self-interlocked metallic strips. As the classic ring buckling model is adopted as the base in this model development, the carcass should be treated as an equivalent rings. Therefore, the focus of Chapter 3 is on proposing an equivalent layer method for that treatment. Since the collapse is a bending-dominant problem, such equivalence should be built based on structural bending stiffness. However, the actual bending stiffness of the carcass is difficult to be obtained due to the geometric nonlinearities of its profile. As an alternative, another property, the absorbed strain energy at the onset of material yielding, is used. With this strain energy and the membrane stiffness of the self-interlocked carcass, the equivalent properties for the ring model can be determined.

Numerical simulation is adopted to verify this equivalent layer method. The interlocked carcass layer and its corresponding equivalent ring are constructed numerically. The wet collapse pressures predicted by these two numerical models are compared, which are in good agreement. This shows the proposed equivalent layer method can be a solid foundation for the following development of analytical model.

The stability theories of ring structures are used to establish the analytical model after the interlocked layers can be addressed by the proposed equivalent layer method. In Chapter 4, the development of analytical model starts from predicting the wet collapse for a flexible riser with initial geometric imperfections. According to the literature review in Chapter 2, the wet collapse resistance is sensitive to the initial ovality of the carcass and the inter-layer gap. To take these two imperfections into account, the collapse process is divided into two phases, pre- and post-contact phases, depending on the gap closure. As the collapse behaviors of the carcass are different in these two phases, the analytical model is established with two sub-models.

In the pre-contact phase, the carcass is buckled as a single ring. The external pressure for layer contact is calculated with the sub-model that develops from ring buckling theories. In the post-contact phase, the radial deformation of the carcass is restrained in the contact area. Under the hydro-static pressure, there is a portion(s) of the carcass detaches from the surroundings, which governs the collapse resistance in this phase. In the second sub-model, this detached portion of the carcass is regarded as a circular arch, in which the surrounding layers are treated as springs that support at the arch ends. The stability theories of arched structures are adopted to solve the buckling

pressure of this spring-supported arch model. As the arch geometry in the second sub-model is decided by the initial geometric ovality and inter-layer gap, the effects of these two imperfections are thereby taken in account.

To verify the analytical model proposed in this chapter, numerical simulations are employed. The numerical model is reproduced from the work of Gay Neto et al., which has been verified by comparing our prediction results with theirs. The effects of initial geometric imperfections on wet collapse resistance are studied through a set of cases, in which both two kind of models are used. The predictions of wet collapse pressure from them are compared. According to the comparison, the analytical predictions correlate well with the numerical results, which indicates that the initial imperfections can be addressed analytically.

Subsequently, the proposed analytical model is improved to consider the curvature effect in Chapter 5. Before introducing the pipe curvature into the analytical model, a mechanism study is conducted numerically to gain insight into the wet collapse behaviors of curved flexible risers. From this study, three factors induced by curvature affect the wet collapse capacity of curved risers, which are the pitch elongation, the squeeze load from surrounding layers, and the deformed cross-sectional shape of the carcass at the collapse moment. Those factors affect the radial stiffness of the detached portion of the carcass, leading to the reduction of the wet collapse strength. In the analytical model, therefore, those curvature-induced factors are introduced to correct the arch properties. The elongated pitch is used to correct the equivalent properties of the carcass. The squeeze and shape effects are adopted to correct the geometry of the arch model. With those corrections, the curvature effect on the wet collapse capacity of flexible risers is involved.

In Chapter 4 and 5, the initial imperfections and pipe curvature are addressed individually in our analytical model. To take their coupling effect into account, an integrated analytical model is established in Chapter 6 with the analytical formulations in previous chapters. Those coupling effects are addressed by correcting the geometric and material properties of the equivalent arch. 3D full FE models constructed based on the work of Gay Neto et al. were adopted to verify this models. The predicted curved wet collapse pressure from those two approaches showed good agreements in this verification, which indicates the integrated analytical model can be an effective tool in the riser design stage.

This integrated analytical model contributes to the hydro-static collapse design of flexible risers, which can provide the designers a rapid feedback for

their designed cross-section configuration. In our research work, the whole collapse analysis conducted by the proposed analytical model takes less than one hour to finish the prediction. Most of the time is spent on modeling the metallic layers for obtaining their equivalent properties. The actually wet collapse calculation given by this analytical model takes only a few seconds. By contrast, the numerical simulation requires 8$\sim$12 hours for modeling and consumes 2$\sim$3 days on average to complete one job. For companies that are developing new riser product to enable the ultra-deep water production, this proposed integrated analytical model can effectively facilitate the collapse design of new riser products.

Samenvatting

Een flexibele stijgpijp (E. ‘flexible riser’) is een pijp die productie in diep water mogelijk maakt door het verbinden van faciliteiten op de zeebodem met vaartuigen aan de oppervlakte. De wand van de pijp is opgebouwd uit meerdere lagen van verschillend materiaal. De pijp moet bestand zijn tegen hoge hydrostatische druk. De ontwerpwaarde van de sterkte van een pijp is mede gebaseerd op ‘nat bezwijken’ (E. ‘wet collapse’), waarbij de buitenzijde van de pijp beschadigd raakt en het zeewater in de wand van de pijp komt. Voor een gegeven waterdiepte moet de hydrostatische bezwijksterkte van de riser worden ondersteund door berekeningen van deze ‘wet collapse’.

Het berekenen van de bezwijkdruk van een flexible stijgpijp is moeilijk doordat de wand van de pijp is opgebouwd uit lagen van verschillende geometrie en verschillend materiaal. Een dergelijke ingewikkelde opbouw maakt dat numerieke simulatie de belangrijkste benadering is voor het bestuderen van het bezwijkmechanisme. Dit is een erg tijdrovend deel van de ontwerpfase. Daar de productie van olie en gas verschuift naar velden in zeer diep water, is er behoefte aan de ontwikkeling van een hulpmiddel om het ontwerp op dit punt te vergemakkelijken.

Doel van dit promotieproject is de ontwikkeling van een analytisch model voor het voorspellen van de natte bezwijkdruk van flexibele stijgpijpen bij gebruik in ultra-diep water. Om de problemen bij de ontwikkeling van zo’n model te leren kennen is een literatuurstudie uitgevoerd van onderzoeken over het bezwijken van flexibele pijpen. Dit literatuuronderzoek wordt gepresenteerd in Hoofdstuk 2. Het onderzoek geeft aan dat er drie problemen zijn bij de ontwikkeling van een analytisch model. Een uitdaging ligt in de aard van de inwendige samenhang van de metalen lagen van risers, waardoor het lastig is om de stabiliteitstheorie voor ringvormige en buisvormige structuren toe te passen. Een andere uitdaging voor de ontwikkeling van een model heeft te maken met initiële onvolkomenheden in de geometrie, waardoor bij de berekeningen rekening moet worden gehouden met die initiële

geometrie en ruimte tussen de lagen. Het belangrijkste probleem ligt in het modelleren van het effect van de buiging van de pijp in een tweedimensionaal ringmodel.

Verwerking van de in elkaar grijpende metalen lagen is de eerste en de belangrijkste stap in de opzet van een model. Het karkas van de pijplichaam vangt de externe druk op; dit karkas is samengesteld uit in elkaar grijpende metalen strips. Daar het klassieke vervormingsmodel voor ringen is gebruikt als basis voor de ontwikkeling van dit model, moet het karkas worden behandeld als een geschikt gekozen, overeenkomende ring. In Hoofdstuk 3 ligt daarom de nadruk op een voorstel voor een lagenmethode daarvoor. Omdat bij het bezwijken buiging dominant is, moet die keuze worden gebaseerd op de buigstijfheid. Maar door de geometrische niet-lineariteit van het karkas is het lastig om de buigstijfheid ervan te bepalen. Als alternatief is de opgenomen spanningsenergie aan het begin van de vloeifase van het materiaal gebruikt. Met deze spanningsenergie en de membraamstijfheid van het karkas kunnen de overeenkomende eigenschappen voor het ringmodel worden bepaald.

Numerieke simulatie is gebruikt voor het verifiëren van de lagenmethode. Het karkas en de daarmee overeenkomende ring zijn numeriek weergegeven. De bezwijkdrukken welke worden voorspeld door de twee modellen zijn vergeleken. De voorspellingen blijken goed overeen te komen. Dit laat zien dat de voorgestelde lagenmethode een goede basis kan zijn voor de ontwikkeling van een analytisch model.

Nu de onderling verbonden lagen kunnen worden behandeld door het voorgestelde equivalente lagenmodel, wordt stabiliteitstheorie van ringvormige structuren gebruikt voor het opzetten van het analytische model. In Hoofdstuk 4 begint de ontwikkeling van het analytische model met het voorspellen van het bezwijken van een flexibele stijgpijp met initiële geometrische onvolkomenheden. Uit het literatuuroverzicht in Hoofdstuk 2 volgt dat de natte bezwijkweerstand gevoelig is voor de initiële onrondheid van het karkas en van de ruimte tussen de lagen. Om met deze twee onvolkomenheden rekening te houden wordt het bezwijkproces verdeeld in twee fasen: de pre-contact fase en de post-contact fase, afhankelijk van het sluiten van de ruimte tussen de lagen. Omdat het bezwijkgedrag in deze twee fasen verschilt, bstaat het analytische model hier uit twee deelmodellen.

In de pre-contact fase vervormt het karkas als een enkele ring. De externe druk welke nodig is voor het contact tussen de lagen wordt berekend met behulp van het deelmodel dat is ontwikkeld op basis van theorie over

de vervorming van ringen. In de post-contact fase wordt de radiale vervorming van het karkas beperkt op plaatsen waar de lagen elkaar raken. Onder hydrostatische druk zijn een of meer delen van het karkas los van de omgevende lagen; dit bepaalt de bezwijkweerstand in deze fase. In het tweede deelmodel wordt zo'n niet-verbonden deel van het karkas beschouwd als een cirkelvormige boog, waarvan de omgevende lagen worden behandeld als veren die zijn ondersteund aan de uiteinden van de boog. Stabiliteitstheorie van gebogen constructies worden gebruikt voor het berekenen van de buigingsdruk. Daar de boogvormige geometrie in het tweede deelmodel wordt bepaald door de initiële onrondheid en de ruimte tussen de lagen, worden zo de effecten van deze twee onvolkomenheden in rekening gebracht.

Het analytische model dat in dit hoofdstuk is opgezet, is geverifieerd met behulp van numerieke simulaties. Het numerieke model is afkomstig uit het werk van Gay Neto e.a., en is geverifieerd door vergelijking van de voorspellingen. De effecten van initiële geometrische afwijkingen op de natte bezwijkweerstand worden onderzocht met behulp van enkele situaties waarin beide soorten modellen worden gebruikt. De gevonden voorspellingen van de natte bezwijkdruk worden vergeleken. Uit de vergelijking volgt dat de analytische voorspellingen goed overeenkomen met de numerieke resultaten. Dit geeft aan dat de initiële afwijkingen analytisch kunnen worden behandeld.

Vervolgens is het voorgestelde analytische model verbeterd door in Hoofdstuk 5 het krommingseffect in beschouwing te nemen. Alvorens de kromming van de pijp aan het model toe te voegen, is het verschijnsel numeriek bestudeerd om inzicht te krijgen in het natte bezwijkgedrag van gebogen flexibele stijgpijpen. Uit dit onderzoek volgen drie, door de kromming veroorzaakte, factoren die invloed hebben op de bezwijksterkte van gekromde stijgpijpen: de lengte van het gebogen stuk, de druk van de omliggende lagen en de vorm van het karkas op het moment van bezwijken. Deze factoren beïnvloeden de radiale stijfheid van het losse gedeelte van het karkas, met verlaging van de bezwijksterkte als gevolg. Deze krommingseffecten worden daarom toegevoegd in het analytische model om te corrigeren voor de invloed van de kromming van de pijp. De lengte van het gebogen stuk wordt gebruikt ter correctie van de overeenkomstige eigenschappen van het karkas. De druk- en vormeffecten worden gebruikt ter aanpassing van de geometrie van het boogmodel. Met die aanpassingen is het krommingseffect op de natte bezwijksterkte van flexibele stijgpijpen verwerkt.

In Hoofdstuk 4 en 5 zijn de initiële vormafwijkingen en de kromming

van de pijp in het analytische model afzonderlijk behandeld. Om hun gezamelijke invloed in rekening te brengen is in Hoofdstuk 6 een geïntegreerd analytisch model opgezet, op basis van de analytische formuleringen in voorgaande hoofdstukken. Die gemeenschappelijke effecten worden in rekening gebracht door aanpassing van de geometrische eigenschappen en de materiaaleigenschappen van de boog. 3D Eindige Elementen modellen, gebaseerd op het werk van Gay Neto e.a., zijn gebruikt om deze modellen te verifiëren. De voorspelde bezwijkdrukken uit deze twee benaderingen kwamen goed overeen. Dit toont aan dat het geïntegreerde analytische model een effectief hulpmiddel kan zijn bij het ontwerp van stijgpijpen.

Dit geïntegreerde model draagt bij aan het ontwerp van flexibele stijgpijpen ten aanzien van bezwijkgedrag onder hydrostatische druk. Dit kan ontwerpers snel inzicht geven in de ontworpen configuratie. De berekening van het natte bezwijkgedrag met behulp van het analytische model kost slechts enkele seconden. Numerieke simulatie van een enkel geval kost gemiddeld 2 tot 3 dagen. Voor bedrijven die een nieuwe riser voor productie in ultra-diep water ontwerpen, kan het voorgestelde geïntegreerde analytische model het ontwerp m.b.t. bezwijkgedrag effectief vergemakkelijken.

About the author

Xiao Li was born on May 30, 1990, in Jingzhou, Hubei, China. He received the Bachelor degree in Naval Architecture and Ocean Engineering from Wuhan University of Technology, Hubei, China, in 2013. At the same year, he started her master study at the same university, under the supervision of Prof. Weiguo Wu. The main work of his master research lay in the field of impact engineering. In 2016, he obtained his Master degree in Naval Architecture and Ocean Engineering.

Sponsored by the China Scholarship Council, Xiao Li started his Ph.D. research in October 2016 at the Department of Maritime Technology and Transport, Delft University of Technology, under the supervision of Prof. Hans (J. J.) Hopman and Dr. Xiaoli Jiang. During his four-year PhD research, he worked on the ultimate strength analysis of flexible pipes, which was mainly focused on the wet collapse of risers. His research interest is structural integrity assessment of marine structures, including hull structures, pipelines, wind turbines and cranes.

Publications

Journal papers

1. **Li X.**, Jiang X., Hopman H. "Development of an analytical model for predicting the wet collapse pressure of curved flexible risers." Ocean Engineering. (under review)

2. **Li X.**, Jiang X., Hopman H. "Curvature effect on wet collapse behaviors of flexible risers subjected to hydro-static pressure." Ships and Offshore Structures, 1861705 (2020).

3. **Li X.**, Jiang X., Hopman H. "Predicting the wet collapse pressure for flexible risers with initial ovalization and gap: an analytical solution." Marine Structures **71**, 102732 (2020).

4. **Li X.**, Jiang X., Hopman H. "Spring-supported arch model for predicting hydrostatic collapse strength of flexible riser with layer gap." Chinese Journal of Ship Research **14**(Supp 2), 15–22 (2019). (In Chinese)

5. **Li X.**, Jiang X., Hopman H. "A strain energy-based equivalent layer method for the prediction of critical collapse pressure of flexible risers." Ocean Engineering **164(15)**, 248–255 (2018).

6. **Li X.**, Jiang X., Hopman H. "A review on predicting critical collapse pressure of flexible risers for ultra-deep oil and gas production." Applied Ocean Research **80**, 1–10 (2018).

7. **Li X.**, Jiang X., Hopman H. "Prediction of the critical collapse pressure of ultra-deep water flexible risers – a literature review." FME Transactions **46(3)**, 306–312 (2018).

Conference papers

1. **Li X.**, Jiang X., Hopman H. "Finite element studies of the curvature effect on collapse behavior of flexible risers subjected to wet collapse." in: MARTECH 2020 5th International Conference on Maritime Technology and Engineering, Lisbon, Portugal (November 2020).

2. **Li X.**, Jiang X., Hopman H. "An analytical approach for predicting the collapse pressure of the flexible risers with initial ovalization and gap." in: ASME 2019 38th International Conference on Ocean, Offshore and Arctic Engineering, Glasgow, Scotland, UK (June 2019).

3. **Li X.**, Jiang X., Hopman H. "A strain energy-based equivalent layer method for the prediction of critical collapse pressure of flexible risers." in: ASME 2018 37th International Conference on Ocean, Offshore and Arctic Engineering, Madrid, Spain (June 2018).

TRAIL Thesis Series

The following list contains the most recent dissertations in the TRAIL Thesis Series, For a complete overview of more than 250 titles see the TRAIL website: www.rsTRAIL.nl.

The TRAIL Thesis Series is a series of the Netherlands TRAIL Research School on transport, infrastructure and logistics.

Li, X., *Development of an Integrity Analytical Model to Predict the Wet Collapse Pressure of Flexible Risers*, T2021/9, February 2021, TRAIL Thesis Series, The Netherlands.

Li, Z., *Surface Crack Growth in Metallic Pipes Reinforced with Composite Repair System*, T2021/8, January 2021, TRAIL Thesis Series, The Netherlands.

Gavriilidou, A., *Cyclists in Motion: From data collection to behavioural models*, T2021/7, February 2021, TRAIL Thesis Series, The Netherlands.

Methorst, R., *Exploring the Pedestrians Realm: An overview of insights needed for developing a generative system approach to walkability*, T2021/6, February 2021, TRAIL Thesis Series, The Netherlands.

Walker, F., *To Trust or Not to Trust? Assessment and calibration of driver trust in automated vehicles*, T2021/5, February 2021, TRAIL Thesis Series, The Netherlands.

Schneider, F., *Spatial Activity-travel Patterns of Cyclists*, T2021/4, February 2021, TRAIL Thesis Series, The Netherlands.

Madadi, B., *Design and Optimization of Road Networks for Automated Vehicles*, T2021/3, January 2021, TRAIL Thesis Series, The Netherlands.

Krabbenborg, L.D.M., *Tradable Credits for Congestion Management: sup-*

port/reject?, T2021/2, February 2020, TRAIL Thesis Series, The Netherlands.

Castelein, B., *Accommodating Cold Logistics Chains in Seaport Clusters: The development of the reefer container market and its implications for logistics and policy*, T2021/1, January 2021, TRAIL Thesis Series, the Netherlands.

Polinder, G.J., *New Models and Applications for Railway Timetabling*, T2020/18, December 2020, TRAIL Thesis Series, the Netherlands.

Scharpff, J.C.D., *Collective Decision Making trough Self-regulation*, T2020/17, November 2020, TRAIL Thesis Series, the Netherlands.

Guo, W, *Optimization of Synchromodal Matching Platforms under Uncertainties*, T2020/16, November 2020, TRAIL Thesis Series, the Netherlands.

Narayan, J., *Design and Analysis of On-Demand Mobility Systems*, T2020/15, October 2020, TRAIL Thesis Series, the Netherlands.

Gong, X., *Using Social Media to Characterise Crowds in City Events for Crowd Management*, T2020/14, September 2020, TRAIL Thesis Series, the Netherlands.

Rijal, A., *Managing External Temporal Constraints in Manual Warehouses*, T2020/13, September 2020, TRAIL Thesis Series, the Netherlands.

Alonso González, M.J., *Demand for Urban Pooled On-Demand Services: Attitudes, preferences and usage*, T2020/12, July 2020, TRAIL Thesis Series, the Netherlands.

Alwosheel, A.S.A., *Trustworthy and Explainable Artificial Neural Networks for choice Behaviour Analysis*, T2020/11, July 2020, TRAIL Thesis Series, the Netherlands.

Zeng, Q., *A New Composite Indicator of Company Performance Measurement from Economic and Environmental Perspectives for Motor Vehicle Manufacturers*, T2020/10, May 2020, TRAIL Thesis Series, the Netherlands.

Mirzaei, M., *Advanced Storage and Retrieval Policies in Automated Warehouses*, T2020/9, April 2020, TRAIL Thesis Series, the Netherlands.

Nordhoff, S., *User Acceptance of Automated Vehicles in Public Transport*,

T2020/8, April 2020, TRAIL Thesis Series, the Netherlands.

Winter, M.K.E., *Providing Public Transport by Self-Driving Vehicles: User preferences, fleet operation, and parking management*, T2020/7, April 2020, TRAIL Thesis Series, the Netherlands.

Mullakkal-Babu, F.A., *Modelling Safety Impacts of Automated Driving Systems in Multi-Lane Traffic*, T2020/6, March 2020, TRAIL Thesis Series, the Netherlands.

Krishnakumari, P.K., *Multiscale Pattern Recognition of Transport Network Dynamics and its Applications: A bird's eye view on transport*, T2020/5, February 2020, TRAIL Thesis Series, the Netherlands.

Wolbertus, *Evaluating Electric Vehicle Charging Infrastructure Policies*, T20 20/4, February 2020, TRAIL Thesis Series, the Netherlands.

Yap, M.D., *Measuring, Predicting and Controlling Disruption Impacts for Urban Public Transport*, T2020/3, February 2020, TRAIL Thesis Series, the Netherlands.

Luo, D., *Data-driven Analysis and Modeling of Passenger Flows and Service Networks for Public Transport Systems*, T2020/2, February 2020, TRAIL Thesis Series, the Netherlands.

Erp, P.B.C. van, *Relative Flow Data: New opportunities for traffic state estimation*, T2020/1, February 2020, TRAIL Thesis Series, the Netherlands.

Zhu, Y., *Passenger-Oriented Timetable Rescheduling in Railway Disruption Management*, T2019/16, December 2019, TRAIL Thesis Series, the Netherlands.

Chen, L., *Cooperative Multi-Vessel Systems for Waterborne Transport*, T2019 /15, November 2019, TRAIL Thesis Series, the Netherlands.